Universidad de Concepción
Facultad de Ciencias Naturales y Oceanográficas
Programa de Doctorado en Oceanografía

VARIABILIDAD ESTACIONAL E INTERANUAL DEL TRANSPORTE DE LA CORRIENTE SUBSUPERFICIAL DE PERÚ-CHILE Y SU RELACIÓN CON EL OXÍGENO DISUELTO FRENTE A LA ZONA CENTRAL DE CHILE (30°-38ºS)

Tesis presentada a la facultad de ciencias naturales y oceanográficas de la Universidad de Concepción para optar al grado de Doctor en Oceanografía

POR: MATIAS BERNARDO PIZARRO KOCH

Profesor Guía: Dr. Oscar Roberto Pizarro Arriagada
Departamento de Geofísica
Universidad de Concepción

Profesor Co-Guía: Dr. Marcel Emilio Ramos Quezada
Depto. Biología Marina, Facultad Cs del Mar
Universidad Católica del Norte

Julio 2021
Concepción, Chile

AUTORIZACIÓN

Quien suscribe, (MATIAS BERNARDO PIZARRO KOCH, 15.479.317-8), alumno del Programa DOCTORADO EN OCEANOGRAFIA, que imparte la Facultad de CIENCIAS NATURALES Y OCEANOGRAFICAS, de la Universidad de Concepción, declara ser autor de la (VARIABILIDAD ESTACIONAL E INTERANUAL DEL TRANSPORTE DE LA CORRIENTE SUBSUPERFICIAL DE PERÚ-CHILE Y SU RELACIÓN CON EL OXÍGENO DISUELTO FRENTE A LA ZONA CENTRAL DE CHILE (30°-38ºS)) y conceder derecho de publicación, comunicación al público y reproducción de esa obra, en forma total o parcial en cualquier medio y bajo cualquier forma del mismo, a la Universidad de Concepción, Chile, para formar parte de la colección material o digital de cualquiera de las Bibliotecas de la Universidad de Concepción y del Repositorio Institucional UdeC. Esta autorización es de forma libre y gratuita, y considera la reproducción de la obra con fines académicos y de difusión tanto nacional como internacionalmente.

Asimismo, quien suscribe declara que dicha obra no infringe derechos de autor de terceros.

……

(FIRMA)

(29/06/2021)

Universidad de Concepción
Dirección de Postgrado

La Tesis de "*Doctorado en Oceanografía*" titulada *"Variabilidad estacional e interanual del transporte de la Corriente Subsuperficial de Perú-Chile y su relación con el oxígeno disuelto en la zona central de Chile (30°-38ºS)"*, del Sr. *MATIAS BERNARDO PIZARRO-KOCH* y realizada bajo la Facultad de Ciencias Naturales y Oceanográficas, Universidad de Concepción, ha sido aprobada por la siguiente Comisión de Evaluación:

Dr. Oscar Pizarro
Profesor Guía
Universidad de Concepción
Concepción – Chile _____

Dr. Marcel Ramos
Profesor Co-Guía
Universidad Católica del Norte
Coquimbo – Chile _____

Dr. Boris Dewitte
Miembro Comité de Tesis
Laboratoire d'Etudes en
Géophysique et Océanographie
Spatiales (LEGOS-IRD) - Francia _____

Dr. Andrés Sepúlveda
Miembro Comité de Tesis
Universidad de Concepción - Chile _____

Dra. Marcela Cornejo D'Ottone
Evaluador Externo
Pontificia Universidad Católica de Valparaíso _____

Dra. Pamela Hidalgo
Directora
Programa de Doctorado en Oceanografía
Universidad de Concepción
Concepción – Chile _____

A mis padres, hermanos e hijos

Otro grano de arena para la playa ;)

Perseverantia: *La permanencia, perseverancia y persistencia a pesar de todos los obstáculos, desalientos e imposibilidades: es eso lo que distingue las almas fuertes de las débiles*.

Thomas Carlyle.

AGRADECIMIENTOS

A mi familia: Bernardo-Karen (padres), quienes me dieron además de la vida, múltiples herramientas y valores para afrontarla. Francisco-Consuelo (hermanos), desde que nací han estado a mi lado siendo un apoyo incondicional en todas mis aventuras y procesos de crecimiento. Martina-Agustín (hijos), ellos sin saberlo condicionan mi existencia para bien y son la razón de ser de mi vida (sus sonrisas llenan mi alma). Andrea (compañera) pilar fundamental en este proceso y mi vida "emocional y racional". Amigos: *M.u.c.h.o.s et al.,* no tengo suficientes hojas para enumerarlos a cada uno, pero todos ellos están incluidos en la sigla.

A mis profesores: don Oscar Pizarro, profesor guía y finalmente un amigo, quien sin interés alguno me entrego todo su apoyo y conocimiento para lograr con éxito este largo proceso. A don Marcel Ramos, guía y amigo, quien me incito a comenzar esta aventura. A don Boris Dewitte, por su incansable y desinteresado apoyo. A don Andrés Sepúlveda, quien silenciosamente siempre estuvo ahí para resolver dudas y me entrego las bases de la modelación numérica.

Finalmente, agradezco el financiamiento otorgado para mi formación en el doctorado y el desarrollo de esta tesis. A la Beca de Doctorado nacional CONICYT, a los proyectos Instituto Milenio de Oceanografía (IMO; ICM 120019), COPAS Sur-Austral, CRN3070-IAI (US national science Foundation; grant GEO-11280040), REDOC.CTA (Red Doctoral en Ciencia, Tecnología y Ambiente, UdeC) y a los proyectos FONDECYT 1181872, 1121041, 1140845, 1151185, 1190276, 1171861, 1120504, 1151299 y 1171895.

Curriculum Vitae

MATIAS BERNARDO PIZARRO-KOCH

Nacido el 13 de Julio de 1983, en Santiago de Chile.

Educación

2021 Doctor (c) en Oceanografía, Universidad de Concepción, Concepcion, Chile.

2009 Biologo Marino, Universidad Catolica del Norte, Coquimbo, Chile.

2008 Licenciado en Cs del mar, Universidad Catolica del Norte, Coquimbo, Chile

Área de investigación

Modelación físico-biogeoquímica del océano con interés en la variabilidad espacio-temporal de las Zonas de Mínimo Oxígeno (ZMO) del Pacífico Suroriental y su relación con los patrones de circulación subsuperficial. Entender y describir los principales mecanismos físicos y bioquímicos que controlan la variabilidad de las ZMOs.

Publicaciones

- **Pizarro-Koch, M**., Pizarro, O., Dewitte, B., Montes, I., Ramos, M., Paulmier, A., & Garçon, V. (2019). Seasonal Variability of the Southern Tip of the Oxygen Minimum Zone in the Eastern South Pacific (30°-38° S): A Modeling Study. *Journal of Geophysical Research: Oceans*. *https://doi.org/10.1029/2019JC015201*

- **Pizarro-Koch, M**., Pizarro, O., Dewitte, B., Montes, I., Ramos, M., Paulmier, A., Garçon, V and Sepulveda, H. H. (2020). Physical drivers of the interannual changes of the Oxygen Minimum Zone off Chile (30ºS-38ºS) during 2000-2008. Submitted to *Journal of Geophysical Research: Oceans.*

- Pizarro, O., Ramirez, N., Castillo, M., Cifuentes, U., Rojas, W. and **Pizarro-Koch**, **M.** (2016). Underwater glider observations in the oxygen minimum zone off central Chile. Bull. Amer. Meteor. Soc. *https://doi.org/10.1175/BAMS-D-14-00040.1*

- Corredor-Acosta, A., Cortés-Chong, N., Acosta. A., **Pizarro-Koch. M**., Vargas, A., Medellín-Mora, J., Saldías. G.S, Echeverry-Guerra, V., Gutiérrez-Fuentes, J. Betancur-

Turizo., S. (2020). Spatio-temporal variability of Chlorophyll-a and environmental variables in the Panama Bight. *Remote Sens*. 2020, 12, 2150; doi:10.3390/rs12132150.

- Rothäusler, E., Hinojosa, I.A., Moraga, J., **Pizarro-Koch, M**., Ramos, M., Thiel, M. (2020), At the mercy of winds: the seasonal dynamics of floating seaweeds at mid latitudes. Submitted to *Limnology and Oceanography.*

- Moraga-Opazo, J., Valle-Levinson, A., Ramos, M., **Pizarro-Koch**, **M**. (2011). Upwelling-Triggered near-geostrophic recirculation in an Equatorward Facing Embayment. Continental Shelf Research, vol 31, pags 1991-1999. *https://doi.org/10.1016/j.csr.2011.10.002*

- I.A. Hinojosa., **Pizarro-Koch**, **M**., Ramos. M, Thiel, M. (2010). Spatial and temporal distribution of floating kelp in the channels and fjords of southern Chile. *Estuarine, Coastal and Shelf Science*, *Volume 87, Issue 3*, 30 April 2010, Pages 367-377. *https://doi.org/10.1016/j.ecss.2009.12.010*

ESTADÍAS DE INVESTIGACIÓN Y CONFERENCIAS INTERNACIONALES

- Laboratoire d'Etudes en Géophysique et Océanographie Spatiales (LEGOS- IRD). Toulouse, Francia. El objetivo fue desarrollar experimentos de modelación numérica (física y biogeoquímica), utilizando los modelos numéricos ROMS (Regional Ocean Model System) y BioEBUS (Biogechemical Eastern Boundary Upwelling System).
- Entrenamiento y análisis de simulaciones numericas en el Instituto Geofísico del Perú. Lima, Perú.
- Participación en el Surface Ocean - Lower Atmosphere Study (SOLAS) summer school 2018. SOLAS es una iniciativa internacional orientado al estudio del la dinámica entre el océano superficial y la atmósfera baja. (más detalles visitar http://www.solas-int.org/)
- Ocean Deoxygenation Conference, Kiel, Alemania (2018)
- 46Th International Colloquium on Low oxygen environments in marine, estuarine and fresh. Liège Bélgica. (2014).
- 11th ICSHMO International Conference of Southern Hemisphere Meteorology and Oceanography. Santiago, Chile. (2015).

Índice de Contenidos

Resumen i
Abstract iii

1. INTRODUCCIÓN 5
    1.1. Oxígeno disuelto en el océano..... 5
    1.2. Zonas de Mínimo Oxígeno..... 6
    1.3. Circulación y masas de agua en el Pacifico Sur-Oriental.....10
    1.4. La Corriente Subsuperficial de Perú-Chile (CSPC).....12
    1.5. Modelación físico-biogeoquímica de la Zona de Mínimo Oxígeno del Pacífico Sur-Oriental (ZMO-PSO) 13
2. HIPÓTESIS Y OBJETIVOS..... 15
3. MATERIAL Y MÉTODOS 16
    3.1. Modelo hidrodinámico (ROMS).....16
    3.2. Modelo biogeoquímico (BioEBUS).....18
    3.3. Acoplamiento físico-biogeoquímico (ROMS-BioEBUS).....19
4. RESULTADOS 22
    4.1. Capítulo 1. Variabilidad estacional del extremo sur de la Zona de Mínimo Oxígeno en el Pacífico Sur Oriental (30ºS-38ºS): Un estudio de modelación.....22
    4.2. Capítulo 2. Factores físicos que controlan los cambios interanuales de la Zona Mínima de Oxígeno frente a Chile central (30ºS-38ºS) durante el periodo 2000-2008.....53
5. DISCUSIÓN 84
6. CONCLUSIONES 95
7. REFERENCIAS 97

RESUMEN

Variabilidad estacional e interanual del transporte de la Corriente Subsuperficial de Perú-Chile y su relación con el oxígeno disuelto en la zona central de Chile (30°-38ºS)

Matias Pizarro-Koch

2021

Dr. Oscar Pizarro, Profesora Guía

Dr. Marcel Ramos, Profesor Co-Guía

La Corriente Subsuperficial de Perú-Chile (CSPC) nace en la región ecuatorial del Pacífico Oriental (~5ºS) y fluye hacia el sur sobre el talud y la plataforma continental de Sudamérica transportando Agua Ecuatorial Subsuperficial (AESS). Esta masa de agua está estrechamente relacionada con la zona de mínimo oxígeno (ZMO) y es la misma que emerge hasta la superficie debido a la surgencia costera frente a Chile central. El AESS se caracteriza por tener un núcleo salino (~35 en su origen y valores cercanos a 34.4-34.6 frente a la costa central de Chile), con bajas concentraciones de oxígeno disuelto (OD) <45µM, altas concentraciones de nutrientes y con altas (bajas) concentraciones de CO_2 (pH). A pesar de la conocida relación que existe entre la CSPC y el transporte de AESS hacia el sur, el rol de la variabilidad espacio-temporal de la CSPC sobre la ZMO en la zona central de Chile ha sido poco explorada. Específicamente, los mecanismos físicos y biogeoquímicos que influyen en la intensidad y variabilidad de la ZMO. Esto debido a la insuficiente cantidad de observaciones existentes y al limitado número de estudios en la región, tanto observacionales como de modelación.

El objetivo general de este estudio es analizar las contribuciones de la advección (horizontal y vertical), la mezcla y los procesos biogeoquímicos en la variabilidad estacional e interanual del oxígeno disuelto en la columna de agua, frente a la costa central de Chile (30ºS-38ºS). Por tanto, se evalua el rol de la CSPS y de la actividad de mesoescala subsuperficial sobre la variabilidad estacional e interanual de la ZMO. Para este propósito, se utilizó una simulación numérica de alta resolución (1/12°) que acopla un modelo hidrodinámico de circulación regional del océano (ROMS) con un modelo biogeoquimíco (BioEBUS). La validación del modelo en

base a observaciones *in-situ* y con datos climatológicos globales, indican una buena representación de los principales procesos oceanográficos de la región de estudio.

Los resultados muestran que el balance estacional e interanual de OD al interior del volumen de la ZMO es dominado por los procesos físicos (principalmente advección) sobre los biogeoquímicos (principalmente respiración oxigénica y nitrificación). En este sentido, la variabilidad estacional e interanual del volumen y la intensidad de la ZMO están altamente correlacionadas con la AESS y la CSPC. A escala estacional, el transporte hacia el sur de la CSPC se relaciona con un mayor volumen de la ZMO, mientras que, a escala interanual la CSPC impacta principalmente la intensidad de la ZMO (es decir, la concentración promedio de OD dentro del volumen de la ZMO) y secundariamente su volumen. No obstante, esta modulación no es homogénea a lo largo de la costa debido a que otros procesos físicos intervienen contribuyendo a modular también la variabilidad del OD; particularmente, procesos como las corrientes (jets) zonales y los flujos turbulentos asociados a los remolinos de mesoescala.

Estos jets zonales se observan intercalados (positivos y negativos) a lo largo de la costa cumpliendo un rol clave en la variabilidad del borde exterior de la ZMO. Los jets positivos (hacia el este) están asociados con flujos de OD hacia la costa, ventilando y comprimiendo la ZMO; en contraste, los jets negativos (hacia el oeste) modulan su expansión costa afuera. Adicionalmente, los flujos turbulentos asociados a la actividad de mesoescala, fluyen generalmente en dirección contraria al gradiente de OD (es decir, hacia la costa) y cumplen un rol significativo en la ventilación oceánica de la OMZ en la región. En consecuencia, estos transportes zonales de OD se presentan como un nuevo mecanismo físico de variabilidad que actúa en el límite oceánico de la ZMO modulando su volumen y extensión zonal frente a Chile central.

ABSTRACT

Seasonal and interannual variability of the Peru-Chile Undercurrent and its relationships with the dissolved oxygen off central Chile (30º-38ºS).

Matias Pizarro-Koch

2021

Dr. Oscar Pizarro, Profesora Guía

Dr. Marcel Ramos, Profesor Co-Guía

The Peru-Chile undercurrent (PCUC) born in the equatorial region and flows southward transporting oxygen depleted Equatorial Subsurface Water (ESSW) along the slope and continental shelf. The ESSW is closely related with the Oxygen Minimum Zone (OMZ) and is the same water that emerges to the upper layer in coastal upwelling periods off central-southern Chile characterized by a saline core ~35 with low dissolved oxygen (DO) concentrations <45µM, high nutrient content and high (low) CO_2 values (pH). Despite the relationship that exists between the CSPC and the ESSW, the role of the spatial and temporal variability of the CSPC over the OMZ in central Chile remain mostly unknow. Specifically, the physical and biogeochemical mechanisms influencing the intensity, and the spatial and temporal variability of the OMZ. This due in part to the insufficient number of observations and limited number of observational and/or modeling studies in the region.

The aim of this study is to evaluated the contribution of the advection (horizontal and vertical), mixing and biogeochemical processes over the seasonal and interannual variability of the DO in the water column off central Chile (30ºS-38ºS). Therefore, we assess the role of the PCUC and the subsurface mesoscale activity on the seasonal and interannual variability of the OMZ. For this purpose, a high horizontal resolution (1/12°) regional coupled physical-biogeochemical model (ROMS-BioEBUS) simulation was used and validated with available *in-situ* observations, and global climatological data indicating a good representation of the main oceanographic dynamics of the study region.

The results suggest that the seasonal and interannual DO budget within the OMZ volume is dominated by the physical (mainly advection) over the biogeochemical processes (mainly

oxic respiration and nitrification). In this sense, the seasonal and interannual variability of the volume and OMZ intensity was highly correlated with the ESSW, and the PCUC. At seasonal time-scale the poleward transport by the PCUC was related with a higher OMZ volume, whereas at interannual time-scale the PCUC transport mainly impact the intensity of the OMZ, and secondarily its volume. Nevertheless, this modulation is not homogeneous along the coast because other simultaneous processes disturb the meridional DO transport, such as the zonal currents (jets) and the turbulent transport associated with the mesoscale eddies.

These zonal transport of DO by meridionally alternating (positive and negative) zonal jets are observed along the coast, playing a key role in the variability of the oceanic OMZ boundary. The positive (eastward) jets are associated with inshore DO flows ventilating and compressing the OMZ volume, meanwhile the intensity of the negative (westward) jets modulate the offshore OMZ expansion. Additionally, the turbulent flows associated with the mesoscale activity generally flowing in the opposite direction of the DO gradient (i.e. inshore) are playing a significant role in the ventilation of the OMZ in the oceanic region off central Chile.

1. INTRODUCCIÓN

1.1 Oxígeno disuelto en el océano

Alrededor del 50% del OD de la Tierra fue producido en los océanos por las cianobacterias (*Holland*, 2006) siendo este gas fundamental para la vida, para los ecosistemas marinos y el clima global de nuestro planeta (*Breitburg et al*., 2018). En el océano, la distribución de OD se encuentra condicionada por un complejo balance entre distintos procesos físicos y biogeoquímicos, los cuales suceden a distintas escalas de variabilidad espacial y temporal. Los procesos biogeoquímicos que modulan la distribución de oxígeno se pueden agrupar en i) procesos biológicos que aportan OD (fuentes de OD), por ejemplo, la fotosíntesis (*Gregg and Rousseaux*, 2019) y ii) procesos biológicos que remueven OD del medio (sumideros de OD) tales como la respiración oxigénica mediada por bacterias (*Kämpf and Chapman et al., 2016; Maßmig et al*., 2020).

Entre los procesos físicos que modulan la concentración de OD se encuentra la circulación profunda, con escalas típicas de cientos de años y decenas de miles de kilómetros (*Ito et al*., 2017; *Schmidtko et al*., 2017). Esta circulación redistribuye las masas de agua en el océano contribuyendo a la ventilación de las aguas profundas e intermedias. Durante la formación de una masa de agua en zonas de altas latitudes, el aumento de la densidad promueve el hundimiento de las aguas superficiales, usualmente saturadas con OD, transportando sus propiedades (oxígeno, nutrientes, temperatura y salinidad, entre otros) hacia el interior del océano (*Warren*, 1981; *Portela et al*., 2020). No obstante, a medida que las aguas se desplazan por las cuencas oceánicas la materia orgánica es respirada, modificando la concentración de nutrientes y de OD. En consecuencia, el OD de una masa de agua está estrechamente ligado a su edad, la que corresponde al tiempo transcurrido desde que la masa de agua perdió contacto con la atmósfera (*Karstensen et al*., 2008).

En las regiones subtropicales/tropicales de los bordes orientales de los océanos, las masas de agua intermedias (es decir, aquellas ubicadas en la zona de la termoclina, primeros 1000 m de profundidad) son pobremente ventiladas por la circulación oceánica de gran escala (e.g *Pedlosky*, 1998; *Lyuten et al*., 1983; *Karstensen et al*., 2008) localizándose allí las

principales Zonas de Mínimo Oxígeno (ZMO). Sin embargo, a escalas espacio-temporales menores (intraestacional a interanual), existen otros procesos físicos que modulan la distribución de OD, por ejemplo: el intercambio gaseoso océano-atmosfera, la solubilidad del gas en el agua de mar, cambios en la estratificación y en la mezcla de pequeña escala, el bombeo de Ekman, la surgencia y *entrainment*, la advección por las corrientes marinas regionales y procesos de sub- y meso- escala (como remolinos oceánicos).

1.2 Zonas de Mínimo Oxígeno

Bajo la superficie del océano entre 100 y 1500 m de profundidad, la combinación de factores físicos y biológicos genera ambientes pobres en OD conocidos como ZMOs (*Cline and Richards*, 1972). Estas zonas se caracterizan por tener altas tasas de respiración microbiana y baja ventilación (*Wirtky*, 1962). En la actualidad, no existe un consenso sobre el umbral exacto de OD para definir las ZMOs. El primer estudio global de aguas hipóxicas consideró un umbral de OD <8 μM (*Kamykowski and Zentara*, 1990). Sin embargo, *Karstensen et al.* (2008) utilizaron tres umbrales para analizar las características de las ZMOs en el Pacífico Oriental Tropical y el Atlántico: OD ~4.5 μM en el rango subóxico, OD ~45 μM y un nivel mayor a ~90 μM para incluir en su análisis la ZMO menos intensa del océano Atlántico Tropical Oriental. Posteriormente, *Paulmier and Ruiz-Pino* (2009), excluyeron la ZMO del océano Atlántico y utilizaron un umbral de 20 μM para describir las ZMOs utilizando la climatología WOA2005 (World Ocean Atlas del año 2005, https://www.nodc.noaa.gov/OC5/WOA05/pr_woa05.html). Del mismo modo, *Fuenzalida et al*. (2009) y *Helly and Levin* (2004) utilizaron el umbral de 20 μM para describir la extensión vertical-horizontal de la ZMO del océano Pacifico Sur-Oriental y las ZMOs sobre los fondos marinos del margen continental, respectivamente. En contraste, *Stramma et al.* (2012) usaron un valor mucho mayor (~150 μM) para analizar la expansión de la ZMO en el océano Atlántico Tropical.

Adicional a la definición de las ZMOs en función del umbral de OD, existen otras clasificaciones definidas de acuerdo a su concentración en el océano, por ejemplo: i) *Suboxia* definida principalmente por biólogos y biogeoquímicos para referirse al rango de transición

entre la respiración de oxígeno y nitrato, con valores entre ~0.7 μM y 20 μM (*Yakusev and Neretin*, 1997; *Hell and Levin,* 2004, *Paulmier and Ruiz-Pino* (2009); ii) *Hipoxia* definida como condiciones de OD en las cuales los macro-organismos no pueden vivir (OD ≤ 62.2 μM) (*Gray et al*., 2002); iii) *Dysoxia* y iv) *Microxia* con rangos de OD < 4 μM y OD < 1μM, respectivamente, asociadas con una transición brusca de OD para los organismos grandes, tales como peces (*Levin*, 2002); y finalmente v) *Anoxia* definida por valores de OD ~ 0.0 μM asociada con la transición entre la respiración de nitrato y sulfato (*Schunck et al*., 2013; *Ulloa et al*., 2012).

De acuerdo a la definición de las ZMOs usada por *Gewin* (2010) equivalente a OD < 0.5 mL L^{-1} (22 μM), las ZMOs actualmente cubren el 8% del área y el 0.1% del volumen del océano, implicando un rol clave en el ecosistema marino y la evolución del clima. Por una parte, las ZMOs impactan la distribución del zooplancton y las pesquerías actuando como una barrera respiratoria (*Levin et al*., 2018; *Sanchez-Velasco et al*., 2018; *Wishner et al*., 2020) y, por otra parte, afectan los ciclos biogeoquímicos del carbono (C) y nitrógeno (N), entre otros (*Bopp et al*., 2002; *Codispoti et al*., 2001; *Paulmier et al*., 2008; *Arévalo-Martínez et al*., 2015; *Chan et al*., 2019), además, estas zonas son una importante fuente de NO_2, un eficiente gas de efecto invernadero (*Arévalo-Martínez et al*., 2015). En las ZMOs alrededor de un 35% del N total se pierde debido a altas tasas de desnitrificación siendo este un proceso bacteriano que convierte el nitrato (NO_3^- - considerado un nutriente inorgánico bio-limitante) en N molecular (N_2) y oxido nitroso (N_2O), los cuales posteriormente se pierden hacia la atmósfera generando un déficit de nitrógeno en el océano (*Gruber and Sarmiento*, 1997; *Tyrrell*, 1999; *Cornejo and Farias et al*., 2012; *Arévalo-Martínez et al*., 2015; *Oschiles et al*., 2019). Estos procesos bacterianos implican además altas tasas de remineralización dejando disponible alto contenido de dióxido de carbono (CO_2) en el agua y una disminución del pH (mayor acidificación) (*Paulmier et al.,* 2008, *Glober and Baumann*, 2016; *Chan et al*., 2019; *Melzner et al*., 2020).

La interacción entre estos mecanismos físicos y biogeoquímicos hace difícil la tarea de comprender, modelar y predecir los cambios espaciales y temporales de las ZMOs (e.g. *Karstensen et al*., 2008; *Oschlies et al*., 2018). Datos *in-situ* y modelos numéricos basados en escenarios de calentamiento global producto de las emisiones de gases efecto invernadero y la

contaminación por nutrientes y desechos orgánicos en zonas costeras, evidencian un aumento en la temperatura, mayor acidificación y pérdida de OD en el océano (desoxigenación oceánica - expansión de las ZMOs) (*Stramma et al*., 2010, 2012, *Shepherd et al*., 2017; *Schmidtko et al*., 2017; *Breitburg et al*., 2018; *Hameau et al*., 2020). En consecuencia, el aumento de la temperatura tendrá un efecto directo en la solubilidad del OD en el océano, mientras que, indirectamente generará una mayor estratificación de la columna de agua impidiendo la mezcla de aguas superficiales, ricas en OD, con aguas profundas deficientes en oxýgeno (*Keeling et al*., 2010; *Gewin*, 2010, *Stramma et al*., 2008, 2012; *Oschiles et al*., 2018).

El borde oriental del océano Pacifico Sur (PSO) presenta una ZMO muy intensa, incluyendo zonas oceánicas anóxicas, con ciclos biogeoquímicos complejos que se retroalimentan y regulan el contenido de OD (*Wyrtki*, 1962; *Chavez and Messié*, 2009; *Fennel and Testa*, 2019). La ZMO-PSO actualmente se considera una de las ZMOs más intensas y someras del océano, debido al efecto combinado de la circulación lenta inducida por el viento, masas de agua relativamente antiguas, alta productividad marina sostenida por la surgencia costera y altas tasas de respiración subsuperficial de materia orgánica (*Luyten et al*., 1983; *Strub et al*., 1998; *Toggweiler et al*., 1991; *Daneri et al*., 2000; *Paulmier et al*., 2006). *Fuenzalida et al*. (2009) utilizando un criterio de OD < 20 μM describieron la extensión horizontal y vertical de la ZMO-PSO en base a datos hidrográficos y climatológicos, caracterizando la ZMO con un área de 9.82 ± 3.60 x 10^6 km^2 y un volumen de 2.18 ± 0.66 x 10^6 km^3, definiendo el límite superior a menos de 50 m de profundidad y el límite inferior alrededor de 1000 m (500 m) de profundidad frente a Perú (Chile). Estos autores señalan que la extensión zonal de la ZMO-PSO disminuye hacia latitudes medias extendiéndose ~3000 km hacia el oeste cerca de los 15°S y ~25 km a los 30°S alcanzando poca extensión zonal frente a Concepción (~36.5°S). Indican además una estrecha relación entre la ZMO y la masa de Agua Ecuatorial Subsuperficial (AESS), caracterizada por alto contenido en nutrientes y CO_2, bajo pH y alta salinidad (>35), la cual es transportada hacia el sur por la Corriente Subsuperficial de Perú-Chile (CSPC) hasta los ~48°S (*Silva & Neshiba*, 1979; *Silva et al*., 2009; *Vergara et al*., 2016b).

Diversos estudios han analizado el rol de la ZMO-PSO en los ciclos biogeoquímicos del nitrógeno (N), carbono (C) y su impacto en los ecosistemas marinos. La implicancia del OD en

el ciclo del N se ha evaluado a través del análisis de los procesos de desnitrificación, reacciones anamox (*Anderson et al*., 1982; *Thamdrup et al*., 2006, *Galan et al*., 2009; *Rich et al*., 2020) y pérdida de N hacia la atmósfera debido a la producción de N_2O por la nitrificación realizada por archeas y bacterias (*Codispoti et al*., 2001; *Gruber and Galloway*, 2008; *Cornejo and Farías*, 2012; *Arevalo-Martinez et al*., 2015; *Callbeck et al*., 2017). En términos del ciclo del C, la remineralización de materia orgánica al interior de la ZMO-PSO se ha relacionado con un alto contenido de CO_2 y aguas de bajo pH (pH ~7.5) (*Paulmier et al*., 2011; *Torres et al*., 2011; *Melzner et al*., 2013; 2020), asociando además los procesos metabólicos y la diversidad genética microbiana de la ZMO-PSO (*Stewart et al*., 2012; *Bertagnolli et al*., 2018; *Ruiz-Fernandez et al*., 2020; *Cantarero et al*., 2020). Siguiendo esta línea, *Paulmier et al*. (2006) propusieron un modelo conceptual para el mantenimiento de la ZMO sugiriendo un alto consumo de OD proveniente de procesos biogeoquímicos tales como la respiración. En tanto que, otros estudios se han enfocado en el análisis ecosistémico de comunidades zooplanctónicas y peces, demostrando una relación directa entre la profundidad de la ZMO-PSO y el rango de las migraciones verticales de ciertas especies (*Escribano et al*., 2009; *Hidalgo et al*., 2012; *Stramma et al*., 2012a; *Wishner et al*., 2018; *Tutasi and Escribano*, 2020).

Aunque existen diversos procesos físicos que son relevantes para la biogeoquímica de la OMZ y su variabilidad, en general frente a las costas de Chile, estos son muy poco conocidos. *Morales et al*. (1999) analizaron los cambios interanuales en el límite superior de la ZMO (oxiclina DO < 1 ml L^{-1}) entre los 18°S y 24°S, mostrando en promedio un aumento en la profundidad de la oxiclina hacia el sur en la banda costera (de 34 m en Arica a 62 m en Antofagasta), indicando una profundización de la oxiclina y la termoclina hasta ~100 m de profundidad durante eventos cálidos (El Niño). Posteriormente, *Hormazabal et al*. (2006) utilizando una década de registros continuos de corrientes cerca del núcleo de la CSPC (33°S) estudiaron la relación entre la variabilidad de la CSPC y la ZMO, mostrando que las variaciones estacionales de la CSPC están fuertemente moduladas por el ciclo El Niño Oscilación del Sur (ENOS). En este sentido, durante los eventos cálidos (El Niño) la variabilidad semianual de la CSPC se intensifica, mientras que durante los eventos fríos (La Niña) la señal anual es dominante, sugiriendo que las ondas Rossby serían un mecanismo físico relevante para explicar

una fracción significativa de la variabilidad estacional de la ZMO en la zona central de Chile. Otros estudios han mostrado que remolinos de mesoescala se desplazan hacia el oeste (~900 km) a una velocidad media de 2 km d^{-1}, transportando un volumen de 1 Sv y se desprenden de la CSPC en condiciones de surgencia (*Hormazabal et al*., 2013). Registros *in situ* de las tasas de utilización aparente de oxígeno al interior de los remolinos oscilan entre 0,29 y 44 nmol L^{-1} d^{-1} y la tasa de consumo de N_2O fue de 3,92 nmol L^{-1} d^{-1} (*Cornejo et al*., 2016). Estos resultados muestran que los remolinos de mesoescala afectan a la biogeoquímica no sólo por el transporte de las propiedades físicas y químicas desde la costa al interior del océano, sino que también durante la advección, el consumo biológico local de oxígeno generando además condiciones favorables para la desnitrificación y la pérdida de fijación de nitrógeno del sistema (*Cornejo et al*., 2016; *Pizarro et al*., 2016)

1.3 Circulación y masas de agua en el Pacífico Sur-Oriental

La circulación y composición de las masas de agua son relevantes para comprender la variabilidad de la ZMO frente a Chile. En el PSO, la circulación oceánica está dominada por el Anticiclón Subtropical del Pacifico Sur, el cual genera un patrón de vientos hacia el ecuador a lo largo de la costa de Chile y un rotor predominantemente negativo (positivo) cerca (lejos) de la costa (*Bakun & Nelson*, 1991; *Aguirre et al*., 2012; *Schneider et al*., 2017). En la región oceánica, el rotor positivo del esfuerzo del viento genera un flujo oceánico hacia el norte, mientras que, en la zona de transición costera el rotor negativo del esfuerzo del viento genera un flujo oceánico hacia el sur (Contracorriente de Perú-Chile) que interactúa con la Corriente Subsuperficial de Perú-Chile (*Aguirre et al*., 2012). El patrón de vientos con dirección hacia el ecuador genera además la surgencia de la AESS en la zona costera, y una corriente superficial somera que sigue la dirección del viento sobre la plataforma continental. Sin embargo, la variabilidad temporal de esta surgencia costera frente a Chile presenta dos distintos regímenes: el primero ubicado entre las latitudes 20°S - 33°S caracterizado por una surgencia semi-permanente, sin cambios estacionales marcados; y el segundo, caracterizado por una surgencia fuertemente estacional entre los 35ºS - 38°S con vientos favorables al ascenso de aguas

subsuperficiales durante primavera-verano, y desfavorables durante otoño-invierno (*Blanco et al*., 2001, *Rutllant & Montecino*, 2002). No obstante, esta circulación regional está también relacionada con forzamientos remotos (ecuatoriales) tales como el ciclo ENOS y la propagación de ondas atrapadas a la costa de origen ecuatorial (*Strub et al*., 1998; *Pizarro et al*., 2001; *Hormazabal et al*., 2006; *Illig et al.,* 2018a, b).

Específicamente, el sistema de corrientes de Humboldt (SCH) en la zona norte y centro de Chile es altamente variable, presentando alternancia de corrientes hacia el ecuador con corrientes hacia los polos. Las corrientes presentes en esta zona destacan por su alta coherencia meridional de miles de kilómetros, sin embargo, ocupan únicamente unas decenas de kilómetros en dirección perpendicular a la costa y unos pocos cientos de metros en profundidad (*Strub et al*., 1998, *Aguirre et al*., 2012). La Corriente de Perú-Chile se alimenta de la Corriente del Pacífico Sur (*Strub et al*., 2013) y en el extremo norte torna hacia el oeste formando la Corriente Ecuatorial del Sur (*Kessler,* 2006). En superficie, sobre la plataforma continental se encuentra la Corriente Costera de Chile que fluye hacia el ecuador, mientras que al oeste de esta corriente se observa la Contra-corriente de Perú-Chile fluyendo en dirección al sur. En conjunto con esta configuración, a nivel subsuperficial cerca del talud continental se encuentra la CSPC con dirección hacia el sur (*Shaffer et al*., 1999; *Pizarro et al*., 2002; *Hormazabal et al*., 2006; *Silva et al*., 2009).

Respecto a la composición de las masas de agua en la región, se han podido identificar cinco masas de agua frente a Chile, tres de ellas situadas en los primeros 500 m de profundidad (*Silva et al*., 2009). En la parte norte de Chile, se encuentra el Agua Subtropical (AST) localizada sobre la termoclina (< 100 m) y caracterizada por una temperatura promedio >18.5°C y salinidad >34.9. En contraste, al sur se encuentra el Agua Subantartica (ASA) con menor temperatura (11.5°C) y muy baja salinidad (33.8) producto de la mayor pluviosidad y descarga de ríos desde la zona continental. Por debajo de estas masas de agua (AST y ASA), se encuentra el Agua Ecuatorial Subsuperficial (AESS) caracterizada por un máximo salino relativo (34.7-34.9) y una temperatura promedio de 12.5°C localizada entre los 200 y ~400 m de profundidad, además de estar directamente relacionada con la ZMO-PSO debido a su bajo contenido de OD. Por debajo de la AESS, abarcando toda la cuenca del PSO se encuentra el Agua Intermedia Antártica (AIA)

localizada entre los ~500 y 1000 m de profundidad, con una salinidad y temperatura promedio de 34 y 3°C, respectivamente. Finalmente, bajo los 1000 m de profundidad se encuentra el Agua Profunda del Pacifico (APP) con temperaturas de 1.75°C y salinidades de 34.68. Otros autores han identificado otras masas de agua acotadas a ciertas latitudes, tales como el Agua Intermedia del Pacifico Sur-Este (AIPSE, *Schneider et al*., 2003) y el Agua Subantártica de Verano (ASAV, *Llanillo et al*., 2012). Asociada a esta configuración oceanográfica y composición de masas de agua, un especial énfasis se ha hecho al rol principal que cumple la CSPC al transportar la AESS hacia el sur, siendo el principal mecanismo físico que afecta la variabilidad de esta masa de agua y el OD subsuperficial frente a Chile (*Silva and Neshyba*, 1979; *Silva et al*., 2009).

1.4 La Corriente Subsuperficial de Perú-Chile (CSPC)

La Corriente Subsuperfical de Perú-Chile se forma debido al gradiente de presión a lo largo de la costa inducido por los vientos favorables a la surgencia (*McCreary*, 1981) y al rotor negativo del viento (*Bakun & Nelson*, 1991). Su origen se ubica cerca de los 4°S frente a Perú (*Penven et al*., 2005; *Montes et al*., 2010; *Chaigneau et al*., 2013) extendiéndose hasta los 48°S (*Gunther*, 1936; *Silva y Neshyba*, 1979; *Silva et al*., 2009). Estudios con modelos numéricos indican que la CSPC es alimentada en parte por la Corriente Ecuatorial Subsuperficial (*Tsuchiya*, 1975; *Montes et al*., 2011) y su ancho es proporcional al radio de deformación baroclínico (*McCreary*, 1987).

Estimaciones directas de la CSPC frente a Perú, basadas en anclajes y estaciones hidrográficas, han mostrado que la CSPC transporta alrededor de 1 Sv ($1x10^6$ m^3 s^{-1}) a los 10°S (*Huyer et al*., 1991). Posteriormente, observaciones directas con un perfilador acústico de corrientes (Acoustic Doppler Current Profiler, -ADCP, siglas en ingles-) realizadas por el Instituto del Mar del Perú (IMARPE) mostraron un mayor transporte hacia el sur relacionado con la CSPC entre los 4°S y 18°S frente a Perú para el periodo comprendido entre los años 2008 y 2012 (*Chaigneau et al*., 2013). Según estas estimaciones, el transporte medio de la CSPC aumenta de ~1.8 Sv en los 5°S a un máximo de 5.2 Sv a los 15°S, sin embargo, al sur de esta última latitud el transporte se reduce ligeramente mostrando un valor medio de ~1,0 Sv a los

30°S a partir de observaciones de anclajes (*Shaffer et al*., 1999; *Chaigneau et al*., 2013). En forma conjunta, estos estudios establecen que la variabilidad estacional de la CSPC en estas latitudes es bastante menor en comparación con las grandes fluctuaciones observadas en los periodos intra-estacionales e interanuales.

En contraste con lo observado frente a la costa de Perú y norte de Chile, la variabilidad estacional de la CSPC frente a la zona central de Chile (~30°S-40°S) se muestra relativamente más importante debido a una mayor amplitud en el ciclo anual del estrés del viento y del rotor del viento (*Bakun y Nelson*, 1991; *Shaffer et al*, 1999; *Aguirre et al*., 2012), asociado a la migración estacional del jet atmosférico de bajo nivel (*Muñoz y Garreaud*, 2005; *Renault et al*., 2009). A escala interanual, la variabilidad de la CSPC está condicionada por la disipación de perturbaciones de origen ecuatorial asociada a forzamientos de origen remoto (*Pizarro et al*., 2001, 2002; *Hormazabal et al*., 2006).

1.5 Modelación Físico-Biogeoquímica de la ZMO-PSO

La representación y simulación de la dinámica temporal de la ZMO asociada al transporte de la CSPC es un tema complejo de abordar con modelos globales de resolución baja o media, debido a las limitaciones para simular de manera realista la dinámica de la surgencia costera y el flujo subsuperficial, el cual es sensible a la forma del talud continental y a la propagación de ondas atrapadas a la costa no resueltas adecuadamente por modelos de baja resolución. Debido a esto, son las simulaciones de alta resolución las que han demostrado ser más útiles para representar varios de los aspectos de la dinámica y circulación oceánica frente a Perú y Chile (*Leth y Shaffer*, 2001; *Montes et al*., 2010; *Aguirre et al*., 2012, 2014; *Combes et al*., 2015; *Vergara et al*., 2016c, entre otros). El realismo de los modelos oceánicos regionales ha permitido abordar cuantitativamente aspectos de la interacción físico-biogeoquímica de la ZMO, tal como lo demuestran estudios recientes en Perú (*Montes et al*., 2014; *Bettencourt et al*., 2015; *Vergara, et al*., 2016a). Si bien las parametrizaciones biogeoquímicas no necesariamente se ajustan con las tasas biogeoquímicas observadas en los sistemas de borde oriental, estos últimos estudios han logrado una representación realista tanto de la variabilidad

espacial y temporal (a escala anual) de la ZMO como de la CSPC, permitiendo incluso abordar el efecto de la circulación inducida por remolinos oceánicos de mesoescala sobre la variabilidad de la ZMO.

A escala interanual, *Mogollon and Calil* (2017) haciendo uso del modelo biogeoquímico BioEBUS observaron cambios en el límite superior de la ZMO asociados con la profundización y desplazamiento costa afuera de la ZMO frente a la costa de Perú durante la fase cálida (El Niño) del ENOS, permitiendo una mayor ventilación de los primeros 100 m en la columna de agua. Los resultados indicaron una mayor actividad de mesoescala durante los años con eventos cálidos impactando positivamente la ventilación de la ZMO a través de flujos de remolinos. Adicional a esto, *Espinoza-Morriberón et al*. (2019) muestran una estrecha correlación entre el límite superior de la ZMO y la profundidad de la termoclina, destacando el papel de los procesos físicos en la variabilidad de la ZMO frente a Perú. A nivel regional, un análisis exhaustivo de la influencia del ENOS en la dinámica de ZMO en el Pacífico Sur Tropical Oriental durante el periodo 1990-2010 muestra una reducción (expansión) de la extensión vertical de ZMO durante la fase cálida (fría) del ENOS debido a cambios en el suministro de OD a profundidades medias, principalmente desde los márgenes laterales (*José et al*., 2019).

Dado este contexto, el presente trabajo de tesis tiene como motivación hacer uso de los recientes avances en la modelación acoplada físico-biogeoquímica (*Montes et al*., 2014; *Bettencourt et al*., 2015; *Vergara et al*., 2016a) para evaluar: i) la relación entre el transporte de la CSPC y la variabilidad estacional e interanual del extremo sur (30°S-38°S) de la ZMO-PSO, indagando hasta qué punto el transporte de la CSPC controla la variabilidad espacio-temporal de la ZMO teniendo en cuenta otros procesos físicos que suceden simultáneamente tales como la actividad de mesoescala; y ii) analizar los principales mecanismos que modulan el presupuesto estacional e interanual del OD al interior de la ZMO, cuantificando la contribución relativa por parte de los procesos físicos versus los procesos biogeoquímicos en el control del presupuesto de OD en la columna de agua frente a Chile central.

2. HIPÓTESIS Y OBJETIVOS

Hipótesis I: La variabilidad estacional e interanual del transporte de la Corriente Subsuperficial de Perú-Chile, regula gran parte (>50%) de los cambios de oxígeno disuelto en la columna de agua frente a Chile central (30º-38°S).

Hipótesis II: La variabilidad estacional e interanual de la mezcla entre las masas de agua SubAntártica, Ecuatorial Subsuperficial e Intermedia Antártica contribuye significativamente (>50%) a los cambios estacionales e interanuales de oxígeno disuelto frente a Chile central (30º-38°S).

Objetivo General: De acuerdo a las hipótesis planteadas anteriormente, el objetivo general de este estudio es analizar las contribuciones de la advección (horizontal y vertical), la mezcla y los procesos biogeoquímicos en la variabilidad estacional e interanual del oxígeno disuelto en la columna de agua, frente a la costa central de Chile (30ºS-38ºS).

Objetivos específicos:

1) Caracterizar la variabilidad estacional e interanual del transporte de la Corriente Subsuperficial de Perú- Chile y su relación con los cambios en las concentraciones de oxígeno disuelto.

2) Determinar la contribución relativa entre la advección y los procesos biogeoquímicos en la variabilidad estacional de la zona mínima de oxígeno frente al talud y plataforma continental de Concepción ~36.5°S.

3) Evaluar el rol de la ventilación del Agua Ecuatorial Subsuperficial mediante la mezcla con el Agua Intermedia Antártica y Agua Subantártica en la variación estacional e interanual del oxígeno disuelto frente a Chile central (30-38°S).

3. MATERIALES Y MÉTODOS

Los modelos numéricos del océano son herramientas muy usadas en la actualidad para estudiar las escalas espacio-temporales que caracterizan la dinámica de diferentes procesos que ocurren en el océano. Las ecuaciones de movimiento que gobiernan la parte hidrodinámica y las ecuaciones de advección-difusión para los diferentes componentes –acopladas a un conjunto de fuentes y sumideros que representan las relaciones que gobiernan los procesos biogeoquímicos– son usadas para resolver el comportamiento del océano. Estas ecuaciones son obtenidas mediante una serie de aproximaciones dinámicas complejas, parámetros físicos y biogeoquímicos, y supuestos numéricos. Todas estas aproximaciones permiten representar directa e indirectamente diversos fenómenos, parametrizando aquellos cuyas escalas de variabilidad no pueden ser resueltas directamente, por ejemplo, la turbulencia de pequeña escala (*Griffies et al*., 2000).

El acoplamiento de los modelos físico y biogeoquímico utilizado en este estudio toma en cuenta los principales procesos de interés que ocurren en los bordes orientales de los océanos, tales como la surgencia costera, las corrientes superficiales y subsuperficiales (como las corrientes hacia el polo que se observan en los bordes orientales de los océanos) y las ZMOs. A continuación, se presenta una pequeña descripción de los modelos hidrodinámico y biogeoquímico usados en este trabajo, para finalizar con una descripción de la simulación físico-biogeoquímica.

3.1. Modelo hidrodinámico (ROMS)

ROMS (Regional Ocean Model System) es un modelo hidrodinámico tridimensional de circulación regional del océano (*Shchepetkin and McWilliams*, 2005), de superficie libre que utiliza diferentes sistemas de coordenadas que siguen la línea de costa y la topografía del fondo, lo cual permite mejorar la resolución espacial del área de interés. Este modelo resuelve las ecuaciones primitivas mediante la aproximación hidrostática y la aproximación de Boussinesq.

Dadas estas aproximaciones, las ecuaciones primitivas, describen la conservación de la cantidad de movimiento horizontal, el equilibrio hidrostático, la conservación de masa, la evolución de la temperatura y la salinidad. En este estudio se usó la versión AGRIF (Adaptive Grid Refinement in Fortran; *Penven et al*., 2005) de ROMS, cuya evolución actual es conocida como CROCO (www.croco-ocean.org; *Debreu et al*., 2012).

Las variables calculadas por ROMS son la elevación de la superficie del mar, las componentes de la velocidad barotrópica y baroclínica, la perturbación de la presión, la temperatura (basada en la ecuación de estado de la UNESCO para los cálculos de la temperatura potencial) y la salinidad (*Marchesiello et al*. 2001). Aspectos generales de la configuración del modelo hidrodinámico se detallan a continuación, otros aspectos más específicos del modelo pueden ser obtenidos en el capítulo 1 de la presente tesis y en *Dewitte et al*. (2012).

***Dominio*:** el dominio completo de la simulación se extiende latitudinalmente desde la zona tropical del Pacífico Norte (12°N), con el fin de captar la conexión de la variabilidad ecuatorial a través de la dinámica de ondas ecuatoriales y ondas atrapadas a la costa y el transporte hacia el sur de la CSPC, hasta los 40ºS. Mientras que longitudinalmente se extiende desde la costa hasta los 95ºW. La topografía del modelo se basó en la base de datos GEBCO suavizada e interpolada según *Penven et al*. (2005).

***Periodo*:** la simulación hidrodinámica comprende el periodo 1958 - 2008. Sin embargo, para el acoplamiento físico-biogeoquímico (usado en esta tesis) solo se utilizaron los últimos 8 años (2000-2008) de la simulación, correspondiente al periodo de observaciones de vientos satelitales de la misión QuikSCAT (https://winds.jpl.nasa.gov/missions/quikscat/).

***Resolución*:** la resolución horizontal es de 1/12º (~8 km) y 37 niveles verticales "*sigma"*. 23 niveles sigma se distribuyen entre la superficie y 500 m de profundidad, permitiendo una mejor representación de la ZMO.

***Forzamiento superficial*:** se utilizó un producto estadístico desarrollado por *Goubanova et al.,* (2011), que refina la resolución espacial de los datos de stress y velocidad del viento provenientes de los datos NCEP-NCAR (National Centers for Environmental Prediction) de 2.5º x 2.5º a 0.5º x 0.5º. Además, este método corrige el sesgo del reanálisis NCEP cerca de la costa de Perú y Chile (*Goubanova et al.,* 2011). El modelo estadístico utiliza los datos del viento

obtenidos de QuikSCAT para el mismo periodo del modelo 2000-2008. El producto atmosférico a su vez es usado en "modo bucle" en conjunto con flujos de calor y agua dulce obtenidos de la climatología COADS (*daSilva et al*., 1994).

***Condiciones de Borde e iniciales*.** Para estas condiciones se utilizaron campos de temperatura, salinidad, nivel del mar y velocidades horizontales fueron obtenidos del reanálisis SODA 1.4.2 (*Smith et al.,* 1992). SODA posee una resolución horizontal de 0.25º (latitud) x 0.4º (longitud) y 40 niveles verticales distribuidos entre los 5 m y 5474 m.

3.2. Modelo Biogeoquímico (BioEBUS)

BioEBUS (Biogeochemical Eastern Boundary Upwelling System) es un modelo biogeoquímico basado en el ciclo del N, proveniente del modelo $N_2P_2Z_2D_2$ (*Koné et al*., 2005). $N_2P_2Z_2D_2$ toma en cuenta las principales comunidades planctónicas de los bordes orientales de los océanos. BioEBUS consta de 12 compartimientos (Figura 1): el compartimento correspondiente al fitoplancton es separado en organismos pequeños (flagelados) y grandes (diatomeas), del mismo modo el zooplancton es dividido en ciliados y copépodos respectivamente. Por su parte, el detritus está dividido por tamaños (partículas pequeñas y grandes). El nitrógeno orgánico disuelto (NOD) está compuesto de solo un compartimiento. Los términos fuentes del NOD en el modelo son la exudación del fitoplancton, la excreción orgánica del zooplancton y la hidrólisis del detritus. Mientras que el único término sumidero en este compartimiento es la amonificación del NOD, el cual fue implementado siguiendo la metodología de (*Dadou et al*., 2001, 2004; *Gutknecht et al*., 2013a, b). El compartimiento de N inorgánico disuelto (NID) es representado por nitrato (NO_3^-) y amonio (NH_4). El modelo también incluye una ecuación para el nitrito (NO_2^-) para tener una mejor descripción del anillo microbiano. Los procesos de amonificacion/nitrificación bajo condiciones óxicas y procesos de desvitrificación/anamox bajo condiciones subóxicas fueron implementados según *Yakushev et al*. (2007). Estos procesos son oxígeno-dependientes, por lo cual están incorporados en la ecuación para el OD del modelo. Finalmente, el óxido nitroso (N_2O) fue introducido usando la

parametrización de *Suntharalingam et al*. (2000, 2012), la cual permite determinar la concentración del N_2O bajo condiciones oxícas y suboxícas.

Condiciones de borde e iniciales: La biomasa fitoplanctónica en la superficie fue derivada de información satelital, específicamente de datos satelitales climatológicos obtenidos de SeaWiFs. Mientras que verticalmente fueron extrapolados usando la metodología de *Morel and Berthon* (1989). Las condiciones iniciales y laterales de los trazadores biogeoquímicos NO_2^-, NH_4^+ and DOM fueron obtenidos de la climatología CARS2006 (www.marine.csiro.au/~dunn/ cars2006/) y establecidos en el modelo usando un perfil vertical constante según *Koné et al.* (2005). En general, los parámetros biogeoquímicos usados en este estudio fueron similares a los utilizados por *Montes et al.* (2014) and *Vergara et al.* (2016a) para Perú y el norte de Chile. Para mayor información de los parámetros biogeoquímicos utilizados en este estudio ver apéndice A en el trabajo de *Montes et al.* (2014).

3.3. Acoplamiento Físico-Biogeoquímico (ROMS-BioEBUS)

El acoplamiento entre ROMS y BioEBUS se realizó en "modo on-line" siguiendo la metodología utilizada por *Montes et al.* (2014) y *Vergara et al.* (2016a). De aquí en adelante nos referiremos a este acoplamiento físico-biogeoquímico como ROMS/BioEBUS. Nótese que la simulación ROMS/BioEBUS abarcó todo el dominio hidrodinámico, sin embargo, la región analizada en este estudio se restringió al límite sur de la ZMO-PSO (ver dominio en sección 3.1). La región norte fue analizada previamente en *Montes et al*., (2014) y *Vergara et al.* (2016a). La evolución de cualquier trazador en ROMS/BioEBUS es determinada por la ecuación de advección/difusión, por ejemplo, para el caso del OD:

$$\frac{\partial OD}{\partial t} = -\nabla \cdot (uOD) + K_h \nabla^2 OD + \frac{\partial}{\partial z}\left(K_z \partial \frac{OD}{\partial z}\right) + SMS \qquad (1)$$

donde el primer término de la mano derecha en (1) es la advección de OD y u es la velocidad del fluido, el segundo término es la difusión horizontal, con K_h el coeficiente difusión turbulenta (100 m^2s^{-1}), y el tercer término es la mezcla vertical, con un coeficiente de difusión turbulenta

$K_z$calculado mediante la parametrización del esquema de mezcla (perfil-K; *Large et al.,* 1994). El último término (SMS) representa las fuentes menos los sumideros de OD y corresponde al consumo y producción de OD asociado a la actividad biológica. Los procesos físicos consideran la sumatoria de los términos advectivos (horizontal y vertical) y la mezcla (difusión horizontal y mezcla vertical). La advección por su parte, también puede ser separada a través de sus contribuciones relacionadas con los diferentes componentes de la velocidad: la advección zonal ($Xadv = -u\partial(\mathrm{OD})/\partial x$), meridional ($Yadv = -v\partial(\mathrm{OD}/\partial y)$ y vertical ($Zadv = -w\partial(\mathrm{OD})/\partial z$) (*Gutknecht et al.,* 2013a). Dado que la velocidad **u** y los trazadores (DO en el ejemplo) son variables en nuestro modelo, cuando se calculan promedios de (1) los términos advectivos incluyen correlaciones entre las variables que contribuyen a los flujos y, eventualmente, a su divergencia y por ende a la variación local del trazador. Estos términos son nombrados aquí como componentes no linealeales de la advección. La estimación de estos términos no-lineales asociados con el transporte de OD fue realizada en "modo offline", mediante una descomposición de Reynolds, ($\langle \mathbf{u}' DO' \rangle$), donde las primas, ( )', representan fluctuaciones respecto a un promedio temporal ($\langle\rangle$), usando diferentes escalas de tiempo para el promedio, la cual depende del proceso a estudiar, por ejemplo, el promedio puede ser de 90 días o intraestacional (en este caso usando anomalías respecto al ciclo anual climatológico), si se quieren evaluar los transportes "turbulentos" asociados a las fluctuaciones de remolinos de mesoescala.

Para calcular el transporte de la CSPC, se usaron secciones perpendiculares a la costa de 200 km de longitud y entre 0 y 800 m de profundidad de la velocidad meridional (norte-sur). El cálculo se realizó para cada latitud entre 30ºS-38ºS. Se utilizó como criterio para definir la CSPC una velocidad ≤ -0.02 m s^{-1}. Luego se construyó una grilla regular (con Δx y Δz constante), así, en cada latitud y tiempo se calculó el transporte de volumen como el área promedio con valores de $v \leq$ -0.02 m s^{-1} por la velocidad promedio. El transporte de la CSPC es expresado en Sverdrups (Sv), donde 1 Sv corresponde a $1x10^6$ m^3 s^{-1}.

Tanto para el capitulo 1 y 2, la ZMO modelada se ha definido como la región de la columna de agua que presenta niveles de OD ≤ 45 μM, debido a que este valor umbral de OD se encuentra en el rango de valores que caracterizan a la hipoxia (*Naqvi et al.,* 2010). Además,

es un valor adecuado para nuestro trabajo ya que aguas con OD ~45 µM en la simulación ROMS/BioEBUS están presentes la mayor parte del tiempo dentro de nuestro dominio de interés.

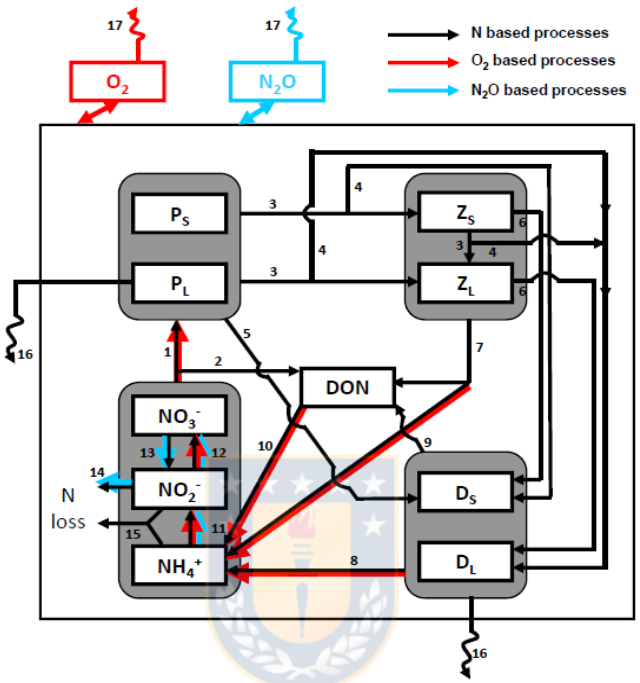

1)	Asimilación de nutrientes	6)	Mortalidad del zooplancton	11,12)	Mortalidad del zooplancton
2)	Exudación	7)	Excreción	13,14)	Excreción
3)	Pastoreo	8)	Descomposicion de detritus	15)	Anamox
4)	Pelets fecales	9)	Hidrolísis	16)	Hundimiento vertical
5)	Mortalidad del fitoplancton	10)	Descomposicion del NOD	17)	Flujo oceano/atmosféra

Figura 1. Representación esquemática de las interacciones entre los diferentes compartimentos del modelo BioEBUS. Las flechas negras representan procesos nitrógeno-dependientes; las flechas rojas procesos oxígeno-dependientes; las flechas azules representan los procesos ligados con la producción de N_2O. Para simplificar la representación de todas las interacciones entre variables, las flechas desde o hacia un rectángulo gris actúan en todas las variables incluidas en este rectángulo. Por ejemplo, la flecha entre nutrientes y fitoplancton (asimilación) es una simplificación de 6 interacciones: NO_3^- a P_S, NO_3^- a P_L, NO_2^- a P_S, NO_2^- a P_L, NH_4^+ a P_S, NH_4^+ a P_L (tomado de *Gutknecht et al*., 2013).

4. RESULTADOS

Artículo publicado en *Journal of Geophysical Research: Oceans* (https://doi.org/10.1029/2019JC015201).

4.1. Capítulo 1: Variabilidad estacional del extremo sur de la Zona de Mínimo Oxígeno en el Pacifico Sur Oriental (30º38ºS): Un estudio de modelación

Matias Pizarro-Koch, Oscar Pizarro, Boris Dewitte, Ivonne Montes, Marcel Ramos, Aurélien Paulmier y Véronique Garçon.

Resumen

Este estudio investiga la variabilidad estacional del extremo sur (30°-38°S) de la Zona de Mínimo de Oxígeno (ZMO) del Pacífico Sur Oriental usando una simulación físico-biogeoquímica del océano con resolución horizontal de 1/12°. La simulación fue validada mediante el uso de observaciones *in situ* disponibles y climatologías globales digitales. La ZMO en el modelo es delimitada por el contorno de 45 μM, presentando un volumen máximo ($4.5x10^4$ km^3) durante el inicio del invierno austral y un volumen mínimo (3.5x104 km^3) al final de la primavera, sólo 1 a 2 meses después que el transporte hacia el sur de la Corriente Subsuperficial de Perú-Chile (CSPC) alcanzará su valor máximo y mínimo, respectivamente. Esto implica que la CSPC impacta significativamente la advección de oxígeno disuelto (OD) a lo largo de la costa central de Chile, modulando la variabilidad estacional de la ZMO. Adicionalmente, se observa un transporte zonal de OD asociado a flujos oceánicos (jets) zonales y al efecto de remolinos de mesoescala. Ambos procesos cumplen un rol importante en la variabilidad estacional y espacial de la ZMO. En conjunto con esto, el análisis del presupuesto de OD revela una contribución significativa de los términos advectivos en la tasa de cambio local (tendencia) del OD y la prominencia de la variabilidad espacial de mesoescala dentro del ciclo estacional de estos términos advectivos. Por otra parte, los procesos físicos de mezcla horizontal y vertical (asociados a los procesos de sub-grilla), así como también los procesos biogeoquímicos, cumplen un papel secundario en el ciclo estacional de la ZMO.

JGR Oceans

RESEARCH ARTICLE
10.1029/2019JC015201

Seasonal Variability of the Southern Tip of the Oxygen Minimum Zone in the Eastern South Pacific (30°-38°S): A Modeling Study

Matias Pizarro-Koch[1,2,3], Oscar Pizarro[2,3,4], Boris Dewitte[5,6,7,8], Ivonne Montes[9], Marcel Ramos[6,7,10], Aurélien Paulmier[8], and Véronique Garçon[8]

[1]Programa de Postgrado en Oceanografía, Departamento de Oceanografía, Facultad de Ciencias Naturales y Oceanográficas, Universidad de Concepción, Concepción, Chile, [2]Millennium Institute of Oceanography, Chile, [3]Centro de Investigación Oceanográfica COPAS Sur-Austral, Universidad de Concepción, Chile, [4]Department of Geophysics, University of Concepcion, Concepción, Chile, [5]Centro de Estudios Avanzados en Zonas Aridas (CEAZA), Coquimbo, Chile, [6]Departamento de Biología Marina, Facultad de Ciencias del Mar, Universidad Católica del Norte, Coquimbo, Chile, [7]Núcleo Milenio de Ecología y Manejo Sustentable de Islas Oceánicas (ESMOI), Universidad Católica del Norte, Coquimbo, Chile, [8]LEGOS-CNRS/IRD/UPS/CNES, Toulouse, France, [9]Instituto Geofísico del Perú, Lima, Perú, [10]Centro de Innovación Acuícola Aquapacífico

Key Points:
- The Oxygen Minimum Zone (OMZ) off Chile is modulated seasonally by the Peru-Chile Undercurrent and by meridionally alternating zonal jets
- Mesoscale eddy fluxes of dissolved oxygen (DO), ventilate the OMZ and play a significant, but secondary, role in its seasonal budget
- The advective term is the main driver of the seasonal budget of DO in the OMZ, biogeochemical and mixing processes play a secondary role

Correspondence to:
M. Pizarro-Koch,
matiaspizarro@udec.cl

Citation:
Pizarro-Koch, M., Pizarro, O., Dewitte, B., Montes, I., Ramos, M., Paulmier, A., & Garçon, V. (2019). Seasonal variability of the southern tip of the Oxygen Minimum Zone in the eastern South Pacific (30°-38°S): A modeling study. *Journal of Geophysical Research: Oceans, 124,* 8574–8604. https://doi.org/10.1029/2019JC015201

Received 15 APR 2019
Accepted 2 OCT 2019
Accepted article online 17 OCT 2019
Published online 5 DEC 2019

Abstract We investigate the seasonal variability of the southern tip (30°–38°S) of the eastern South Pacific oxygen minimum zone (OMZ) based on a high horizontal resolution (1/12°) regional coupled physical-biogeochemical model simulation. The simulation is validated by available *in situ* observations and the OMZ seasonal variability is documented. The model OMZ, bounded by the contour of 45 μM, occupies a large volume ($4.5x10^4$ km^3) during the beginning of austral winter and a minimum ($3.5x10^4$ km^3) at the end of spring, just 1 and 2 months after the southward transport of the Peru-Chile Undercurrent (PCUC) is maximum and minimum, respectively. We showed that the PCUC significantly impacts the alongshore advection of dissolved oxygen (DO) modulating the OMZ seasonal variability. However, zonal transport of DO by meridionally alternating zonal jets and mesoscale eddy fluxes play also a major role in the seasonal and spatial variability of the OMZ. Consistently, a DO budget analysis reveals a significant contribution of advection terms to the rate of change of DO and the prominence of mesoscale variability within the seasonal cycle of these terms. Biogeochemical processes and horizontal and vertical mixing, associated with subgrid scale processes, play only a secondary role in the OMZ seasonal cycle. Overall, our study illustrates the interplay of mean and (mesoscale) eddy-induced transports of DO in shaping the OMZ and its seasonal cycle off Central Chile.

Plain Language Summary Dissolved oxygen in the ocean strongly impacts most marine ecosystems. Its distribution depends mainly on physical and biogeochemical processes. In the eastern South Pacific, water with very low oxygen is present at intermediate depths (100-800 m). This oxygen minimum zone (OMZ) is associated with a regional water mass called Equatorial Subsurface Water which is transported southward along the coast by the Peru-Chile Undercurrent. Here, using a physical/biogeochemical model we investigate the main mechanisms controlling the seasonal variability of the OMZ off central Chile. We found that the total volume of the low-oxygen waters is reduced by 25% during spring. This seasonal change is closely related to changes in the water mass composition and is mainly driven by changes in the undercurrent transport, but zonal currents and eddy fluxes, largely related to mesoscale variability, play also a major role in the seasonal and spatial variability of the OMZ, while biogeochemical and mixing processes play only a secondary role.

1. Introduction

Despite the large primary productivity that takes place along the coast off central Chile during the upwelling season, surface waters are commonly undersaturated with oxygen (e.g. Letelier et al., 2009). Near the coast subsurface waters with very low dissolved oxygen (DO) are transported to the surface by the upwelling circulation cells. In fact, the presence of an intense and relatively shallow oxygen minimum zone (OMZ) is one of the most striking oceanographic features along most of the eastern boundary of the Eastern South Pacific (ESP). A relative high rate of microbial decomposition of organic matter and weak subsurface circulation

combine to generate these oxygen-poor environments (e.g. Helly & Levin, 2004; Karstensen et al., 2008; Wyrtki, 1962). The OMZ of the ESP is quite intense, there, regions of the open ocean may frequently reach values of DO lower than 20 μM, in the suboxia range (Fuenzalida et al., 2009; Naqvi et al., 2010; Paulmier et al., 2006; Paulmier & Ruiz-Pino, 2009), or even anoxic zones may also be found (e.g. Schunck et al., 2013; Ulloa et al., 2012). Such a low DO concentration largely impacts marine communities and biogeochemical cycling (Helly & Levin, 2004; Niemeyer et al., 2017; Stramma et al., 2011).

During the last two decades several studies have focused on the physical variability, the biogeochemical processes and bacteria communities present in this OMZ of the ESP (e.g. Frenger et al., 2018; Levin et al., 2002; Montes et al., 2014; Morales et al., 1999; Paulmier et al., 2006; Stramma et al., 2010; Ulloa et al., 2012; Ulloa & Pantoja, 2009; Vergara, Dewitte et al., 2016), which have led to a better understanding of the natural and forced variability of DO within OMZs as a whole. However, most of the studies have been conducted in the tropical part of the ESP, off Peru and northern Chile, where the OMZ extends deeper and further offshore and experiences only relatively small seasonal variability. In this work we focus on the extratropical region, near the southern tip of the OMZ. In contrast to the tropical ESP, where zonal flow originating from the equatorial region dominates the surface and subsurface circulation feeding the OMZ (e.g., Montes et al., 2010; Stramma et al., 2010), close to the coast of Chile the subsurface circulation is governed by a poleward undercurrent, namely, the Peru-Chile Undercurrent (PCUC) (e.g., Silva & Neshyba, 1979; Strub et al., 1998). Since the pioneer work of Gunther (1936), the PCUC has been associated with the presence of oxygen depleted waters at intermediate depths along northern and central Chile. Subsequently, many other works have confirmed this relationship (Wooster & Gilmartin, 1961; Silva & Neshyba, 1979; Codispoti 1989; Hormazábal et al., 2006; Silva et al., 2009) and have related the variability of the OMZ to changes in the PCUC transport. This undercurrent transports oxygen depleted Equatorial Subsurface Water (ESSW) southward along the continental slope and shelf edge off Chile, which can be traced as far south as 48°S (Silva & Neshyba, 1979). The PCUC undergoes large variability at a wide range of timescales, standing out the intraseasonal one (from about 20 to 90 days) and the interannual that characterize the El Niño-La Niña cycles (e.g. Shaffer et al., 1997, 1999; Pizarro et al., 2001, 2002; Dewitte et al., 2012; Illig, Bachèlery, et al., 2018 Illig, Cadier, et al., 2018). To date, the paucity of DO data has prevented a thorough assessment of the temporal variability of the OMZ off Chile associated with temporal and spatial changes of the PCUC.

Direct estimations of the PCUC off Peru, based on data from current meter moorings and hydrographic stations, showed that the PCUC transports about 1 Sv at 10°S (Huyer et al., 1991). Nevertheless, recent shipboard ADCP observations conducted between 4°S and 18°S off Peru –between 2008 and 2012 by Instituto del Mar del Perú (IMARPE)– showed a much larger southward transport related to the PCUC (Chaigneau et al., 2013). According to those estimates the mean PCUC transport increases from about 1.8 Sv at 5°S to a maximum of 5.2 Sv at 15°S. South of this last latitude the transport reduces slightly (Chaigneau et al., 2013). PCUC transport estimation at 30°S –based on current-meter and hydrographic observations– showed a mean value of about 1.0 Sv (Shaffer et al., 1999). All the above studies –Huyer et al. (1991), Shaffer et al. (1999), Chaigneau et al. (2013)– emphasize that the seasonal variability of the PCUC is rather small compared to the large fluctuations observed at intraseasonal and interannual periods. Table 1 shows a comparison of the mean and seasonal transport of the PCUC off Peru and Chile obtained from different observational and model studies.

In contrast to that observed off Peru and northern Chile, off central Chile (~30°S- 40°S) seasonal variability may be relatively more important due to the large increase of the seasonal fluctuation of the alongshore wind-stress and the wind-stress curl (e.g. Aguirre et al., 2012; Bakun & Nelson, 1991; Shaffer et al., 1999) associated to the seasonal migration of the energetic atmospheric low-level jet (Muñoz & Garreaud, 2005; Renault et al., 2009) and the dissipation of perturbations of equatorial origin. The relatively weak seasonal variability of the PCUC associated to marked latitudinal fluctuations questions the extent to which the OMZ characteristics are linked to the PCUC transport at seasonal timescale. This issue is hard to tackle with from low to medium resolution global models owing to their limitations in simulating realistically coastal upwelling dynamics and parametrisations in the biogeochemical models not necessarily tuned for eastern boundary current systems. High-resolution modeling has been proven more useful to address many aspects of the oceanic dynamics and circulation of the ESP-OMZ (Aguirre et al., 2012, 2014; Combes et al., 2015; Leth & Shaffer, 2001; Montes et al., 2010; Vergara, Echevin et al., 2016, among others).

Table 1
Mean and Seasonal Values of the Peru-Chile Undercurrent Transport Reported by Different Modeling and Observational Studies Along the Peruvian and Chilean Coasts

Latitude	This study (2019)[a]	Vergara, Echevin, et al. (2016)[a]	Combes et al. (2015)[a]	Chaigneau et al. (2013)[b]	Aguirre et al. (2012)[a]	Leth et al. (2004)[a]	Shaffer et al. (1997, 1999)[b]	Huyer et al. (1991)[b]
5°S								
Average				1.8				
10°S								
Average								1
15°S								
Average				5.2				
20°-25°S								
Average			2.7 ± 1.7					
28°S								
Average						1.3		
30°S								
Fall	0.84 ± 0.90	0.85 ± 0.36			1.06			
Winter	0.75 ± 0.28	0.68 ± 0.37			0.86			
Spring	0.78 ± 0.55	0.94 ± 0.41			0.87			
Summer	1.18 ± 0.85	0.73 ± 0.54			0.81			
Average	0.88 ± 0.70	0.80 ± 0.40			0.90		1	
33°S								
Fall	0.85 ± 0.92	0.82 ± 0.23			0.81			
Winter	0.75 ± 0.30	0.46 ± 0.29			0.61			
Spring	0.66 ± 0.40	0.81 ± 0.29			0.70			
Summer	0.56 ± 0.39	0.90 ± 0.24			0.73			
Average	0.71 ± 0.56	0.76 ± 0.17			0.71			
35°S								
Fall	0.74 ± 0.65							
Winter	0.56 ± 0.23							
Spring	0.49 ± 0.35							
Summer	0.35 ± 0.30							
Average	0.53 ± 0.43	0.76 ± 0.36				1.3		
36°S								
Fall	0.20 ± 0.14	0.50 ± 0.32			0.68			
Winter	0.18 ± 0.03	0.22 ± 0.26			0.55			
Spring	0.19 ± 0.18	0.45 ± 0.35			0.43			
Summer	0.14 ± 0.12	0.71 ± 0.49			0.85			
Average	0.17 ± 0.13	0.47 ± 0.17			0.62			
39°S								
Fall		0.48 ± 0.16			0.34			
Winter		0.15 ± 0.10			0.20			
Spring		0.08 ± 0.09			-			
Summer		0.34 ± 0.17			0.17			
Average		0.26 ± 0.09			0.27 ± 0.09			
43°S								
Average						1.1		

Note. Values are in Sverdrups (1 Sv = 10^6 m^3/s).
[a]reported by different modeling. [b]reported by observational studies.

The realism of the regional oceanic models allows in particular addressing quantitatively aspects of the physical-biogeochemical interaction and OMZ variability as shown by recent studies off Peru (Bettencourt et al., 2015; Montes et al., 2014; Vergara, Dewitte, et al., 2016). These latter studies have in particular shown a realistic representation of both spatiotemporal variability of the OMZ and the PCUC, and allows addressing the effect of the eddy-induced circulation on the OMZ variability. Thus, here we take advantage of these recent progresses in coupled modeling to investigate the seasonal variability of the southern tip of the eastern South Pacific Oxygen Minimum Zone between 30°S and 38°S. Our study focused on the role of the meridional changes of the PCUC transport and its seasonal cycle on the OMZ. We question the extent to which the PCUC transport controls the OMZ variability taking also into account other important aspects of the OMZ variability associated to mesoscale activity (Bettencourt et al., 2015; Vergara, Dewitte, et al., 2016).

The rest of the paper is organized as follows: In section 2 we described the data used for model validation, followed by a brief description of the coupled physical-biogeochemical model. An extensive model assessment is included in the Appendix. In section 3 we present (1) a description of different metrics that characterize the southern tip of the ESP OMZ and its annual variability, (2) the seasonal variability of the PCUC and its relationships with the OMZ, and the role of the zonal transport of the DO in the OMZ, (3) an integrated seasonal budget of DO in the OMZ and the role of mesoscale variability, and (4) an estimation of the oxygen eddy fluxes. In section 4 we discuss our key findings and the main strengths and limitations of the presented results, and finally, a summary of our main finding and conclusion are presented in section 5.

2. Data, model description and methods

2.1. Data

Satellite-derived sea surface temperature (SST) and chlorophyll-a (Chl-a) concentration data used in this study were the level-3 products of the Moderate Resolution Imaging Spectro-radiometer-MODIS-Aqua mission available from the National Aeronautics and Space Administration Jet Propulsion Laboratory PO.DAAC (https://oceancolor.gsfc.nasa.gov). These products have been pre-processed by PO.DAAC to obtain a daily resolution and a spatial resolution of ~4 km (NASA Goddard Space Flight Center, O. E. L and O. B. P. G., 2014). Sea level height and geostrophic currents were obtained from the Archiving, Validation, and Interpretation of Satellite Oceanographic (AVISO; currently processed and distributed by Copernicus Marine and Environment Monitoring Service (CMEMS) with no changes in the scientific content; see http://marine.copernicus.eu). These data were used to evaluate the simulated velocities near the surface. A comparison of model and satellite derived eddy kinetic energy (EKE) can be found in Vergara et al. (2017) (their Figure).

In situ data of temperature, salinity and dissolved oxygen concentration from different oceanographic cruises conducted off south-central Chile (35.5°- 40°S) were also used to assess the model performance. The cruises were supported by the "Fondo de Investigación Pesquera" (FIP; MOBIO-BIO project) and were carried out during Nov-2004, Dec-2005, Oct-2006 and Mar-2008. A total of 358 CTD profiles between 0 and 600 m depth were collected during those cruises and processed by the Physical Oceanography Group at the University of Concepcion. A monthly ship-based time series from the University of Concepcion at 36°30′S over the continental shelf (~90 m depth) for the period 2002-2008 was used to evaluate the seasonal variability near the coast at this latitude [see Sobarzo et al. (2007) and Escribano et al. (2012) for more details].

Climatological information of temperature, salinity, dissolved oxygen and nutrients for the study region were obtained from the Commonwealth Scientific and Industrial Research Organisation (CSIRO) Atlas of Regional Seas (CARS) gridded compilation (CARS 2009; www.marine.csiro.au/~dunn/cars2009/), it comprises gridded (0.5° latitude by 0.5° longitude every one month) fields of the different variables recorded over the period of modern ocean measurements. The seasonal cycle is based on an annual and semi-annual harmonic over the first km of the ocean. We use this atlas, along with other data sets, for the model assessment described in the Appendix.

Ocean current observations from a current-meter mooring located over the continental slope at 30°S, were used to assess the time variability of the model PCUC. The mooring was equipped with an upward-looking 300 kHz acoustic Doppler current profiler (ADCP) at ~120m depth –set up with a bin size of 4 m– and 4 Aanderaa current meters (RCM 8) at 220, 330, 480 and 750 m depth. The sampling interval for all the equipments changed during the measuring period between 0.5 h and 1 h. These current time series started originally in November 1991 and was maintained until 2010 (the ADCP was added to the mooring in May 2003). Here comparisons between model and observed currents were performed during the period 2003 and 2006.

2.2. Coupled physical/biogeochemical model

The regional high-resolution coupled physical-biogeochemical model used for this study takes into account the main processes linked with the eastern boundary upwelling systems (EBUS) and associated OMZ, it extends up to the equatorial region (12°N) in order to grasp the connection with the equatorial variability through coastal wave dynamics and transport by the PCUC. However, the region analyzed in this study is limited to the southern tip of the OMZ, comprised from 30° to 38°S (Figure 1). The model encompasses the period 2000-2008.

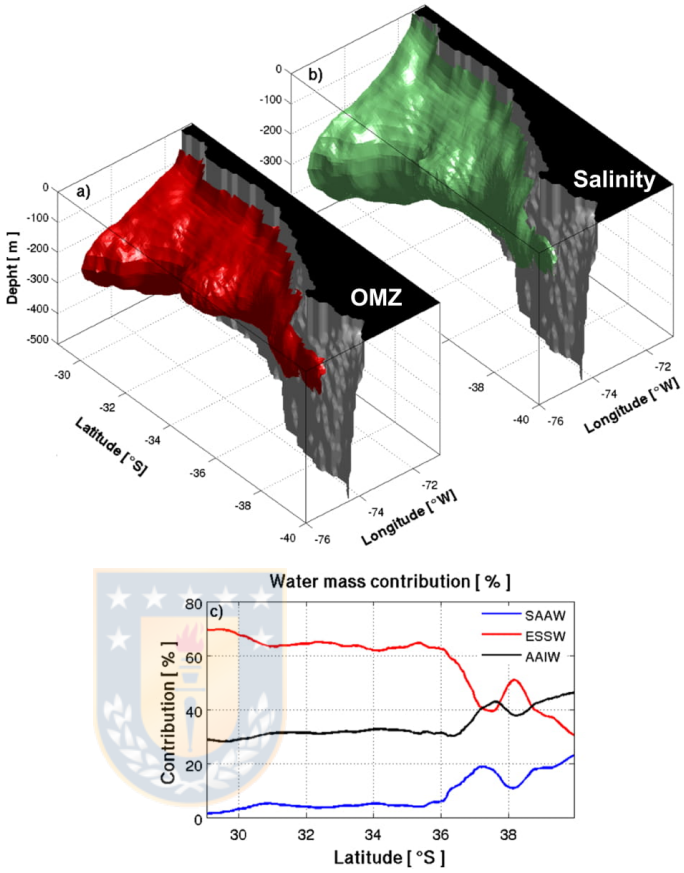

Figure 1. Annual mean extension of the eastern South Pacific OMZ between 30°S and 40°S obtained from the model. The red surface encompasses waters with DO <45 μM (a). The green surface shows the isohaline of 34.55 representative of the ESSW (b). Water masses proportion (in %) in the first 200 km from the coast and from the surface to 1500 m depth (c). Water masses are Subantarctic Water (SAAW; 11.5°C, 33.8), Equatorial Subsurface Water (ESSW; 12.5°C, 34.9) and Antarctic Intermediate Water (AAIW; 3°C, 34). The corresponding temperature and salinity values indicated above were obtained from Silva et al., 2009 and were used here to compute the water mass proportions.

The hydrodynamics was modeled by the Regional Ocean Model System (ROMS), an ocean model widely used for regional studies. It is a free-surface, terrain-following coordinate model with split-explicit time stepping and with Boussinesq and hydrostatic approximations that allows achieving adequate resolution to resolve mesoscale dynamics (see Shchepetkin & McWilliams, 2005, for a full description of the model). The ROMS simulation extend from 1958 to 2008 and has been validated using mean sea surface temperature data, EKE (based in geostrophic surface currents estimated from satellite altimetry) and vertical current structure (Dewitte et al., 2012; Vergara et al., 2017). Only the last nine years were used here. The complete domain extends from 12°N to 40°S, and from the coast to 95°W having a horizontal resolution of 1/12° (~8 km) and 37 sigma levels in the vertical. Most of the sigma levels (23) are distributed in the first 500 m depth, the remaining levels are distributed down to 4500 m depth, which allows a good representation of

the OMZ, even in the deep ocean. The atmospheric forcing consists in a statistical downscaling product from NCEP-NCAR (2.5° x 2.5°) data that provides wind stress and wind speed (see Goubanova et al., 2011), this method refines the NCEP-NCAR resolution to 0.5° x 0.5° and correct for the biases of the NCEP reanalyses near the Peru-Chile coast. The latter is used in the bulk formula combined with COADS monthly climatology (1° x 1°) (da Silva et al., 1994), air temperature and humidity to estimate latent heat fluxes. The statistical model is constructed from the QuikSCAT data so that the atmospheric forcing is almost equivalent to the original data over the period 2000-2008, which also motivates to focus on this period. Other flux terms also are from the COADS. The lateral open boundary conditions for temperature, salinity and horizontal velocity were obtained from SODA 1.4.2 reanalysis (Smith et al., 1992). The SODA 1.4.2 horizontal resolution is 0.25° (lat) x 0.4°(lon) and with 40 vertical levels with 10 m spacing near the surface. For further description of the hydrodynamic model simulation and validation see Dewitte et al. (2012) and Vergara et al. (2017).

The ROMS model was coupled to a biogeochemical model named BioEBUS following similar methodology than Montes et al. (2014) and Vergara, Dewitte, et al. (2016). Hereafter to this physical-biogeochemical coupled we will refer as ROMS/BioEBUS. The BioEBUS model is a nitrogen-based model developed for EBUS (Gutknecht, Le vu, Dadou, et al., 2013; Gutknecht, Le vu, Marchesiello, et al., 2013) derived from $N_2P_2Z_2D_2$ model (Koné et al., 2005). This model consists of 12 compartments having two classes of phytoplankton ("small" and "large", the small class is representative of small-flagellates named PS, while the large is representative of diatoms named PL), two classes of zooplankton (representing small-ciliates ZS and large-copepods ZL) and two classes of detritus (small DS, large DL). Dissolved organic nitrogen (DON) is represented in one compartment, while dissolved inorganic nutrients are represented by nitrate, nitrite and ammonium. The biogeochemical initial and open boundary conditions for nitrate and DO were obtained from CSIRO Atlas of Regional Seas (CARS, 2006). The nitrous oxide concentrations were estimated from DO using the parameterization given by Suntharalingam et al. (2000, 2012). The phytoplankton biomass is initially derived from satellite information (climatological data based on SeaWiFS observations) and vertically extrapolated using the Morel and Berthon (1989) methodology. Finally, initial and lateral boundary conditions for other biogeochemical tracers (NO_2^-, NH_4^+ and DOM) are established using constant vertical profiles based on Koné et al. (2005), similar to those used by Montes et al. (2014) and Vergara, Dewitte, et al. (2016). In general, the biogeochemical parameters used in our model simulation were the same as those used by Montes et al. (2014) and Vergara, Dewitte, et al. (2016) for Peru and northern Chile. See appendix in Montes et al. (2014) for a quantitative description of the parameters used for BioEBUS in this study.

The evolution of any tracer in BioEBUS is determined by the advection-diffusion equation (Gutknecht, Dadou, Le Vu, et al., 2013). In particular, for DO we can write:

$$\frac{\partial DO}{\partial t} = -\nabla\cdot(\boldsymbol{u}DO) + K_h\nabla^2 DO + \frac{\partial}{\partial z}\left(K_z\partial\frac{DO}{\partial z}\right) + SMS \tag{1}$$

The first term on the right-hand side of (1) is the advection, where **u** is the fluid velocity, the second term is horizontal subgrid-scale diffusivity, where K_h is the horizontal eddy diffusion coefficient –equal to 100 m^2s^{-1} in this version of the model–, and the third term is the vertical mixing. (with a turbulent diffusion coefficient K_z calculated using the K-profile parameterization mixing scheme; Large et al., 1994). Note that the model also has numerical diffusion associated with inherent spurious diapycnal mixing of the numerical scheme, so that K_h has to be empirically adjusted. The last term, *SMS* (sources minus sinks), includes all biogeochemical processes considered by the model that act as sources and sinks, in this case, for DO. Note that the tracer equation (1) was evaluated online at each time step. The total physical term (named *PHYS* below) is the summed-up contribution of the advective term ($ADV = -\nabla\cdot(\mathbf{u}DO)$) plus the horizontal diffusion ($K_h\nabla_h^2 DO$) and vertical ($\frac{\partial}{\partial z}\left(K_z\frac{\partial DO}{\partial z}\right)$) mixing, hereafter called *Hmix* and *Vmix*, respectively. The *ADV* can also be represented separately through its contributions related to the different components as: the zonal ($Xadv = -u\partial(DO)/\partial x$), meridional ($Yadv = -v\partial(DO/\partial y$) and vertical ($Zadv = -w\partial(DO)/\partial z$) advection e.g. Gutknecht, Dadou, Le Vu, et al., (2013), where *u, v* and *w* are the zonal, meridional and vertical velocity components, respectively. Note that *ADV* contains also diffusion inherent to the numerical advection scheme. *Hmix* and *Vmix* are explicit source of mixing, however, they are not the only term contributing to mixing in the model. The term mixing will refer to the integrated effect of all processes contributing to mixing directly

or indirectly. Besides horizontal diffusion and vertical mixing, mixing can be also caused by non-linear advection. e.g. eddy fluxes (cf. Vergara, Dewitte, et al., 2016). Here non-linear advection (of *DO*) refers to the cross products of the anomalous velocity field (**u'**) and the anomalous *DO* (*DO'*) -i.e. in the context of Reynolds decomposition, this corresponds to the term (**u**'*DO*') where prime stands for an anomaly with regards to any preferred baseline (either mean climatology or 3-month running mean in this study). Note that equation (1) would involve the divergence of this term. Linear advection refers to either the mean advection of anomalous gradient in *DO* ($\overline{\mathbf{u}}\partial DO'/\partial z$) or anomalous advection of mean gradients in *DO* ($\mathbf{u}\partial\overline{DO}/\partial z$). Here also mean and anomalies are defined by the a priori Reynolds decomposition that is considered. In this context the mean quantities are "constant" while the anomalies are variable in time.

2.3. Characterizing the extratropical OMZ

At the present time, there is still no full agreement about the best threshold in oxygen that defines the OMZs. The first global study of hypoxic waters considered a DO threshold of <8 μM (Kamykowski & Zentara, 1990). However, Karstensen et al. (2008) used three thresholds to analyze the characteristics of the OMZ in the eastern tropical Pacific and Atlantic: DO ~4.5 μM in the suboxic range, DO ~45 μM, and a more relaxed level of ~90 μM in order to include in their analysis the less intense OMZ of the eastern Tropical Atlantic. Paulmier and Ruiz-Pino (2009), in contrast, excluded the Atlantic OMZ when they used (~20 μM) to describe the different OMZs using the WOA2005 climatology. Helly and Levin (2004) used also a threshold of ~20 μM in their global study of the OMZs on continental margin seafloors. In contrast, Stramma et al. (2012) used a much larger value (~150 μM) to analyze the expansion of the OMZ in the tropical Atlantic.

Here we define the OMZs as the region where DO levels are ≤ 45 μM, because this threshold value is in the range of values characterizing hypoxia (e.g. Naqvi et al., 2010). For more practical reason, we also note that waters with DO ~45 μM are present most of the time inside our domain of interest. Also, as the model overestimates somewhat DO in the southern part of the domain (see Appendix), a lower value, like DO <20 μM, would narrow the extent of the OMZ within our domain compared to the observations. Considering that low value in DO concentration (i.e DO< 20 μM) is required to stimulate denitrification, this model bias needs to be kept in mind when interpreting the results (Section 3).

Finally, it is worth noting that in our analysis we use the volume of the OMZ as a metric to characterize its seasonal variability, but for analyzing the budget of DO we use a fixed volume defined as the region with 9-year (2000-2008) mean DO ≤ 45 μM.

2.4. Estimation of DO eddy fluxes

To evaluate the contribution of the eddy-induced circulation on the DO seasonal variability, we consider a Reynolds decomposition of the DO and the three velocity fields, where the departure from the "mean state" accounts for fluctuations having a typical time scale lasting from weeks to a few months so that eddy variability refers here mostly to the mesoscale turbulence. This writes as follows:

$$\varnothing(x,y,z,t) = \widetilde{\varnothing}(x,y,z,t) + \varnothing'(x,y,z,t) \tag{2}$$

where ∅ represents DO or any velocity component, $\widetilde{\varnothing}$ is the 3-month running mean and ∅′ is the deviations from $\widetilde{\varnothing}$. Time series with a temporal resolution 5-day mean model output are used for this calculation. To estimate the mesoscale eddy fluxes of DO we compute the covariance between horizontal velocity fluctuations (*u*', *v*') and *DO*', i.e. $\langle u'DO'\rangle_{3\text{-m}}$ and $\langle v'DO'\rangle_{3\text{-m}}$, where "$\langle\rangle_{3\text{-m}}$" stands for a 3-month moving average. Hereafter, for simplicity, we refer to eddy fluxes for theses quantities (instead of mesoscale eddy fluxes). The methods to derive the eddy flux is similar to that used in Vergara, Dewitte, et al. (2016).

We thus obtained covariance time series every 5 days, from which we estimate the climatology. In this paper, we focus on the seasonal cycle of the horizontal eddy flux, $\langle u'DO'\rangle_{3\text{-m}}$ and $\langle v'DO'\rangle_{3\text{-m}}$, that consists in the climatology of the eddy flux ($\langle u'DO'\rangle$, $\langle v'DO'\rangle$) where the braket indicates here the mean over the entire period (2000-2008). The latter will be compared to the mean seasonal flux that corresponds to the flux associated to mean seasonal cycle, i.e. $\left(\left\langle\widetilde{u}\widetilde{DO}\right\rangle, \left\langle\widetilde{v}\widetilde{DO}\right\rangle\right)$.

3. Results

3.1. Seasonal and spatial variability of the southern tip of the OMZ

As a first step, we document the main characteristics of the southern tip of the OMZ and its seasonal variability, including dynamical and morphological features that are used for the interpretation of the subsequent diagnostics. Along the Chilean coast the zonal extension and thickness of the OMZ (represented here by the region with DO $\leq$ 45 μM or ~1 mL L^{-1}, i.e. near the suboxia range, e.g. Naqvi et al., 2010) rapidly decrease southward, but near the coast it remains at intermediate depth as far south as 38°S (Figure 1). Observations show that the OMZ may extend even farther south, exceeding the southern border of our study region (e.g., Silva et al., 2009). The tongue of low-oxygen waters is rather well associated with a tongue of high salinity (salinity > 34.55) and both are largely reduced southward by mixing with low-salinity and well ventilated AAIW and SAAW (Figures 1b and c, and Figure A4; cf. Silva et al., 2009 and Llanillo et al., 2012). Although on average the offshore extension of the OMZ decreases southward , its offshore boundary zigzags with maximum (minimum) extent near 30°S and 33°S (31°S and 34°S; Figures 2 and 3, central rows). At 100 m depth lower values of DO are observed along the coast during summer (Figure 2a, top panels), when upwelling reaches a maximum in the region.

The seasonal cycle of salinity and DO are inversely correlated inside the whole OMZ. To illustrate this, we present results for 3 cases, in all of them both DO and salinity time series are obtained by spatially-averaging the corresponding variable in the whole OMZ region. The 3 cases are the following: 1) Just the 12- month time series that conform the seasonal cycle (r = -0.87; this represent the correlation between the time series shown in the lower panels of Figures 4d and 4e); 2) 9-year (2000-2008) monthly time series of DO an Salinity (r=-0.97), and 3) similar to case 2, but only the region between 35°S and 38°S was considered (r=-0.83). These last 2 correlation values are significantly different from zero at the 95% confidence level (using an integral time scale of 3 months; Emery & Thompson, 2004). South of ~36°S, the seasonal cycle of DO increases and it differs from that observed in the northern part of the study region (Figure 4). For instance, the minimum DO found during fall in most of the domain is not present south of 36.5°S (Figure 4d). In this region the relative contributions of the different water masses present inside the OMZ display an abrupt change. ESSW decreases from about 64% at 36°S to ~40% at 37°S, while AAIW increases from ~30% to 40% between those latitudes. The increase of SAAW in this region accounts for the other 14% (Figure 1c).

The above results suggest that the seasonal and spatial variability of DO inside the model OMZ are related to changes in the proportion of ESSW more than to biological processes. The OMZ is less intense and it volume is smaller during spring (Figure 2 and Figure 3; in this context a less intense OMZ means that the concentration of DO inside the OMZ, i.e. inside the volume for which DO < 45 μM, is larger). It is worth noting that the PCUC is weaker in austral winter (August-September), just a couple of months before the decrease in intensity of the OMZ is less intense (Figure 4). In the next subsection we analyze in more detail the variability of this poleward flow and it relationship with the OMZ.

3.1.1. Seasonal variability of the PCUC and the OMZ

The meridional component of the velocity within the OMZ is mostly southward year-round, but around August-September this poleward flow is largely reduced and may be slightly northward. Conversely, maximum poleward currents are observed near late April-May (Figure 4f). North of 36.5°S this flow shows an important semi-annual component, with a secondary maximum in December, and a secondary minimum during the end of the austral summer. This semi-annual component in the poleward flow has been well documented based on direct current observations at 30°S and its forcing has equatorial and local origins (cf. Shaffer et al., 1999; Pizarro et al., 2002; Ramos et al., 2006; see section 4). Note that the OMZ is located in a region dominated by the PCUC (see white contours on Figure 3) and the weakness of this flow –centered around August (Figure 4f)– is followed by an increase of the DO in the OMZ about 2 months later (Figure 4d). Conversely, the maximum poleward flow centered around April-May coincides with a reduction of the mean DO.

In our model the mean position of the poleward undercurrent does not always coincide with the mean position of the core of the OMZ (Figure 3). The undercurrent commonly extends deeper than the 45 μM isopleth, and this isopleth may extend farther offshore than the undercurrent, particularly in the northern part of the

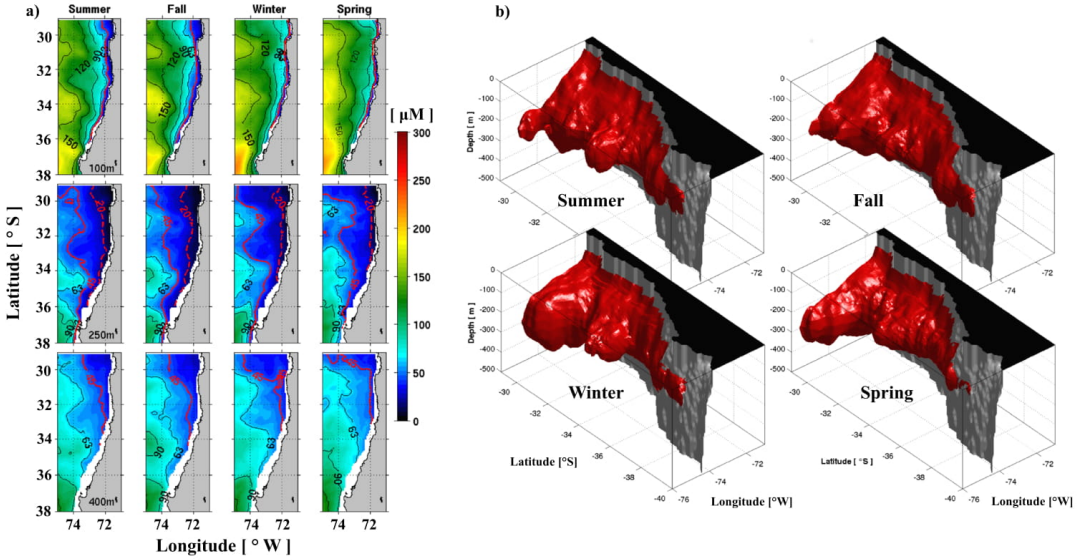

Figure 2. Spatial and seasonal distribution of DO modeled at three different depths: 100 m (top), 250 m (middle) and 400 m (bottom) (a). The solid and dashed red contours represent 45 µM and 20 µM, respectively. The seasonal 3-D volume of the southern tip OMZ obtained from the model (b). The red surface contains waters with DO <45 µM. Summer (JFM), fall (AMJ), winter (JAS) and spring (OND).

study region. We estimate the transport of the PCUC by spatially averaging the southward flow between 80 and 800 m depth, and between the coast and 200 km offshore (only values smaller than -0.02 m s^{-1} were considered in the calculation). The mean transport of the PCUC decreases southward from about 1.2 Sv at 30°S to 0.5 Sv at 37°S (Figure 5a). The former value is slightly larger than the ~1.0 Sv estimated using direct currentmeter observations and hydrographic data by Shaffer et al. (1997, 1999) over a different period. The mean southward transport of the PCUC in the study region was ~0.7 Sv, consistent with the mean value estimated by Aguirre et al. (2012) and Vergara, Echevin, et al. (2016), both estimates are also based on numerical simulations using the same source of data for the atmospheric forcing (i.e QuikSCAT data). These studies also showed that the PCUC transport decreases southward and has a minimum value in winter off central Chile. Unfortunately, there are not enough published data available to contrast these model estimations southward of 30°S (see Table 1). The variability of the PCUC transport in our model showed an important semi-annual component, particularly north of 36°S, consistent with the semi-annual variability described above and also observed in the alongshore flow over the slope at 30°S (see Figure 5a). South of 36°S the transport of the PCUC is drastically reduced (Figure 5a). A similar, relatively abrupt, change was observed in the meridional velocity and DO concentration inside the OMZ (Figures 4d and 4f), but somewhat farther south. The seasonal cycle of DO averaged inside the whole OMZ showed a maximum of ~32 µM in austral spring (i.e. October-November, see bottom panels of Figures 4d), about 2 month later than the PCUC velocity reached a minimum (see bottom panels of Figures 4f). This result is consistent also with the estimated transport of the PCUC and with the DO averaged inside the region dominated by this current (Figure 5).

To further illustrate the PCUC control on the OMZ variability we show the variability of DO inside the core of the PCUC (Figure 5b). The mean DO concentration within PCUC core varies from ~26 µM at 30°S to > 60 µM at 37°S. This concentration tends to be smaller when the southward transport is weaker, that is in part, because when the PCUC is weaker its core tends to be restricted to the core of the OMZ (Figure 3). On the other hand, the minimum poleward transport of the PCUC in August is related to a rapid increase in DO concentration particularly south of 34°S (Figure 5b).

3.1.2. Seasonal variability of the zonal flow and the OMZ

The zonal components of the velocity, averaged inside the OMZ region (which is near cross-shore in our study region), shows small seasonal variability (~0.5 cm s^{-1}) with an important semi-annual component (Figure 4c). Given the large cross-shore gradient of DO (Figures 3 and 4), small changes in the zonal speed may contribute to modulate the DO seasonal cycle in the OMZ through anomalous zonal advection of mean oxygen gradient. The most striking feature of the zonal speed is its large spatial variability, with the presence of alternating zonal jets of positive (eastward) and negative (westward) currents. For instance, bands of eastward speeds are centered around ~31°S, 34°S and ~37°S, although their latitudes may change somewhat during the year. These zonal jets are closely related with the offshore extension of the lateral boundaries of the OMZ (contrast Figure 2 with 4c), that is, where the cross-shore velocity is predominantely eastward, the oxygen isopleths that bound the OMZ approaches the coast, while at those latitudes where the velocity is predominantly westward, the lateral OMZ boundary extends further offshore.

From figure 4c we can distinguish 3 bands of zonal velocity (here we refer to the zonal velocity averaged inside the OMZ at each latitude: u_{OMZ} (*Lat,t*), where *Lat* is latitude and *t* is time) dominated by positive (onshore) flow. The first band is centered around 31°S and has a maximum (onshore) flow in winter (u_{OMZ} ~1.5 cm s^{-1}, this value is the average of the velocity in the band from 30.3°S to 31.6°S), the second band is located between ~33°S and ~35°S with a small maximum also in winter (u_{OMZ} ~0.5 cm s^{-1}) and the third one, laying around 36°S and 37°S, with a small maximum in summer (u_{OMZ} ~0.8 cm s^{-1}) (Figure 4c). Thus, the onshore flow is somewhat more intense in winter north of 36°S, when the poleward flow is minimum, contributing to the increased DO –and to the reduction of the OMZ offshore extension. The increase in the onshore transport of DO and the weakening of the PCUC result in a well-defined maximum of DO inside the OMZ and a reduction of its total volume during spring. Despite the fact that the amplitudes of the seasonal cycles of u_{OMZ} averaged inside these bands are small, they are significant at the 90% confidence level. To calculate the significance of the amplitude of the seasonal cycle we use a Monte Carlo method. It involves the generation of an artificial time series by randomly sampling the original one (with replacement), and to fit an annual harmonic to the artificial time series. This process was repeated 1000 times. Then, based on the 1000 artificial amplitudes a P% percentile was calculated. If the observed amplitude was larger than this percentile the amplitude was considered to be significant at (100-P)% of confidence level.

To summarize, our analysis suggests that the mean OMZ (i.e. zonal and meridional extent) is heavily constrained by the mean circulation as evidenced by the existence of a "high salinity tongue" matching the limits of the OMZ and the meridional variability of the off-shore limit following approximately latitudinally alternating bands of weak and stronger zonal "jets". The seasonal variability of the OMZ seems also tightly linked to the variability of the PCUC with a stronger PCUC in austral spring associated to the intensification and southward extension of the OMZ. There is also a significant contribution of the semi-annual cycle to the seasonality in both the PCUC and OMZ structure. While the PCUC variability appears as a key driver of the OMZ seasonal change, our description of the OMZ mean state and seasonal variability also suggest that other processes are occurring simultaneously that are documented below in the light of the results of a DO budget.

3.2. DO budget

3.2.1. Integrated seasonal budget of DO in the OMZ

To analyze the contribution of the different drivers to the DO seasonal cycle we consider the seasonal variability of the RHS terms in the advection-diffusion equation (1). The tendency terms were averaged inside the volume delimited for the mean position of the 45 μM isoline (i.e. inside the fixed volume that encompass the annual mean of the OMZ shown in Figure 1a). We present the climatological variation of the different terms including their mean value to assess their relative magnitude (Figure 6). The zonal advection (*Xadv*), *SMS* and the horizontal mixing (*Hmix*) are negative, while meridional advection (*Yadv*), vertical advection (*Zadv*) and vertical mixing (*Vmix*) are positive. *Xadv* shows the largest magnitude, while *Yadv* is the second largest. In contrast, the mixing terms (*Vmix* and *Hmix*) are, in the total average, 2 orders of magnitude smaller than the other terms conforming the RHS of (1) with vertical mixing (positive) larger in absolute value than horizontal mixing (negative). The amplitude of the annual harmonic of DO (fitted to the dashed black curve shown in Figure 6a) is 4.3 μM and represents about ~14% of the mean DO (30.7 μM) concentration inside the whole OMZ control volume. This harmonic explains ~82% of the seasonal cycle of DO and has

a maximum in austral spring. The seasonal cycle of DO within the OMZ volume is also represented in Figure 4d (bottom panel), but in that case the amplitude of the variability is much smaller because the volume changes according to the seasonal variability of the 45 μM isopleth, so we are only considering waters with DO lower than 45 μM. The rate of change of the DO (∂DO/∂t, red line in Figure 6a) peaks in July, about 2 months before the DO peaks (Figure 6a, red line), when the DO is increasing most rapidly. There is only a qualitative consistency when the averaged seasonal cycles of DO and ∂DO/∂t are compared, revealing the relative importance of non-linear terms (i.e non-linear advection and mixing). The seasonal cycle of ∂DO/∂t has a secondary maximum in April, which accounts for the presence of semi-annual variability. The main peak in this series is in August and may be associated with the weakening of the southward transport of DO (cf. Figure 4f).

The summed-up contribution of the physical tendency terms (*PHYS* formed by *ADV* + mixing) is the largest contributor to the seasonal cycle of ∂DO/∂t within the OMZ (Figure 6b). Consistently, *PHYS* and ∂DO/∂t time series show similar seasonal variability, which emphasizes the prominent role of physical processes in controlling the averaged seasonal variability of DO inside the OMZ. Furthermore, the *ADV* terms, and in particular, the zonal advection of DO (*Xadv*; Figure 6b) dominates the seasonal variability of *PHYS*, while the mixing terms (*Hmix*, *Vmix*) are much smaller (Figure 6c) and their mean contribution to the seasonal variability of DO (averaged inside the OMZ) is only significant during the transition phase when ∂DO/∂t changes sign or remains weak (like in May-June). It is worth noting that *ADV* may also generate mixing (i.e. eddy-induced advection; see section 3.3) associated with mesoscale turbulence, so *Hmix* and *Vmix* are mainly related here to small-scale (subgrid-scale processes) mixing.

The biogeochemical term (*SMS* in Eq. (1)) has small seasonal variability compared with *PHYS* and it permanently behaves as a sink of DO inside the OMZ with a single maximum in austral winter. The yearly means of *PHYS* and *SMS* have similar magnitude (1.8 and 1.4 $x10^{-6}$ μM s^{-1}, respectively), but opposite signs. On average, the meridional (*Yadv*) and vertical (*Zadv*) advection behaves as oxygen sources, while the zonal advection (*Xadv*) acts as a sink for the whole volume. The amplitude of the annual and semi-annual harmonics adjusted to the different terms showed in Figure 6 is provided in Table 2.

The sum of all averaged terms shown in Figure 6 does not necessarily have to be zero, even if ∂DO/∂t was zero, due to the important influence of non-linear terms that make up *PHYS*. In fact, the magnitude of *PHYS* exhibits large mesoscale variability (see below), which suggests a relevant contribution of non-linear eddy fluxes –related to mesoscale processes– to the variability of the OMZ. Thus, the spatially-averaged terms inside the whole volume may not represent properly the characteristics of the seasonal cycle of the DO budget. On the other hand, the mean of ∂DO/∂t inside the whole volume for the period 2000-2008 was of the order of 10^{-8} μM s^{-1}. This small trend can be associated with decadal variability present in the study region (note that, for the full simulation period, 1958-2008, the model is stable and the mean ∂DO/∂t is practically zero). Table 3 shows the total mean values inside the OMZ for the period 2000-2008 and the climatological variability (standard deviation) of ∂DO/∂t and *ADV*, including the *Xadv*, *Yadv* and *Zadv* components (all values are in μM s^{-1}×10^{-6}). The explained variance of ∂DO/∂t in term of the advection (R^2, in percentage) is also shown. As the different non-linear advection components are correlated among them (not shown), they cannot be regarded as independent contribution to ∂DO/∂t. In general, all advective terms contribute to ∂DO/∂t in the OMZ, but *Xadv* seems to play a major contribution as also was suggested by Figure 6b.

3.2.2. The role of the mesoscale activity

While the previous analysis indicates seasonality in the processes, there are also indications of high frequency fluctuations which may result from the intricate circulation in relation with mesoscale features. To visualize the spatial structure of the seasonal variability associated with the different terms that control the oxygen budget inside the OMZ we use an EOF analysis applied to the seasonal fields of *PHYS* (particularly *Xadv*, *Yadv* and *Zadv*) and *SMS*. These fields were previously averaged between the isopycnal surfaces of 26.4 and 26.8 kg m^{-3}, where the core of the OMZ is located (Figure 3). Note that the seasonal time series of each field are monthly i. e each time series have only 12 values. The analysis was restricted to the region delimited by the mean position of the 45 μM isopleth, consistently with the above analysis (i.e. we remove from the analysis the white area showed in Figure 7. To evaluate the sensitivity of the EOF results to the selected region we also considered a

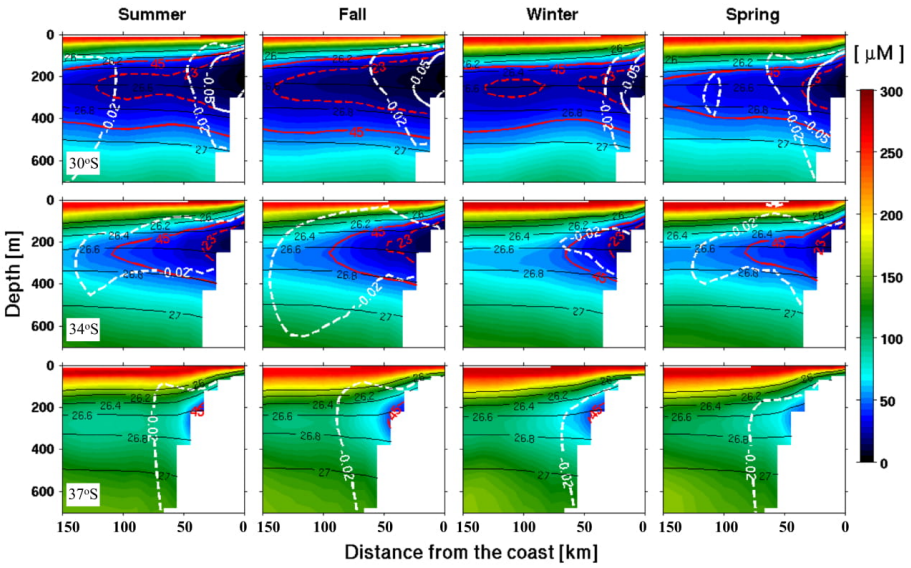

Figure 3. Cross-shore sections of DO modeled (background color and red contours) and southward velocity (white contours) representing the PCUC at 30°S (top), 34°S (middle) and 37°S (bottom) in the first 150 km from the coast at different seasons: summer (JFM), fall (AMJ), winter (JAS) and spring (OND). The continuous and dashed red contours represent 45 µM and 20 µM respectively. The solid and dashed white contours represent southward speeds of 0.05 m s^{-1} and 0.02 m s^{-1}, respectively.

wider region, including the region outside the OMZ. The structure of the EOF of the different terms was rather similar with most of the variance near the coast, i.e. where the OMZ is observed (not shown).

The first EOF mode for *PHYS* explains 16% of the total variance and its spatial structure shows large variability with length-scale typical of mesoscale processes (Figure 7a). The explained variance for the first EOF mode of different *ADV* terms was around 20% (Figures 7b to d). The EOF mode 1 of *Xadv* and *Yadv* are spatially well anti-correlated (r =-0.7; Figure 7b and c). Eddy flows and their rectification on the mean flows seem to be relevant, contributing to this large spatial variability. Time series (EOF principal components) of *Xadv* and *Yadv* show an important semi-annual component with maxima in March and July-August, coincident with the periods of weaker poleward undercurrent (Figure 4f). In contrast to *PHYS*, the first EOF of *SMS* showed a uniform (in phase) structure in the whole study region and its time series showed a well-defined annual variation with a maximum in July. This EOF mode explains 72% of the total variance. In this density range (26.4 and 26.8 kg m^{-3}) *SMS* was always a sink for DO, so the EOF time series indicates that DO consumption was minimum during austral winter.

In order to gain further insight into the spatial variability of *ADV* inside the OMZ, we perform an EOF analysis in three cross-shore coastal sections: 30°S, 34°S and 37°S, delimited by the 45 µM and the first 150 km (Figure 8). The first EOF mode of all advective terms showed rather similar structures, with maxima near the continental slope, just inside the core of the PCUC (dashed black contour in Figure 8). Nodal lines, centered around 250 m depth for *Xadv* and *Zadv*, and 150 m depth for *Yadv*, are observed in the different sections (Figure 8). The principal components of *Xadv* in the 3 locations showed a rather consistent semi-annual fluctuation (Figure 8m) similar to that observed in the horizontal EOF analysis. Conversely, *Yadv* and *Zadv* time series were quite variable (Figure 8n, o). The first EOF mode of *SMS* explain a large fraction of the total variability and was vertically in phase in all sections, with larger amplitude toward the upper limit of the OMZ. Their time series are similar to those observed in the horizontal sections with a maximum in July, but the time series from 30°S, which showed a maximum centered around April.

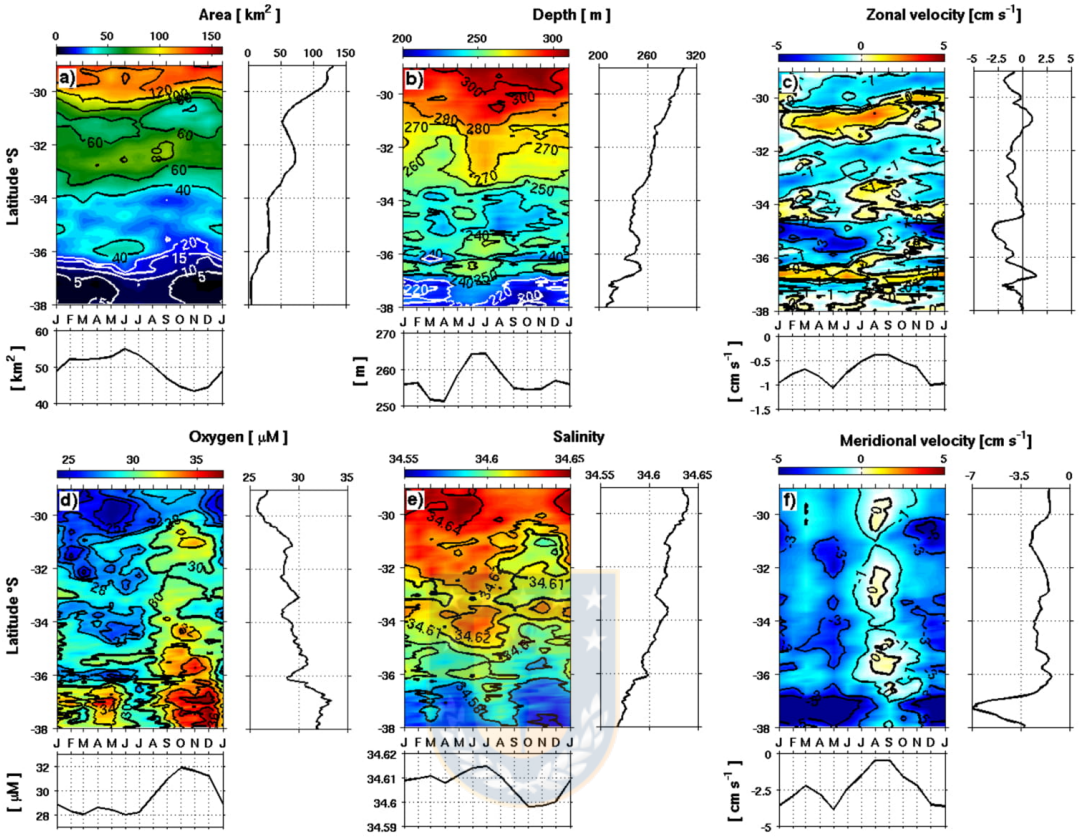

Figure 4. Seasonal cycle of different metrics that characterize the OMZ between 29°S and 38°S (in this case the OMZ was defined as the variable volume enclosed by the isopleth of DO ≤ 45 μM, which change with the time). The area of cross-shore sections covered by the OMZ in km^2 at different latitudes (a), the mean depth (m) of the OMZ (b), zonal velocity (cm s^{-1}) (c), DO concentration (μM) (d), salinity (e) and meridional velocity (cm s^{-1}) (f). The insets at the right and bottom of each main panel show the annual mean at different latitude (right) and the latitudinal averaged seasonal cycle (bottom) of the corresponding variable, respectively.

To summarize, the three advective terms (*Xadv*, *Yadv* and *Zadv*) are the main contributors to the seasonal variability of the DO budget in the OMZ, these terms have large and correlated mesoscale variability and vertical structure with a node typically centered around 200 m depth. The typical annual change is not dominated by one harmonic, it shows large semiannual and shorter variability. These results, along with previous studies from the northern region of the eastern South Pacific OMZ [cf. Montes et al., 2014; Bettencourt et al., 2015; Vergara, Dewitte, et al., 2016), as well as from other OMZ (Resplandy et al., 2012), suggest that the DO budget in our study region is impacted by mesoscale processes. The formalism of the oxygen budget does not allow an estimate of the separate contribution of mesoscale variability to the rate of change in DO since eddies are embedded into the total circulation from which advection terms are derived. To get insights on the role of mesoscale variability in shaping the seasonal cycle of the OMZ, the DO eddy flux can be estimated (see section 2.4) and compared to the mean seasonal flux (i.e. the DO flux associated with the seasonal variability of the "mean" circulation) to infer its role on the OMZ seasonal cycle.

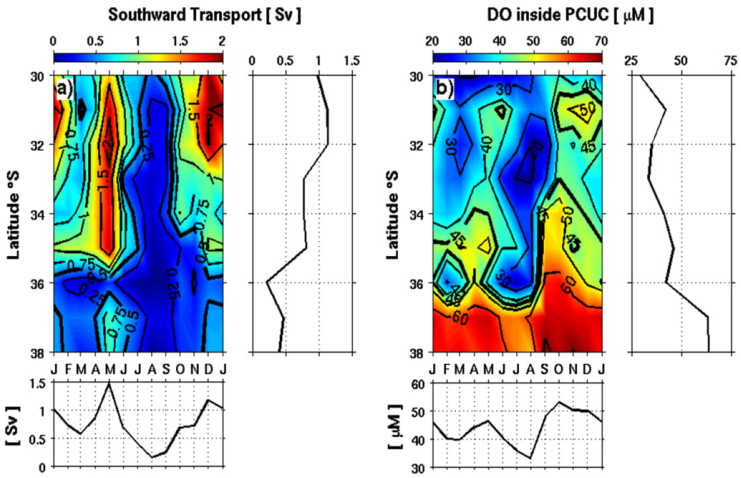

Figure 5. Seasonal cycle of the alongshore southward transport associated to the PCUC modeled (in Sv, 1 Sv = 10^6 m^3s^{-1}) (a) and mean DO inside the PCUC defined by the isopleth of -0.02 m s^{-1} in the first 150 km from the coast and above 700m depth (b). The insets at the right and bottom of the main panels show the annual mean at different latitude and the mean seasonal cycle latitudinally averaged of the corresponding variable, respectively.

3.3. Mesoscale eddy fluxes of dissolved oxygen

The mean eddy flux (MEF) and its seasonal variability across the OMZ averaged between the isopycnal surface of 26.4 and 26.8 kg m^{-3} are presented in Figure 9 (top panels), which can be compared to the mean seasonal flux (bottom panels). The arrows provide the two components of the horizontal eddy flux (i.e. ($\langle u'DO' \rangle$, $\langle v'DO' \rangle$) for MEF) while the shading indicates the amplitude of MEF, that is $\sqrt{\left(\left\langle u'\widetilde{DO'}\right\rangle_{3-m}^{2}+\left\langle v'\widetilde{DO'}\right\rangle_{3-m}^{2}\right)}$. First we note that the mean eddy flux, although smaller than the mean seasonal flux, is of the same order of magnitude, with regions (e.g. north of 34°S) where the amplitude of the mean eddy flux is comparable to that of the mean seasonal flux. MEFs showed large spatial variability with lower values (<0.3 m s^{-1} μM) in the OMZ. In the offshore region outside the OMZ the fluxes were larger (~1 m s^{-1} μM) and predominantly eastward. The regions with larger eastward MEFs, like those centered around 32°S and 34.5°S, are related to a smaller offshore extension of the OMZ, as can be observed following the 90 μM contour (Figure 9a). Thus, the MEFs seem to contribute to ventilate the OMZ in some regions, particularly during summer and spring (Figure 9b to e), and to shape the offshore extension of the OMZ. The mean horizontal DO advective fluxes ($\widetilde{u}\widetilde{DO}$ and $\widetilde{v}\widetilde{DO}$) are, in general, larger than the MEFs and they have also large spatial variability with eddies and meanders in the offshore region. Near the coast these fluxes are mainly southward, consistent with the predominance of the PCUC in this density range (i.e. 26.4 and 26.8 kg m^{-3}). The seasonal anomalies of these advective fluxes during the different seasons are also consistent with the shape of the 45, 60 and 90 μM contours showed in Figures 9g to 9j.

To better visualize the relative contributions of the horizontal fluxes of DO to the oxygen budget of the OMZ and its seasonal variability we show the mean flux across the 60 μM surface between 26.4 and 26.8 kg m^{-3} isopycnals (Figure 10). The mean position of this surface is shown in Figure 9 as a black contour (surfaces of 90 μM and 45 μM, are also shown there). We use the 60 μM surface because it better represents the boundary of the OMZ than the 90 μM one, and it is present in the complete domain most of the year, while the 45 μM surface is not present in the southern part of the domain during some periods or is restricted to a small range of depths and does not cover the entire chosen density range. Results showed that the MEFs of DO

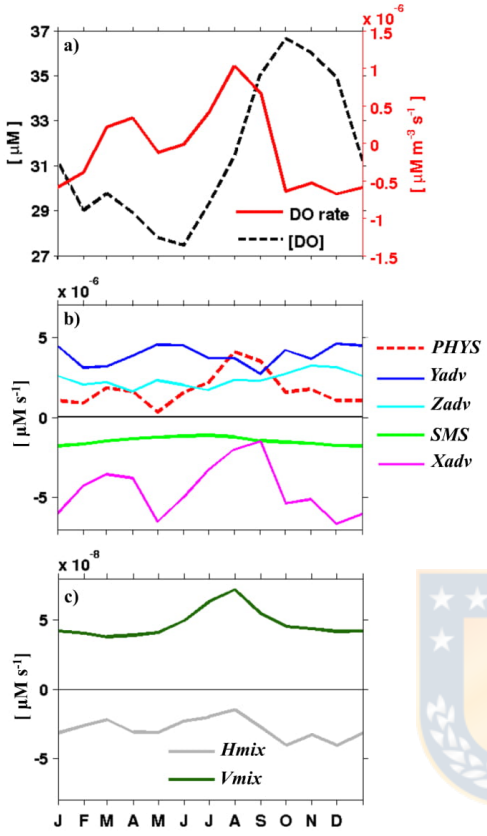

Figure 6. Seasonal DO budget within the mean OMZ volume (in this case the OMZ is considered as fixed volume defined as the region with 9-year (2000-2008) mean DO ≤ 45 µM; see Figure 1a). Seasonal cycle of DO and DO rate of change (∂DO/∂T) (a). The different terms of the right-hand side of Eq. (1) are also shown (b): The physical term (*PHYS* red dashed line) is the summed-up contribution of advection and mixing. The advection term (*ADV*) is composed, in turn, by zonal (*Xadv*, magenta line), meridional (*Yadv*, blue line) and vertical (*Zadv*, cyan line) advections. The biogeochemical fluxes (*SMS*, light green line) represents the "source-minus-sink" contribution to the DO rate of change due to biogeochemical processes. The mixing terms are the summed-up contribution of the horizontal diffusion (*Hmix*; grey line) and vertical diffusivity (*Vmix*, dark green line) (c).

predominantly transport DO toward the OMZ, particularly in the region located northward of 34°S. These fluxes have small annual variability (about 20% of the total variability of the DO fluxes) and they do not have a clear seasonal signal (Figure 10a and c). Conversely, the mean advective fluxes of DO are predominantly negative (Figure 10d), except in August, September and October (Figure 10f, bottom panel). The seasonal cycle of this flow has also a semi-annual component that is coherent with the seasonal variability of the zonal current shown above (contrast Figures 4c and 10f). Thus, in average for the whole study region, while zonal MEF contribute to transport DO toward the OMZ, the mean advective flows tend to transport DO in the opposite direction and both fluxes have the same order of magnitude, but the second one showed a larger seasonal variability, with minimum in fall and spring consistently with the seasonal variability observed in different metrics of the OMZ described above (Figure 4) and with the total DO budget (Figure 6). These results also show the relevance of the MEFs in ventilating the OMZ.

4. Discussion

The lack of observations of both dissolved oxygen and currents off central Chile has limited the ability to evaluate the relationship between the PCUC and the OMZ and to explore the role of other concurrent processes that may also contribute to modulate the OMZ in this region. Here, we used a coupled physical/biogeochemical model to tackle this problem. Although the model may have important limitations associated to uncertainties in the parameter values of the model parametrisations or to inaccurate representation of key biogeochemical processes taking place in the OMZ (Gutknecht, Dadou, Le Vu, et al., 2013), it provides a powerfull tool to explore quantitatively the diversity of forcing mechanisms associated to seasonal variability of the OMZ in a region where observations are crucially lacking.

The model assessment showed that the model has biases in both mean state and seasonality (Appendix). The extent to which the model bias could influence our results would require undertaking sensitivity experiments to a number of processes, which is beyond the scope of the present work. The improvement of the mean state could be achieved through using more realistic wind forcing in particular near the coastal region where along-shore winds of most products including scatterometer data are stronger than observed (cf. Astudillo et al., 2017) producing a cool bias near the coast. The realism of the model simulations could be also improved through tuning the biogeochemical parameters to the study region since the model parameters were originally best fitted for simulating the OMZ off Peru (see Montes et al., 2014; Table A1) (e.g. maximum growth rate of phytoplankton, hydrolysis rate of detritus, nitrification and anamox processes among others). On the other hand, an improvement of the seasonal variability would require to include river run-off and consider air-sea interacction at mesoscale (e.g. Oerder et al., 2018). Sediment processes, that can be very relevant for the dynamics of DO near the coast (Bianucci et al., 2012; Siedlecki et al., 2015), could be also included to improve the realism of the model in term of DO near the coast. Despite of these limitations, we consider that our regional ocean simulation is realistic enough for carrying out process studies focused on seasonal timescale.

Dissolved oxygen and salinity in the model simulation were spatially well correlated inside the OMZ and both co-varied simultaneously throughout the year. Most of the DO variability was associated with

Table 2
Amplitude, Phase, and Explained Variance (in %) of the Annual and SemiAnnual Harmonics of the DO Concentration and the Different Terms of equation (1) Integrated in the Omz, as Showed in Figure 6

	Annual harmonic			Semiannual harmonic		
	Amplitude	Phase	% explained	Amplitude	Phase	% explained
DO	4.3	10.6	82	1.3	8.2	8
∂DO/∂T	5.4e-7	6.7	47	4.2e7	5.0	27
PHYS	1.0e-6	8.4	43	8.2e-7	5.0	29
SMS	3.1e-7	6.3	90	5.9e-9	9.6	0
Xadv	1.1e-6	7.5	23	1.7e-6	5.1	64
Yadv	8.1e-8	3.3	0	6.8e-7	11.5	60
Zadv	5.6e-7	11.2	63	2.7e-7	10.8	15
Hmix	6.6e-9	6.1	36	6.5e-9	3.8	36
Vmix	1.2e-8	8.0	63	7.1e-9	3.2	23

Note. The physical term (*PHYS*) is the summed-up contribution of all advection and mixing terms. The advection terms are the zonal (*Xadv*), meridional (*Yadv*), and vertical (*Zadv*) advections. The biogeochemical fluxes (*SMS*) represents the "source minus sink" contribution to the rate of change of DO (∂DO/∂t) due to biogeochemical processes. The subgrid mixing terms are the summed-up contribution of the horizontal diffusion (*Hmix*) and vertical diffusivity (*Vmix*). The DO amplitude is in μM and the terms of the equation (1) are in μM/s. The phase indicates the month of the annual and (first) semiannual maximum.
Abbreviations: DO = dissolved oxygen; OMZ = oxygen minimum zone.

changes in water mass composition rather than with changes driven by biogeochemical processes. Nevertheless, according to our results those changes are not only driven by changes in the PCUC, as was firstly hypothesized, but by zonal advection and by eddy fluxes associated to mesoscale variability wich contribute to ventilate the OMZ. In the following we discuss in detail this and the rest of our main findings.

The seasonal cycles of the PCUC showed to be well correlated with all the metrics used here to characterize the OMZ (Figures 4 and 5) and also with several terms that are relevant in the DO budget of the OMZ (Figures 6a, 6b, 7f, 7h and 10f). Thus, our results support the interpretation that the variability of the PCUC is an important driver of the OMZ seasonal cycle. A striking feature of the seasonal cycle of the PCUC is its semi-annual variability. In fact, north of 36°S both the annual and semiannual harmonics of the undercurrent have about the same amplitude. This semi-annual variability was also evidenced in the metrics of the OMZ (Figures 4 and 5) and in the dominant advective terms in the DO budget of the OMZ (Figures 6a, 6b, 7f, 7h and 10f). For instance, the OMZ volume (DO concentration inside the OMZ) has two maxima (minima). This volume reaches the absolute minimum –and the DO concentration inside the OMZ reaches an absolute maximum– about one or two months after the PCUC southward transport reaches its absolute minimum. According to Pizarro et al. (2002) the semi-annual component of the PCUC seasonal cycle is of equatorial origin, while the annual harmonics results from a combination of equatorial and local wind forcing (see also Shaffer et al., 1999). Nevertheless, the seasonal variability of the alongshore wind varies in phase and amplitude along the west coast of South America, which may also introduce semi-annual variability in the PCUC. Off Peru these winds are maximum in winter, while off Chile they are more intense during spring and summer. Off northern Chile (between ~18°S and 25°S) the seasonal cycle is weaker and increases toward the central coast off Chile associated to the presence of an atmospheric coastal jet that develops in spring and summer (Muñoz & Garreaud, 2005). This jet migrates meridionally during the calendar year and thus may also induces semi-annual alongshore variability of central Chile (cf. Dewitte et al., 2008, their Figure 7a).

Table 3
Total Mean Values Inside the Oxygen Minimum Zone for the Period 2000–2008 and the Corresponding Standard Deviations for ∂Do/∂T and the Adv, Including the Xadv, Yadv, and Zadv Components Showed in Figures 6a and b (all values are in 10^{-6} μM/s)

	$\frac{\partial DO}{\partial t}$	*ADV*	*Xadv*	*Yadv*	*Zadv*
Mean (μM/s)	0.02	1.76	−4.43	3.84	2.35
SD (μM/s)	0.56	1.12	1.67	0.63	0.50
R^2 (%)	—	62	75	25	36

Note. The values of R^2 (explained variance in percentage) among ∂DO/∂t and the different advection terms are also shown.
Abbreviations: *ADV* = advection term; *Xadv* = zonal advection; *Yadv* = meridional advection; *Zadv* = vertical advection.

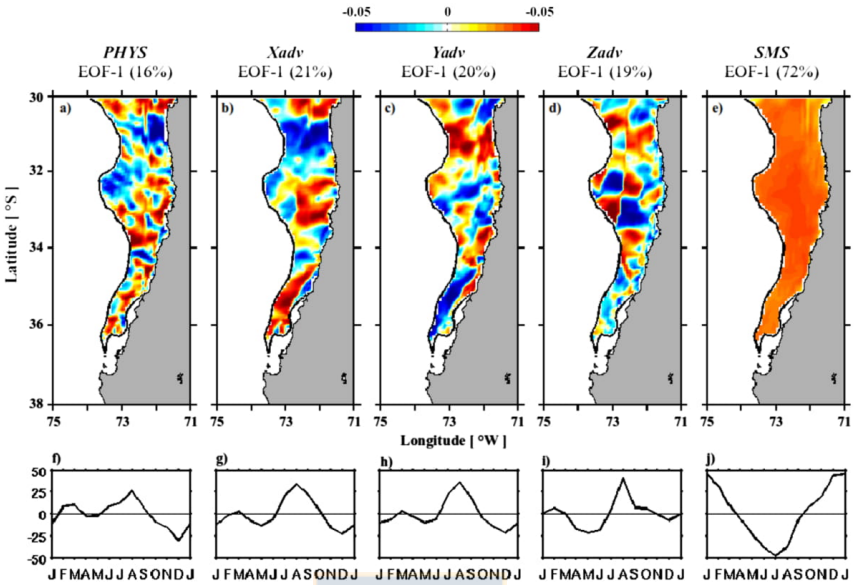

Figure 7. Spatial structure of the first EOF mode for *PHYS*, *Xadv*, *Yadv*, *Zadv* and *SMS* seasonal cycles averaged between the 26.4 and 26.8 kg m^{-3} isopycnals. The offshore extension of the domain in these calculations was given by the mean position of the 45 μM isopleth showed in Figure 1a). The explained variance for the first mode is indicated in the upper part of each panel. The bottom panels show the corresponding principal components associated with the first EOF patterns.

In contrast to the semi-annual variability observed in the different metrics representing the core of the OMZ, over the continental shelf the seasonal cycle of the oxycline, and oxygen concentration in the whole water column, is dominated by a single annual harmonic. There, the minimum depth of the oxycline coincides with the season of maximum upwelling-favorable winds (cf. Figure 5a). This is also observed off northern Chile between around 20°S and 24°S (e.g. Reyes et al., 2007, see their Figure 158). Thus, seasonal changes in DO over the continental shelf seem to be more tightly related to the annual upwelling cell than to the drivers that control DO in the OMZ core. Nevertheless, different ship-based, monthly, time series from northern and central Chile show also large month to month and interannual variability of the oxycline not well related to the local upwelling favorable winds, but to coastally trapped waves of equatorial origin, which may largely disturb the pycnocline, as well as the oxycline and the PCUC (Shaffer et al., 1997, Morales et al., 1999; Ulloa et al., 2001; Illig, Cadier, et al., 2018; Illig, Bachèlery, & Cadier, 2018). Thus, the dynamics of the OMZ over the continental shelf seems to be different from that described here for the core of the OMZ. The variability of DO over the continental shelf and its relationship with the coastal upwelling and the offshore OMZ was not specifically addressed in our study, because it would require a model with better spatial resolution to correctly represent the continental shelf and the biogeochemical processes taking place therein. e.g. a sediment compartment which our model did not incorporate.

Along with the alongshore advection, the cross-shore transport of DO plays also a key role in the seasonal cycle of the OMZ and so in the DO budget in our study region. This cross-shore or near zonal transport in the oceanic region was related to the presence of inserted zonal bands of positive and negative striations (Figure 4c). These striations have been observed in different regions of the global ocean through satellite altimetry (e.g. Maximenko et al., 2005), Argo float (Cravatte & Marin, 2012) and cruise data (Brandt et al., 2010), and have been reproduced in global and regional models (Belmadani et al., 2017; Nakano & Hasumi, 2005; Sinha & Richards, 1999). The presence of eastward and westward jets seems to result from the eddy field generated in the presence of planetary vorticity gradient and they efficiently develop near eastern boundaries

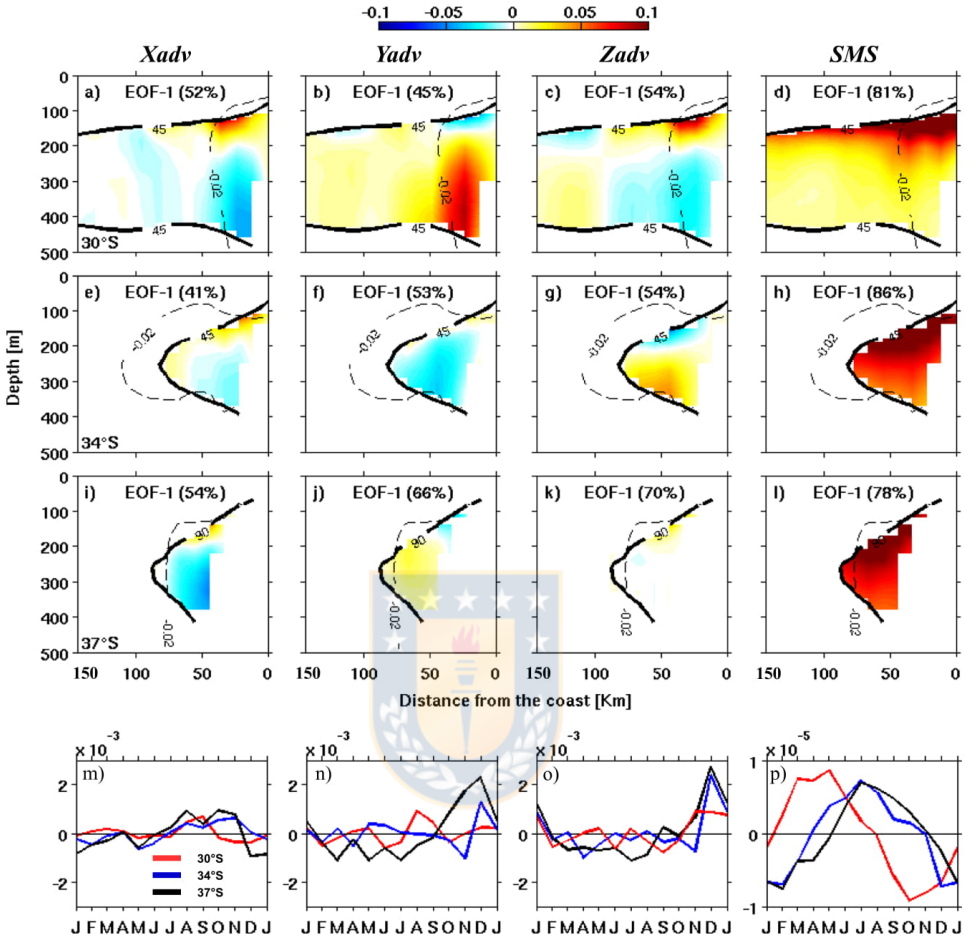

Figure 8. Offshore-vertical structure of the first EOF mode for *Xadv*, *Yadv*, *Zadv* and *SMS* seasonal cycles in three different sections (30°S, 34°S and 37°S) inside the OMZ. Solid and dashed black lines (in a-i) show the mean boundary of the OMZ and the PCUC (–0.02 m s^{-1}), respectively. The bottom panels show the principal components associated with the respective EOF patterns at 30°S (red), 34°S (blue) and 37°S (black).

related to particular coastal features (Belmadani et al., 2017; Davis et al., 2014). They may play also a role in ventilating the OMZs located at the eastern ocean boundaries as was shown for the tropical North Atlantic, where these meridionally alternating jets contribute to modulate the zonal advection of DO along the isopycnals surfaces at interannual and decadal timescales (e.g. Brandt et al., 2010; Hahn et al., 2017).

Our results suggest that this kind of zonal jets contribute as much as the PCUC to the transport of DO toward the OMZ and both play a major role controlling its seasonal cycle. These jets also shape the offshore boundary of the OMZ modulating its extension. Regions that are dominated by westward (eastward) velocities extend (reduce) the offshore distance of the OMZ boundary. Thus, these meridional jets add a dimension to the paradigm of PCUC-driven OMZ variability, which was the starting point of this study. On average,

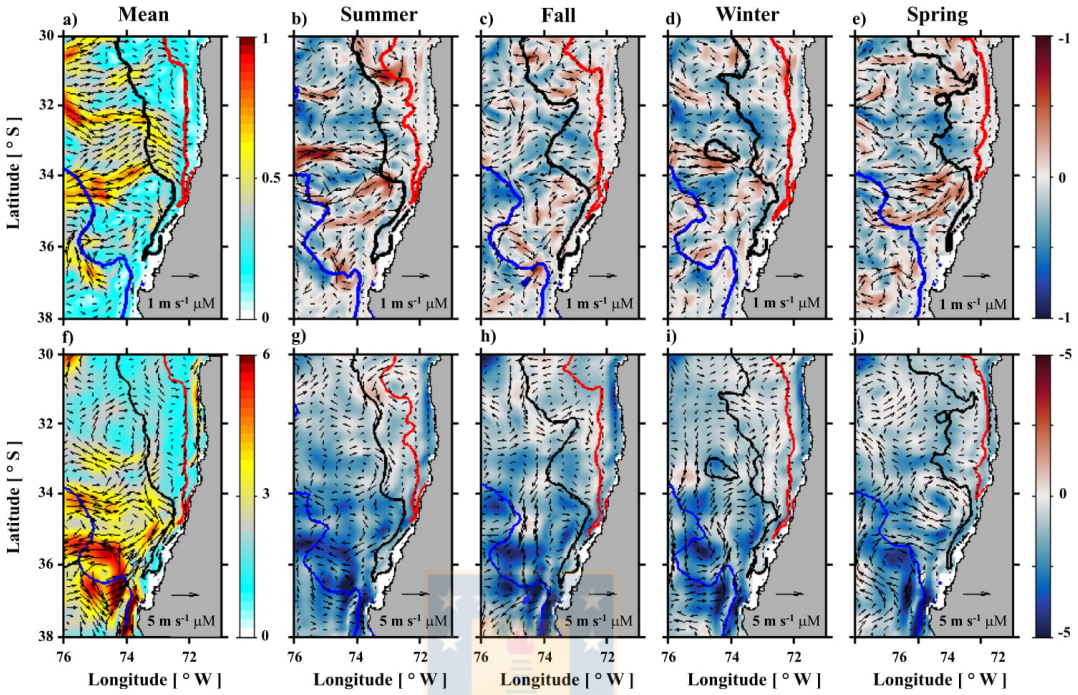

Figure 9. Mean and seasonal averaged DO fluxes integrated between the 26.4 and 26.8 kg m^{-3} isopycnals. The mesoscale eddy fluxes ($\mathbf{u}'DO'$) are depicted in the top panels (a-e), while the bottom panels (f-j) show the mean advective fluxes ($\langle\widetilde{\mathbf{u}}\widetilde{DO}\rangle$). Background color (in m s^{-1} μM) and arrows show the magnitude and direction of the fluxes, respectively. The red, black and blue contours show 45 μM, 60 μM and 90μM, respectively.

the zonal currents transport low oxygen waters offshore extending the OMZ, except during end of winter and beginning of spring (Figure 10f), when the zonal advection of DO is toward the OMZ, contributing along with the weakening of the PCUC to reduce the total volume occupied by the OMZ in the study region and to increase the DO concentration inside it. In contrast to the mean westward transport of DO due to the zonal advection, mesoscale eddies fluxes contribute, on average, to transport DO eastward, i.e. toward the OMZ, during all the year (Figure 10c) playing also a key role in the dynamics of the OMZ. A relevant uncertainty related to eddy fluxes results from the role of subsurface mesoscale eddies. Those eddies are ubiquitous in the study region (Colas et al., 2012; Combes et al., 2015; Hormazábal et al., 2013), and they are not well enough captured by satellite data nor *in situ* data which is too sparse to have a reliable quantification of them. The role of these subsurface eddies in the offshore transport of oxygen depleted waters and in the overall dynamics of the OMZ and on its biogeochemistry is poorly understood (e.g., Frenger et al., 2018). Recent studies from the west coast of South America have shown that the PCUC plays also a key role in the generation of subsurface mesoscale eddies (e.g. Thomsen et al., 2016). Thus, the PCUC contributes directly to the southward transport of oxygen depleted ESSW and indirectly to its offshore transport by promoting the generation of subsurface mesoscale eddies.

The above discussion calls for further investigation and sensitivity experiment with the model considering that the representation of mesoscale activity in the model is critically dependent on a number of parameters, including horizontal resolution and the way the air-sea interaction at mesoscale is taken into account. This may have a significant influence on the net primary production and thereby on oxygen content through export (see Renault et al., 2016). While sensitivity experiments would be important to investigate further

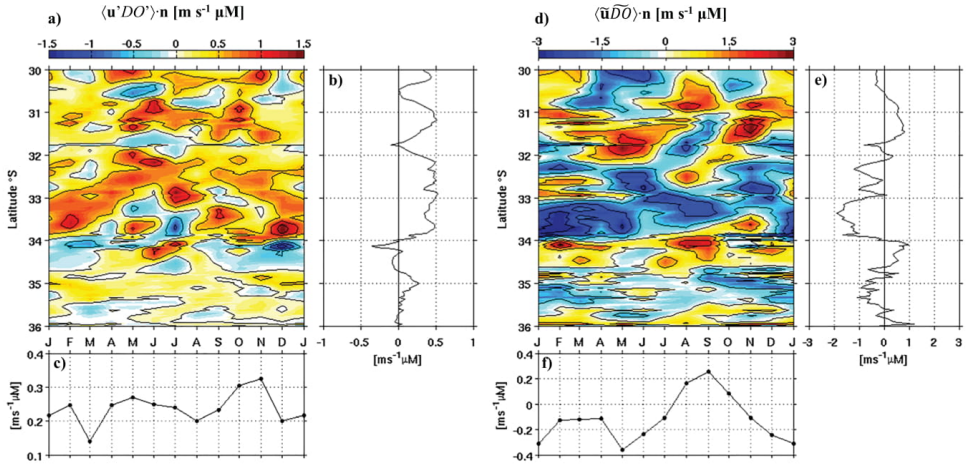

Figure 10. Seasonal cycle of the mesoscale eddy fluxes of DO (integrated between the 26.4 and 26.8 kg m^{-3} isopycnals) across the mean position of the 60 µM isoplethu'*DO*'·**n,** where **n** is a unitary horizontal vector perpendicular to the 60 µM isopleth showed in Figure 9 (a). The curve in (b) shows the averaged annual value at different latitudes. The curve in (c) shows the latitudinal averaged values for different months. The panels (d), (e) and (f) are similar to those showed above but for $\langle \tilde{\mathbf{u}}\tilde{DO}\rangle\cdot\mathbf{n}$.

the role of eddy activity in shaping the OMZ off Central Chile, as a preliminary step, it may be necessary to consider other processes important in our study region. In particular, the biogeochemical model used here tends to overestimate the DO near the coast, which has been also observed off Peru for this particular model (Montes et al., 2014; Vergara, Dewitte, et al., 2016). Such a bias may be detrimental for our conclusions on the role of the PCUC on the OMZ variability since, in our study region, DO concentration is sensitive to the amount of oxygen advected southward along the slope by the PCUC. Sensitivity experiments to the northern boundary conditions of the domain considered here (i.e. 30°-38°S) may thus be necessary to evaluate the extent to which the amount of DO is critical for explaining the OMZ seasonal fluctuations. Another approach would be to tune the biogeochemical model for the study region considering that the model configuration used in our study was calibrated for the tropical part of the OMZ (Montes et al., 2014), and no specific calibration was performed to improve comparison among model outputs and observations off central Chile. In particular, in different OMZs the biogeochemical BioEBUS model was shown to be highly sensitive to the rate of organic matter decomposition and its vertical distribution (as well as to the sinking rate of particles; Gutknecht, Dadou, Le Vu, et al., 2013). Finally, it is worth noting that sediment processes, that can be relevant for the dynamics of DO near the coast (Bianucci et al., 2012; Siedlecki et al., 2015), are not included here, although sediment may act as an important sink of DO near the coast. Future work will need to consider these improvements in the model setup in order to refine our estimate of the physical control of the OMZ by the PCUC and eddy activity.

5. Summary and conclusions

A high resolution coupled physical-biogeochemical model was used to assess the seasonal variability of the southern tip of the Southeastern Pacific OMZ between 30°S and 38°S. The model was able to capture relatively realistically the mean structure of the OMZ and its spatial and temporal variability in the study region, although DO is somewhat overestimated near the coast and the very southern tip. We used different metrics to characterize the seasonal variability of the OMZ: (1) The amplitude of the typical seasonal variability of DO concentration inside the OMZ itself (i.e. inside the volume enclosed by the isosurface of DO = 45 µM) is about 2 µM (about 7% of the mean DO), with larger values in austral spring. (2) The mean volume of the OMZ between 30°S and 38°S was ~4×10^4 km^3 changing annually by ~25%, from 4.5 ×10^4 km^3 during

early austral winter to 3.5 $\times 10^4$ km^3 in austral spring. Thus, we can conclude that the amplitude of the seasonal cycle of the OMZ is relatively weak. However, south of 35°S the volume of the OMZ is reduced, DO increases rapidly and seasonality becomes more relevant. The OMZ volume and its seasonal variability is highly correlated to subsurface waters with high salinity (salinity >34.5) in the study region consistent with the common idea that the OMZ is closely related to the warm, salty and nutrient rich ESSW.

Our analyses suggest that there is a close relationship between the PCUC transport variability and the seasonal cycle of OMZ. Intense poleward transport by the PCUC is related to a larger OMZ volume off south-central Chile. However, this modulation would not be homogeneous alongshore due to other simultaneous processes such as disturbances in the transport by the meridionally alternating jets and eddy activity. These processes play also a role in shaping the mean characteristics of the OMZ, including changes observed in the offshore extension of the OMZ at different latitudes and the alongshore rate of decreasing of its volume. In addition, by evaluating the DO budget, it was determined that advective terms (*ADV*) are the main contributors (~90%) to the rate of change of DO, while subgrid mixing and biogeochemical (SMS) terms play a minor role in the seasonal variability of the OMZ off Chile. The seasonal cycle of these advective terms showed large mesoscale variability in the OMZ region, consistent with the significant contribution of non-linear advection, and accordingly, it was shown that mesoscale fluxes of DO play also a significant role in the seasonal variability of the OMZ.

Appendix: Model assessment

In this section we assess the model's realism in terms of the mean state and seasonal cycle of the OMZ. Many aspects of the circulation have been previously validated using remote and in situ observations in Dewitte et al. (2012) with a main focus on mean state and interannual variability (e.g., SST, EKE, the Peru Chile Undercurrent) off Peru. Vergara et al. (2017) complemented this assessment by validating the thermocline depth, EKE, coastal currents and sea level anomalies over the whole model domain. The coupled

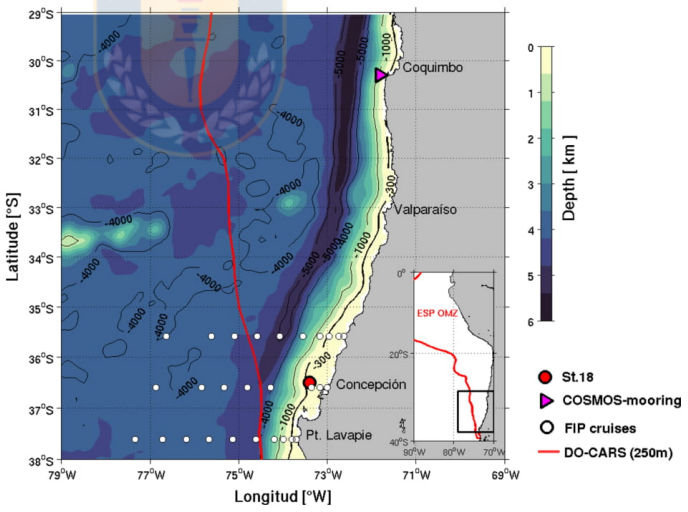

Figure A1. Geographic locations of in-situ data used for ROMS/BioEBUS model validation. The red dot shows the position of the time-series station over the continental shelf (36°30′S). The white dots show the hydrographic stations visited by the FIP cruises during Nov-2004, Dec-2005, Oct-2006 and Mar-2008. The current-meter mooring located over the upper slope (~1000 m total depth) near 30°S is shown by the magenta triangle. The inset shows the eastern South Pacific Oxygen Minimum Zone where the red contour represents the climatological isopleth of 45 μM of DO at 250 m depth obtained from CARS 2009 climatology.

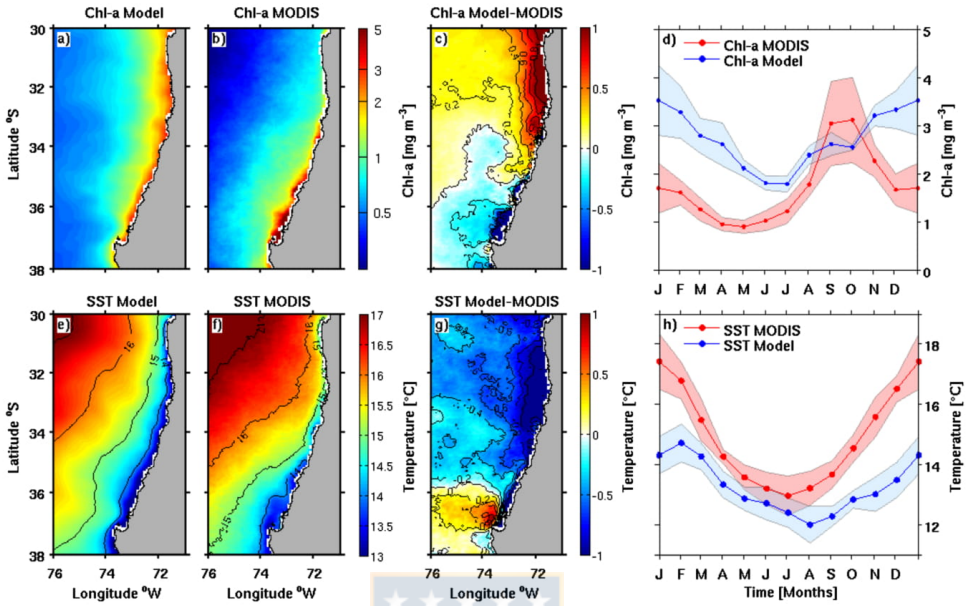

Figure A2. Annual mean and seasonal cycle of the chlorophyll-a (Chl-a) (top panels) and sea surface temperature (SST) (bottom panels) for both ROMS/BioEBUS and MODIS based on the 2003-2008 period. For Chl-a (mg m^{-3}, note that the log scale). The biases in (c) and (g) represent the difference between the ROMS/BioEBUS model and MODIS data. The seasonal cycles showed in (d) and (h) were estimated in a coastal band (first 80 km) extending from 30°S to 38°S. The blue (red) line show the model (MODIS) averages. Shaded areas show the corresponding standard deviations.

ROMS/BioEBUS simulation has been evaluated by Montes et al. (2014) and Vergara, Dewitte, et al. (2016), also with an emphasis in the OMZ off Peru. Here we focused our assessment off central Chile from 30°S to 38°S, which comprises our study region. Figure A1 shows the study region and the positions of several oceanographic stations and a currentmeter mooring located over the slope (at 1000 m total depth) near 30°S used for the model assessment.

Sea Surface Temperature and Chlorophyll-a

Monthly SST and Chl-a data from MODIS-Aqua satellite were used to evaluate the model skills in reproducing the observed mean fields and seasonal cycles of these variables (Figure A2). The model reproduces the main features of the observed SST and Chl-a mean fields. Near the coast and north of 34°S the model showed larger mean values of Chl-a than the observations, while south of 35°S the model values were a bit underestimated. The coastal SST was about 0.8°C to 1°C colder in the model, which is largely due to an overestimation of the coastal winds used in the forcing (Astudillo et al., 2019). In the offshore region the differences between model and observed mean fields were, in general, much smaller than the differences observed near the coast (Figure A2c and g). The seasonal cycle of the SST near the coast (first 80 km) showed also important differences with the observations. Consistently with the coastal cold bias associated to a stronger upwelling rate than that observed, the model overestimates Chl-a during most of the year. It does not reproduce an observed increase of Chl-a in austral spring as shown by observations (Figure A2d). In contrast to the coastal region, the model and observed seasonal cycles of Chl-a and SST were rather similar offshore. The larger Chl-a and the lower SST observed in the model simulation near the coast may be associated with an overestimation of upwelling, which may be,

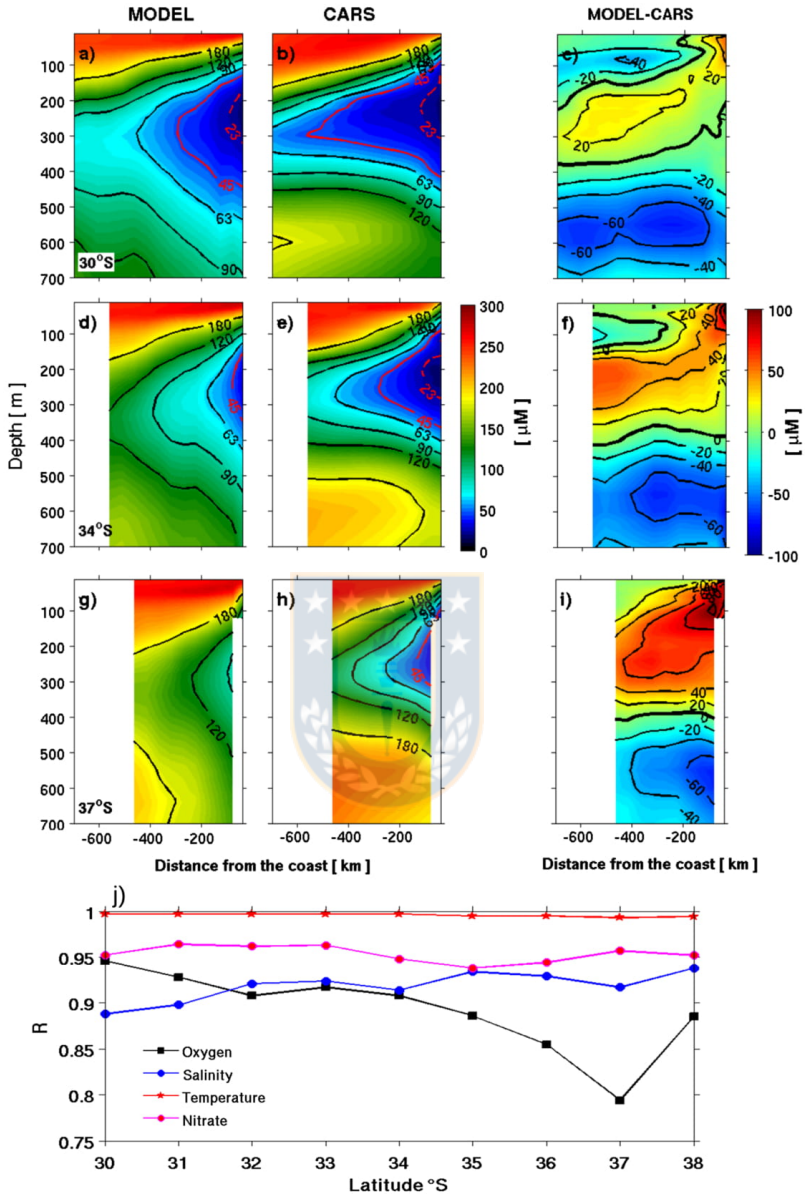

Figure A3. Mean DO based on ROMS/BioEBUS model (left column) and CARS climatology (central column) at three cross-shore sections: 30° (first row), 34° (second row) and 37°S (third row) between surface and 700m depth and from the coast to ~500km offshore. The right column shows the difference between ROMS/BioEBUS model and CARS (positive values indicate an overestimation of DO by the model). The spatial correlation between modeled and CARS sections at different latitude are shown in the bottom panel. There, we have included oxygen (black), salinity (blue), temperature (red) and nitrate (magenta).

in turn, related to an overestimation of the wind stress near the coast when satellite-based winds are used. Experiments carried out by one of the authors showed that coastal SST is more realistic when a shoreward decrease of the wind stress near the coast is considered. This may also have an impact on net primary production and thereby on the export production and oxygen inventory (see Renault et al., 2016). Presently, we are working with a new coupled ROMS/BioEBUS simulation to evaluate the response of Chl-a when a realistic wind drop-off near the coast is considered.

Vertical structure of the variables and water masses

To evaluate the model ability to represent the mean vertical structure of temperature, salinity, DO and nitrate we use the CARS climatology as a benchmark. Noteworthy, oxygen data are rather scarce in the study region and the oxygen climatology from CARS may have also limitations, which should be kept in mind. The Figure A3 shows zonal sections of DO at 30°S, 34°S and 37°S. The model exhibits marked biases consisting mostly in a sea-sow pattern resulting from an overestimation of DO in the core and an underestimation below the OMZ (Figures A3c, A3f, A3i). Despite this mean bias, the model is able to simulate realistically its mean depth and the positions of the upper and lower oxyclines, but the offshore extension of the OMZ (bounded by the isopleth of 45 μM in our study) is much smaller in the model than in CARS. The simulated vertical gradients of DO in the upper and lower oxyclines are also smaller than the observed ones, particularly in the lower part of the OMZ. The overestimation of DO is more pronounced in the southern part of the study region and may exceed ~70 μM close to the coast. This misfit is analyzed further by comparing the model outputs and the data at a coastal site located at 36°30′S. Spatial correlation between model and CARS (using zonal sections that expand from the surface and 700 m depth and from the coat and 80°W) at different latitudes indicates a general good agreement for salinity, temperature and nitrate (figures not shown). Nevertheless, nitrate showed a large bias (5-10 μM) near the coast, between surface and 200 m depth. For temperature, salinity and nitrate the spatial correlations between simulated and CARS variables were larger than ~0.85 at all latitudes (Figure A3j), while for DO, the correlations tend to decrease southward reaching the lowest value ($r = 0.79$) at 37°S. Model T-S diagrams were also compared with those from CARS in the first 200 km and from the surface to 1500 m depth. The core of the OMZ in the model coincides with a salinity maximum centered around the 26.5 kg m^{-3} isopycnal surface and is consistent with CARS based T-S diagrams (Figure A4). Despite the model underestimating the salinity maximum related to ESSW and overestimating the salinity minimum related to AAIW (i.e ESSW is less salty and AAIW is saltier in the model) it reproduces reasonably well the subtropical water masses structure around the OMZ, namely: Subantarctic Water, Equatorial Subsurface Water and Antarctic Intermediate Water (Figure A4).

Seasonal cycle of DO at 36°30′S

We used cruise data at 36°30′S to evaluate the seasonal cycle of the model DO in the southern tip of the OMZ near the coast (Figure A5). Since September 2002 a monthly, ship-based time series has been maintained over the continental shelf (~90 m depth) at 36°30′S by the University of Concepcion (e.g. Escribano et al., 2012; Escribano & Schneider, 2007). The data were depth-averaged over the whole water column (between 0 and 90 m depth) and a seasonal cycle was estimated over the period 2003-2015 for the observations and 2000-2008 for the model data. The comparison indicates that the model has skill in simulating the seasonal variability of DO, both amplitude and phase. Negative DO anomalies are observed during the upwelling season in austral spring and summer and positive ones during fall and winter. While both seasonal cycles were well correlated ($r = 0.85$), the amplitude of the simulated annual harmonic was somewhat smaller (32.5μM) than that from the observations (44.5μM).

Comparison of model and observed *in situ* DO

Cruise data offers the opportunity to compare some mesoscale features that are relevant for our study and that are not present in a climatology like CARS. Firstly, we compare the simulated vertical structure of DO and alongshore velocities with *in-situ* data (and geostrophic velocity) in a zonal transect at 35.5°S carried out during November 21, 2004 (Figure A6). During that month the model and the observations showed a mesoscale eddy at that latitude (our simulation did not assimilate observations, so it is expected that mesoscale eddies do not coincide in space and time). The model reproduced fairly well both the magnitude and vertical structure of DO related to mesoscale eddies, and the alongshore velocities also were consistent with observations, although concentrations of DO were overestimated by ~20-30 μM at the core of the OMZ.

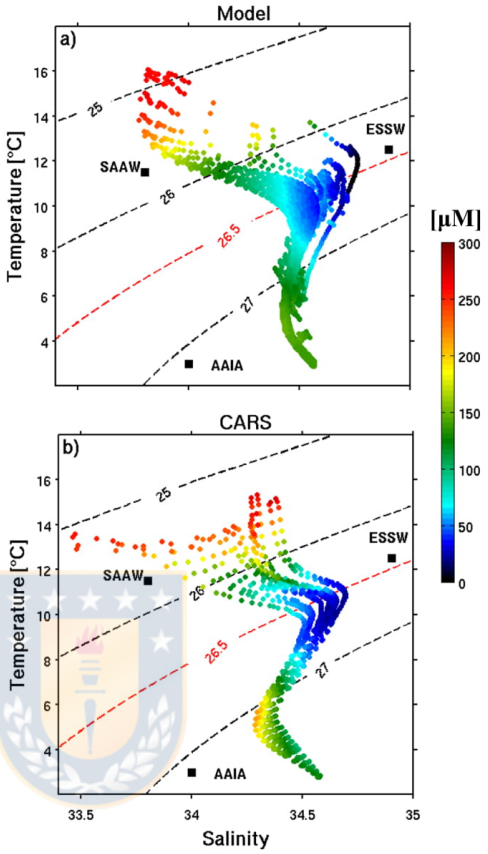

Figure A4. T-S-DO diagrams for ROMS/BioEBUS model (a) and CARS climatology (b). Only water encompassing the region within the first 200 km from the coast and from the surface to 1500 m depth in whole domain were considered. DO (in µM) is represented by color. The Surface Subantarctic Water (SAAW, 11.5°C; 33.8), Equatorial Subsurface Water (ESSW, 12.5°C; 34.9) and Antarctic Intermediate Water (AAIW, 3°C; 34) are shown. The corresponding values of temperature and salinity to each water mass is indicated between parenthesis. These values were obtained from Silva et al. (2009).

Below 500 m depth DO was underestimated by ~50 µM. As shown above (A.3) the simulated AAIW has relatively high oxygen and low salinity below ~500 m depth. The comparison of the T-S diagrams near the coast (first 200 km) corroborates that observed in Section A.2 using CARS data and the whole period (compare Figures A6 and A4).

We use also cruise data to evaluate the vertical oxygen structure near the continental slope, where the oxycline is more intense. We considered DO profiles between 0 and 600m depth from two different sites (35.5°S; 73.2°W and 37.5°S; 74.0°W). The observations (and model profiles) were obtained in November- 2004, December-2005, October-2006 and March-2008. The Figure A7 shows a comparison between the different profiles at both sites. As mentioned before, the model reproduces the OMZ, but it shows, in general, larger values of DO than the observations, while below the OMZ the model underestimates DO by ~16 µM at 35.5°S

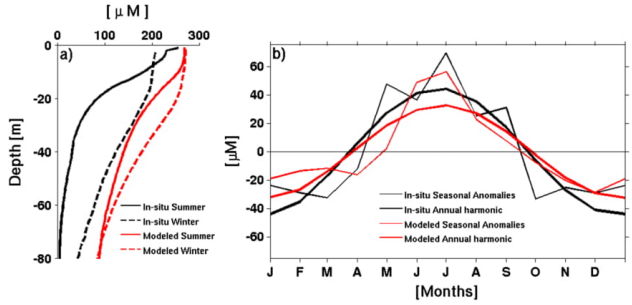

Figure A5. Mean profiles of DO for summer and winter (a) and seasonal anomalies of DO averaged from surface to 80 m depth (b) over the continental shelf at ~36.5°S (location of the time series maintained by University of Concepcion) for both ROMS/BioEBUS model and in-situ data. In (a) the black lines represent *in situ* data and the red line the model ones. Solid curves are for summer and dashed curves for winter. In (b) the thin black curve shows the seasonal cycle of DO anomalies and the red thin line the DO anomalies based on the model results. Thick lines show the corresponding annual harmonics.

and 19 µM at 37.5°S. The upper oxycline is relatively well reproduced, except during 2005 at 37.5°, when a very sharp and unusually deep upper oxycline was observed. In contrast, the lower oxycline was, in general, smoothed resulting in a large bias between modeled and observed DO.

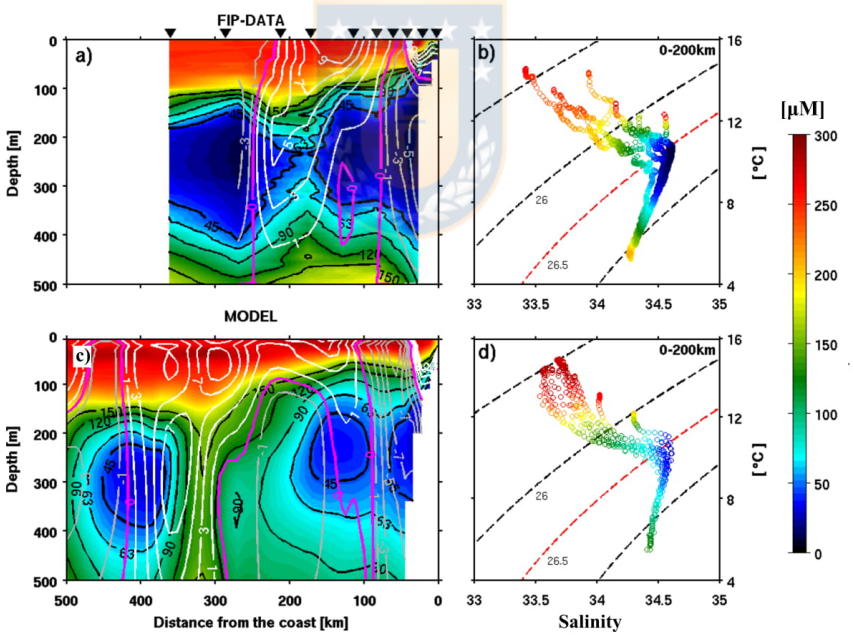

Figure A6. Cross-shore sections of DO and meridional geostrophic velocity (a and c), and T-S-DO diagrams (b and d) for both ROMS/BioEBUS model and *in situ* data. The *in situ* data were collected during November 2004 (for more detail see FIP cruise Letelier et al., 2009; and Section 2.1). In (a) and (c) the background colors show DO (in µM) and the white (grey) contours indicate northward (southward) flow. The magenta contours indicate zero velocity. The T-S-DO diagrams are represented in (b) for *in-situ* data and in (d) for the model. The T-S-DO are representative of the first 200 km from the coast. Colors in the T-S-DO diagrams show DO.

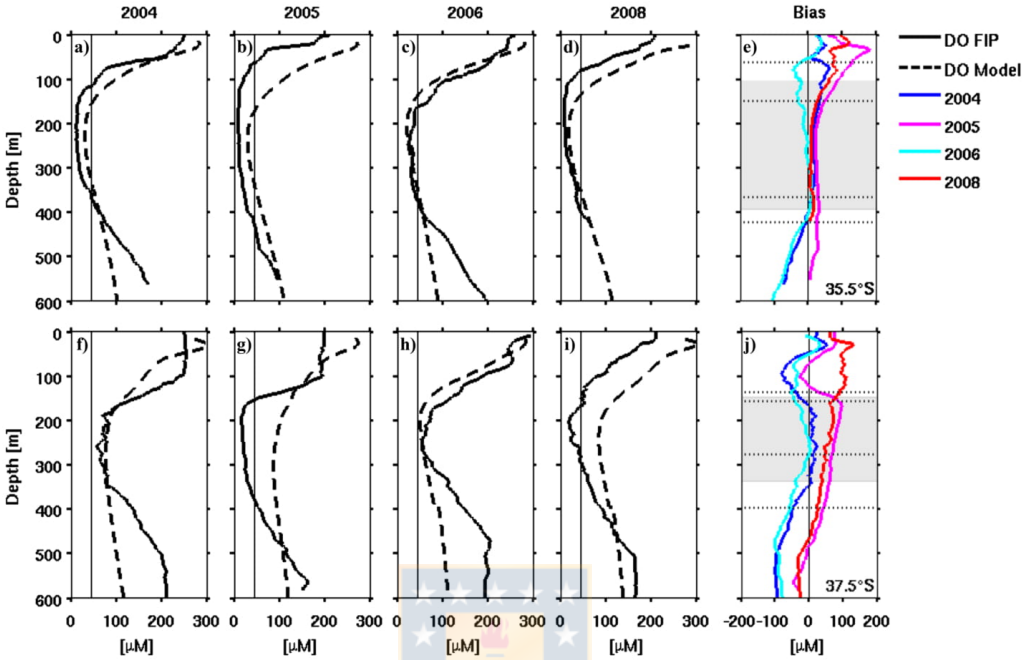

Figure A7. Vertical DO distribution near the continental slope at two different positions: 35.5°S; 73.2°W (top panels) and 37°S; 74°W (bottom panels) during spring-summer for both ROMS/BioEBUS and *in situ* data. The *in situ* (model) DO is represented by solid (dashed) lines. The biases (Figures e and j) are represented as the difference between ROMS/BioEBUS and *in situ* data. Different years are represented by the different colors. The gray area represents the mean position of the observed OMZ and the dashed black lines show the standard deviation of the depth of the upper and bottom boundaries of the OMZ.

The PCUC near 30°S

To assess the ability of the model in reproducing the vertical structure and seasonal variability of the PCUC, we used data from a current-meter mooring located over the slope at ~1000 m total depth near

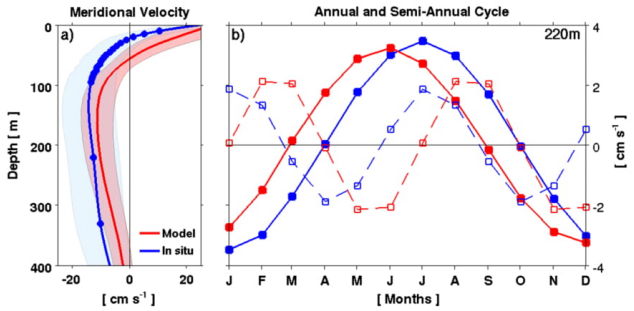

Figure A8. A comparison of the observed and model Peru-Chile Undercurrent (PCUC). Mean vertical profiles of the observed (blue solid line) and model (red solid line) alongshore currents at 30°S (a). The standard deviation of the observed and model current is shown by the shaded areas. Annual and semi-annual harmonics of the observed (blue) and model (red) alongshore current at 220m depth, near the core of the PCUC (b).

30°S (cf. pink triangle in Figure A1). The data used here expand only from 2003 to 2006 to include a period where an ADCP was present in the mooring. The ADCP (an RDI workhorse 300 kHz) was located at 120 m depth (upward-looking) with a vertical resolution of 4 m. In addition, the mooring had 4 punctual Aanderaa RCM 8 currentmeters located at 220 m, 330 m, 480 m and 750 m depth. As we are interested here in the seasonal cycle, the original hourly data were monthly averaged and then used to estimate a mean vertical profile and typical annual variability (Figure A8). The seasonal cycle of the current at 220m (near the PCUC core) was estimated by averaging monthly values from 2003 to 2006. In general, the PCUC shows very large intraseasonal variability at this site [cf. Pizarro et al., 2002, their Figure 3] and consistent semi-annual and annual fluctuations. The mean profile of the model PCUC in the same location is somewhat deeper and weaker than the observed one (Figure A8a), resulting in a small vertical shear near the upper 100 m. The variability, based on monthly means, is also smaller in the model PCUC (shaded areas in Figure A8b). Here, we compare also the annual and semi-annual harmonics of the current at 220m (Figure A8b). The amplitudes of both harmonics are well reproduced by the model, but the harmonics are lagged by 1-month. Despite, the fact that the model slightly underestimates a bit the magnitude of the mean PCUC in this location, the total transport at this latitude is rather similar to the transport estimated using *in situ* currents and hydrography (see main text).

Acknowledgments

MP-K was supported by a Doctoral Scholarship from CONICYT (Ministry of Education, Chile). This study was partial funded by the FONDECYT projects: 11811872 leaded by OP, 1140845 leaded by MR and 1151185 leaded by BD. BD acknowledges support from Fondecyt (project 1190276). Funds from the Instituto Milenio de Oceanografia, Chile (ICM grant IC 120019), COPAS Sur-Austral CONICYT PIA APOYO CCTE AFB170006 and project CRN3070-IAI (US national science Foundation; grant GEO-11280040), and the financial support for MP-K internships at LEGOS and IGP from the REDOC.CTA (Red Doctoral en Ciencia, Tecnología y Ambiente, University of Concepción, Chile) are also acknowledged. BD, OP and MR also acknowledge supports from FONDECYT 1171861. The university of Concepcion and the "Fondo de Investigación Pesquera" (FIP; MOBIO-BIO program) provided *in situ* data. The authors acknowledge: MODIS-Aqua for providing SST and chlorophyll satellite data (http://oceancolor.gsfc.nasa.gov); AVISO for altimeter products (http://marine.copernicus.eu); CARS for climatological data (www.marine.csiro.au/~dunn/ cars2009/). Cruise data used in Figures A5, A6 and A7 and mooring data used in Figure A8 are freely available under request to the Chilean National Center for Hydrographic and Oceanographic Data (Centro Nacional de Datos Hidrográficos y Oceanográficos de Chile; http://www.shoa.cl/n_cendhoc/). ROMS model code is available at http://www.croco-ocean.org. All input data set and configuration of our ROMS/BIOEBUS simulations are described in section and in the references therein. This work was granted access to the HPC resources of CALMIP supercomputing center at the Toulouse University under the allocations 2017-1044 and 2018-1044.

References

Aguirre, C., Garreaud, R., & Rutllant, J. (2014). Surface ocean response to synoptic-scale variability in wind stress and heat fluxes off south-central Chile. *Dynamics of Atmospheres and Oceans*, *65*, 64–85. https://doi.org/10.1016/j.dynatmoce.2013.11.001

Aguirre, C., Pizarro, O., Strub, P. T., Garreaud, R., & Barth, J. (2012). Seasonal dynamics of the near-surface alongshore flow off central Chile. *Journal of Geophysical Research*, *117*, C01006. https://doi.org/10.1029/2011JC007379

Astudillo, O., Dewitte, B., Mallet, M., Frappart, F., Rutllant, J. A., Ramos, M., et al. (2017). Surface winds off Peru-Chile: Observing closer to the coast from radar altimetry. *Remote Sensing of Environment*, *191*, 179–196. https://doi.org/10.1016/j.rse.2017.01.010

Astudillo, O., Dewitte, B., Mallet, M., Rutllant, J. A., Goubanova, K., Frappart, F., et al. (2019). Sensitivity of the near-shore oceanic circulation off Central Chile to coastal wind profiles characteristics. *Journal of Geophysical Research: Oceans*, *124*, 4644–4676. https://doi.org/10.1029/2018JC014051

Bakun, A., & Nelson, C. S. (1991). The seasonal cycle of wind-stress curl in subtropical eastern boundary current regions. *Journal of Physical Oceanography*, *21*, 1815–1834. https://doi.org/10.1175/1520-0485(1991)021<1815:TSCOWS>2.0.CO;2

Belmadani, A., Concha, E., Donoso, D., Chaigneau, A., Colas, F., Maximenko, N. A., & Di Lorenzo, E. (2017). Striations and preferred eddy tracks triggered by topographic steering of the background flow in the eastern South Pacific. *Journal of Geophysical Research: Oceans*, *122*, 2847–2870. https://doi.org/10.1002/2016JC012348

Bettencourt, J. H., López, C., Hernández-García, E., Montes, I., Sudre, J., Dewitte, B., et al. (2015). Boundaries of the Peruvian Oxygen Minimum Zone shaped by coherent mesoscale dynamics. *Nature Geoscience*, *8*, 937–940. https://doi.org/10.1038/ngeo2570

Bianucci, L., Fennel, K., & Denman, K. L. (2012). Role of sediment denitrification in water column oxygen dynamics: comparison of the North American East andWest Coasts. *Biogeosciences*, *9*, 2673–2682. https://doi.org/10.5194/bg-9-2673-2012

Brandt, P., Hormann, V., Kortzinger, A., Visbeck, M., Krahmann, G., Stramma, L., et al. (2010). Changes in the ventilation of the oxygen minimum zone of the Tropical North Atlantic. *Journal of Physical Oceanography*, *40*, 1784–1801. https://doi.org/10.1175/2010JPO4301.1

Chaigneau, A., Dominguez, N., Eldin, G., Vasquez, L., Flores, R., Grados, C., & Echevin, V. (2013). Near-coastal circulation in the Northern Humboldt Current System from shipboard ADCP data. *Journal of Geophysical Research: Oceans*, *118*, 5251–5266. https://doi.org/10.1002/jgrc.20328

Codispoti, L. A. (1989). Phosphorus vs. nitrogen limitations of new andexport production. In W. H. Berger et al. (Eds.), Productivity of the ocean: Present and past (p. 377–394). Wiley.

Colas, F., McWilliams, J. C., Capet, X., & Kurian, J. (2012). Heat balance and eddies in the Peru-Chile current system. *Climate Dynamics*, *39*(1–2), 509–529.

Combes, V., Hormazábal, S., & Di Lorenzo, E. (2015). Interannual variability of the subsurface eddy field in the Southeast Pacific. *Journal of Geophysical Research: Oceans*, *120*, 4907–4924. https://doi.org/10.1002/2014JC010265

Cravatte, S., Kessler, W. S., & Marin, F. (2012). Intermediate zonal jets in the tropical Pacific Ocean observed by Argo floats. *Journal of Physical Oceanography*, *42*(9), 1475–1485. https://doi.org/10.1175/JPO-D-11-0206.1

da Silva, A. M., Young, C. C., & Levitus, S. (1994). *Atlas of Surface Marine Data 1994, vol. 1, Algorithms and Procedures, NOAA Atlas NESDIS* (Vol. 6, p. 83). NOAA, Silver, Spring, Md.

Davis, A., Di Lorenzo, E., Luo, H., Belmadani, A., Maximenko, N., Melnichenko, O., & Schneider, N. (2014). Mechanisms for the emergence of ocean striations in the North Pacific. *Geophysical Research Letters*, *41*, 948–953. https://doi.org/10.1002/2013GL057956

Dewitte, B., Purca, S., Illig, S., Renault, L., & Giese, B. (2008). Low frequency modulation of the intraseasonal equatorial Kelvin wave activity in the Pacific ocean from SODA: 1958–2001. *Journal of Climate*, *21*, 6060–6069.

Dewitte, B., Vazquez-Cuervo, J., Goubanova, K., Illig, S., Takahashi, K., Cambon, G., et al. (2012). Change in El Niño flavours over 1958–2008: Implications for the long-term trend of the upwelling off Peru. *Deep Sea Research Part II: Topical Studies in Oceanography*, *77-80*, 143–156. https://doi.org/10.1016/j.dsr2.2012.04.011

Emery, W. J., &Thomson, R. E. (2004). *Data Analysis Methods in Physical Oceanography* (2nd Ed.). New York: Elsevier BV.

Escribano, R., Hidalgo, P., Fuentes, M., & Donoso, K. (2012). Zooplankton time series in the coastal zone off Chile: Variation in upwelling and responses of the copepod community. *Progress in Oceanography*, *97-100*, 174–186. https://doi.org/10.1016/j.pocean.2011.11.006

Nakano, H., & Hasumi, H. (2005). A series of zonal jets embedded in the broad zonal flows in the Pacific obtained in eddy-permitting ocean general circulation models. *Journal of Physical Oceanography*, *35*, 474–488.
Naqvi, S. W. A., Bange, H. W., Farias, L., Monteiro, P. M. S., Scraton, M. I., & Zhang, J. (2010). Marine hypoxia/anoxia as a source of CH4 and N2O. *Biogeosciences*, *7*, 2159–2190. https://doi.org/10.5194/bg-7-2159-2010
NASA Goddard Space Flight Center, Ocean Ecology Laboratory, Ocean Biology Processing Group; (2014): Sea-viewing Wide Field-of-view Sensor (SeaWiFS) Ocean Color Data. NASA OB.DAAC. doi: https://doi.org/10.5067/ORBVIEW-2/SEAWIFS_OC.2014.0
Niemeyer, D., Kemena, T. P., Meissner, K. J., & Oschlies, A. (2017). A model study of warming-induced phosphorus-oxygen feedbacks in open-ocean oxygen minimum zones on millennial timescales. *Earth System Dynamics*, *8*(2), 357–367. https://doi.org/10.5194/esd-8-357-2017
Oerder, V., Colas, F., Echevin, V., Masson, S., & Lemarié, F. (2018). Impactsof the mesoscale ocean-atmosphere coupling on the Peru-Chile ocean dynamics:The current-induced wind stress modulation. *Journal of Geophysical Research:Oceans*, *123*, 812–833. https://doi.org/10.1002/2017JC013294
Paulmier, A., & Ruiz-Pino, D. (2009). Oxygen minimum zones (OMZs) in the modern ocean. *Progress in Oceanography*, *80*(3–4), 113–128. https://doi.org/10.1029/j.pocean.2008.08.001
Paulmier, A., Ruiz-Pino, D., Garçon, V., & Farias, L. (2006). Maintaining of the East South Pacific Oxygen Minimum Zone (OMZ) off Chile. *Geophysical Research Letters*, *33*, L20601. https://doi.org/10.1029/2006GL026801
Pizarro, O., Clarke, A. J., & Van Gorder, S. (2001). El Niño sea level and currents along the South American coast: Comparison of observations with theory. *Journal of Physical Oceanography*, *31*, 1891–1903. https://doi.org/10.1175/1520-0485(2001)031<1891:ENOSLA>2.0.CO;2
Pizarro, O., Shaffer, G., Dewitte, B., & Ramos, M. (2002). Dynamics of seasonal and interannual variability of the Peru-Chile Undercurrent. *Geophysical Research Letters*, *29*(12), 1581. https://doi.org/10.1029/2002GL014790
Ramos, M., Pizarro, O., Bravo, L., & Dewitte, B. (2006). Seasonal variability of the permanent thermocline off northern Chile. *Geophysical Research Letters*, *33*(9), L09608. https://doi.org/10.1029/2006GL025882
Renault, L., Deutsch, C., Mc Williams, J. C., Frenzel, H., Liang, J. H., & Colas, F. (2016). Partial decoupling of primary productivity from upwelling in the California Current System. *Nature Geoscience*, *9*, 505–508. https://doi.org/10.1038/NGEO2722
Renault, L., Dewitte, B., Falvey, M., Garreaud, R., Echevin, V., & Bonjean, F. (2009). Impact of the atmospheric coastal jet off central Chile on sea surface temperature from satellite observations (2000–2007). *Journal of Geophysical Research*, *114*, C08006. https://doi.org/10.1029/2008JC005083
Resplandy, L.,Lévy, M., Bopp, L., Echevin, V., Pous, S., Sarma, V. V. S. S., & Kumar, D. (2012). Controlling factors of the oxygen balance in the Arabian Sea'sOMZ. *Biogeosciences*, *9*(12), 5095–5109. https://doi.org/10.5194/bg-9-5095-2012
Reyes, H., Letelier, J.,Pizarro, M.,Catasti, V. (2007). Monitoreo de lascondiciones bio-oceanográficas entre la I y IV. regiones, año 2006. IFOP Proyecto FIP 2006-01. Octubre 2007.
Schunck, H., Lavik, G., Desai, D. K., Großkopf, T., Kalvelage, T., Löscher, C. R., et al. (2013). Giant Hydrogen Sulfide Plume in the Oxygen Minimum Zone off Peru Supports Chemolithoautotrophy. *PLoS ONE*, *8*(8), e68661. https://doi.org/10.1371/journal.pone.0068661
Shaffer, G., Hormazábal, S., Pizarro, O., & Salinas, S. (1999). Seasonal and interannual variability of currents and temperature off central Chile. *Journal of Geophysical Research*, *104*, 29,951–29,961. https://doi.org/10.1029/1999JC900253
Shaffer, G., Pizarro, O., Djurfeldt, L., Salinas, S., & Ruttlant, J. (1997). Circulation and low-frequency variability near the Chilean coast: Remotely forced fluctuations during the 1991–1992 El Niño. *Journal of Physical Oceanography*, *27*, 217–235. https://doi.org/10.1175/1520-0485(1997)027<0217:CALFVN>2.0.CO;2
Shchepetkin, A., & McWilliams, J. C. (2005). The regional oceanic modeling system (ROMS): a split-explicit, free-surface, topography-following- coordinate oceanic model. *Ocean Modelling*, *9*, 347–404. https://doi.org/10.1016/j.ocemod.2004.08.002
Siedlecki, S. A., Banas, N. S., Davis, K. A., Giddings, S., Hickey, B. M., MacCready, P., et al. (2015). Seasonal and interannual oxygen variability on the Washington and Oregon continental shelves. *Journal of Geophysical Research: Oceans*, *120*, 608–633. https://doi.org/10.1002/2014JC010254
Silva, N., & Neshyba, S. (1979). On the southernmost extension of the Peru-Chile Undercurrent. *Deep Sea Research Part I. Oceanographic Research Papers*, *26*, 1387–1393. https://doi.org/10.1016/0198-0149(79)90006-2
Silva, N., Rojas, N., & Fedele, A. (2009). Water masses in the Humboldt Current System: properties, distribution, and the nitrate deficit as a chemical water mass tracer for equatorial subsurface water off Chile. *Deep Sea Research Part II: Topical Studies in Oceanography*, *56*, 1004–1020. https://doi.org/10.1016/j.dsr2.2008.12.013
Sinha, B., & Richards, K. (1999). Jet structure and scaling in Southern Ocean models. *Journal of Physical Oceanography*, *29*, 1143–1155.
Smith, R. D., Dukowicz, J. K., & Malone, R. C. (1992). Parallel ocean general circulation modeling. *Physica D*, *60*, 38–61. https://doi.org/10.1016/0167-2789(92)90225-C
Sobarzo, M., Bravo, L., Donoso, D., Garcés-Vargas, J., & Schneider, W. (2007). Coastal upwelling and seasonal cycles that influence the water column over the continental shelf off central Chile. *Progress in Oceanography*, *75*, 363–382. https://doi.org/10.1016/j.pocean.2007.08.022
Stramma, L., Prince, E. D., Schmidtko, S., Luo, J., & Hoolihan, J. P. (2011). Expansion of oxygen minimum zones may reduce available habitat for tropical pelagic fishes. *Nature Climate Change*, *2*, 33–37. https://doi.org/10.1038/nclimate1304
Stramma, L., Prince, E. D., Schmidtko, S., Luo, J., Hoolihan, J. P., Visbeck, M., et al. (2012). Expansion of oxygen minimum zones may reduce available habitat for tropical pelagic fishes. *Nature Climate Change*, *2*, 33–37. https://doi.org/10.1038/nclimate1304doi:10.1038/nclimate1304
Stramma, L., Schmidtko, S., Levin, L. A., & Johnson, G. C. (2010). Ocean oxygen minima expansions and their biological impacts. *Deep Sea Research Part I: Oceanographic Research Papers*, *57*, 587–595. https://doi.org/10.1016/j.dsr.2010.01.005
Strub, P. T., Montecino, V., Ruttlant, J., & Salinas, S. (1998). Coastal ocean circulation off western South America. In A. R. Robinson, & K. H. Brink (Eds.), *The sea, vol. 11, The Global Coastal Ocean: Regional Studies and Syntheses* (pp. 273–314). Hoboken, N. J: John Wiley.
Suntharalingam, P., Sarmiento, J. L., & Toggweiler, J. R. (2000), Globalsignificance of nitrous-oxide production and transport from oceanic low-oxygenzones: A modeling study. *Global Biogeochemical Cycles*, *14*, 1353–1370. https://doi.org/10.1029/1999GB900100
Suntharalingam, P., Buitenhuis, E., Le Quere, C., Dentener, F., Nevison, C., & Butler, J. (2012). Quantifying the Impact of Anthro-pogenic Nitrogen Depositionon Oceanic Nitrous Oxide. *Geophysical Research Letters*, *39*, L07605. https://doi.org/10.1029/2011GL050778
Thomsen, S., Kanzow, T., Krahmann, G., Greatbatch, R. J., Dengler, M., & Lavik, G. (2016). The formation of a subsurface anticy-clonic eddy in the Peru-Chile Undercurrent and its impact on the near-coastal salinity, oxygen, and nutrients distributions. *Journal of Geophysical Research: Oceans*, *121*, 476–501. https://doi.org/10.1002/2015JC010878

Ulloa, O., Canfield, D. E., DeLong, E. F., Letelier, R. M., & Stewart, F. J. (2012). Microbial oceanography of anoxic oxygen minimum zones. *Proceedings of the National Academy of Sciences of the United States of America*, *109*(40), 15,996–16,003. https://doi.org/10.1073/pnas.1205009109

Ulloa, O., Escribano, R., Hormazábal, S., Quiñones, R., González, R., & Ramos, M. (2001). Evolution and biological effects of the 1997-98 El Niño in the upwelling ecosystem off northern Chile. *Geophysical Research Letters*, *28*, 1591–1594. https://doi.org/10.1029/2000GL011548

Ulloa, O., & Pantoja, S. (2009). The oxygen minimum zone of the eastern South Pacific. *Deep Sea Research Part II: Topical Studies in Oceanography*, *56*(16), 987–991. https://doi.org/10.1016/j.dsr2.2008.12.004

Vergara, O., Dewitte, B., Montes, I., Garçon, V., Ramos, M., Paulmier, A., & Pizarro, O. (2016). Seasonal variability of the oxygen minimum zone off Peru in a high-resolution regional coupled model. *Biogeosciences*, *13*, 4389–4410. https://doi.org/10.5194/bg-13-4389-2016

Vergara, O., Dewitte, B., Ramos, M., & Pizarro, O. (2017). Vertical energy flux at ENSO time scales in the subthermocline of the Southeastern Pacific. *Journal of Geophysical Research: Oceans*, *122*, 6011–6038. https://doi.org/10.1002/2016JC012614

Vergara, O., Echevin, V., Sepulveda, H. H., Colas, F., & Quiñones, R. (2016). Modeling the seasonal dynamics of the Peru-Chile undercurrent of Central Chile (30-40°S). *Continental Shelf Research*, *123*, 61–79. https://doi.org/10.1016/j.csr.2016.04.001

Wooster, W. S., & Gilmartin, M. (1961). The Peru–Chile Undercurrent. *Journal of Marine Research*, *19*, 97–122.

Wyrtki, K. (1962). The oxygen minima in relation to ocean circulation. *Deep Sea Research and Oceanographic Abstracts*, *9*, 11–23. https://doi.org/10.1016/0011-7471(62)90243-7

Artículo enviado a *Journal of Geophysical Research: Oceans*

4.2. Capítulo 2: Factores físicos que controlan los cambios interanuales de la Zona Mínimo de Oxígeno frente a Chile (30ºS-38ºS) durante el periodo 2000-2008

Matias Pizarro-Koch, Oscar Pizarro, Boris Dewitte, Ivonne Montes, Hector Hito Sepulveda, Marcel Ramos, Aurélien Paulmier y Véronique Garçon

Resumen

En este artículo se analizan los principales mecanismos físicos de la variabilidad interanual de la zona mínima de oxígeno (ZMO) frente a la zona central de Chile. Para este fin se utilizó la misma simulación numérica descrita en el trabajo anterior considerando los años 2000-2008. Durante este periodo, se observó una variabilidad interanual en el volumen de la ZMO, definido como el volumen con OD $\leq$ 45 μM. Particularmente, el RMS interanual del volumen fue ~31% mayor que el ciclo estacional a pesar de la débil amplitud del ciclo ENOS durante el periodo de estudio. Se observo un importante contraste en el volumen y el OD medio de la OMZ durante los años 2001 (máximo volumen) y 2007 (mínimo volumen).

Las anomalías negativas centradas el año 2007 están asociadas principalmente con una marcada disminución de la Corriente Subsuperficial de Perú-Chile (CSPC) y un debilitamiento de las corrientes oceánicas (jets) zonales que transportan agua desde la ZMO hacia el océano abierto. Mientras que las anomalías positivas observadas el año 2001 muestran un mayor transporte hacia el sur de la CSPC, un flujo advectivo de OD negativo (hacia el oeste) asociado a los jets zonales y un marcado debilitamiento del transporte turbulento de OD hacia la ZMO asociado a los remolinos de mesoescala.

En consecuencia, los cambios interanuales en el volumen e intensidad de la ZMO para el periodo evaluado frente a Chile central son el resultado de los efectos combinados de la variabilidad de la CSPC, las corrientes zonales (jets) y los flujos turbulentos asociados a los remolinos de mesoescala. La variabilidad interanual de la CSPC modula principalmente la intensidad de la ZMO más que su volumen. Mientras que el transporte advectivo de OD perpendicular a la costa (jets zonales y los flujos turbulentos de remolinos) muestran un rol importante en la ventilación y extensión oceánica de la ZMO.

59 **Plain Language Summary**
60

61 The southern tip of the Oxygen Minimum Zone (OMZ) in the Eastern South Pacific off Chile is
62 very sensitive to the global deoxygenation trend. Here, using a physical-biogeochemical model
63 we investigate the main physical mechanisms controlling its interannual variability. The study
64 period study (2000-2008) comprises El Niño-La Niña cycles with a relative weak amplitude.
65 Nevertheless, we found large contrast of the OMZ volume and its intensity during the years 2001
66 and 2007. Dissolved oxygen changes within OMZ were closely related to the southward
67 transport of the Peru-Chile Undercurrent, while changes of the OMZ volume were mainly related
68 to changes in zonal currents and in the eddy fluxes, largely related to mesoscale variability.
69 Thus, the interplay of the meridional and zonal transport of dissolved oxygen modulate the
70 interannual oxygen budget and shape of the OMZ off central Chile.

71
72
73
74

Physical drivers of the interannual changes of the Oxygen Minimum Zone off Chile (30ºS-38ºS) during 2000-2008

Matías Pizarro-Koch[1,2,3], Oscar Pizarro[2,3,4], Boris Dewitte[5,6,7,9], Ivonne Montes[10], Marcel Ramos[6,7,8], Aurélien Paulmier[9], Véronique Garçon[9] and Hector Hito Sepulveda[4]

[1] Programa de Postgrado en Oceanografía, Departamento de Oceanografía, Facultad de Ciencias Naturales y Oceanográficas, Universidad de Concepcion, Concepción, Chile.

[2] Millennium Institute of Oceanography, Chile.

[3] Centro de Investigación Oceanográfica COPAS Sur-Austral, Universidad de Concepcion, Concepción, Chile.

[4] Department of Geophysics, University of Concepcion, Concepcion, Chile.

[5] Centro de Estudios Avanzados en Zonas Aridas (CEAZA), Coquimbo, Chile.

[6] Departamento de Biología Marina, Facultad de Ciencias del Mar, Universidad Católica del Norte, Coquimbo, Chile.

[7] Núcleo Milenio de Ecología y Manejo Sustentable de Islas Oceánicas (ESMOI), Universidad Católica del Norte, Coquimbo, Chile

[8] Centro de Innovacion Acuícola Aquapacífico, Coquimbo, Chile.

[9] LEGOS-CNRS/IRD/UPS/CNES, Université de Toulouse, Toulouse, France.

[10] Instituto Geofísico del Perú, Lima, Perú.

Submitted to Journal of Geophysical Research: Oceans (19/03/2020)

Corresponding author: Matias Pizarro-Koch (matiaspizarro@udec.cl)

Key Points:

- The Oxygen Minimum Zone (OMZ) off Chile is modulated interannually by the Peru-Chile Undercurrent and by the alternating zonal jets.
- Zonally advective and mesoscale eddy fluxes of dissolved oxygen play a key role ventilating and shapping the OMZ at interannual time-scale.
- The OMZ intensity is modulated interannually mainly by the Peru-Chile Undercurrent variability near to continental slope.

Abstract

The main physical drivers of the interannual variability of the oxygen minimum zone (OMZ) off central Chile were analyzed using a high-resolution (1/12º) coupled physical-biogeochemical model simulation between the years 2000 and 2008. During this period a relatively large interannual variability was observed in the OMZ volume (OMZ_{VOL}), defined as the volume with dissolved oxygen concentration (DO) $\leq$ 45 μM in the region between 30°S-38°S. Interannual OMZ_{VOL} RMS was ~31% larger than the seasonal one despite relatively weak El Niño Southern Oscillation (ENSO) amplitude. Particularly, larger positive (negative) anomalies of OMZ_{VOL} were observed during 2001 (2007). We showed that these anomalies were associated with changes in (1) the Peru-Chile Undercurrent (PCUC) that transports low-DO waters poleward, (2) in the intensity of narrow zonal jets that meridionally alternate, transporting water from and toward the OMZ and (3) in the zonal eddy transport related to mesoscale eddy activity. The interannual variability of the PCUC modulates mainly the DO contents of the OMZ, while cross-shore DO transport by the zonal jets and the eddy fluxes play a major role ventilating and shaping the offshore extent of the OMZ. When the OMZ_{VOL} was maximum (minimum) the PCUC transport was relatively normal (abnormally reduced), but the zonal advective and eddy fluxes of DO showed negative (positive) anomalies, reducing (increasing) ventilation. Thus, the OMZ_{VOL} interannual changes observed off central Chile during the study period resulted from the compensating effects associated with the PCUC, zonal jets and mesoscale eddy flux variability.

1 Introduction

The tropical and subtropical regions of the eastern South Pacific Ocean (ESP) undergo large variability at interannual time scales that may modulate the spatial extension and intensity of the oxygen minimum zone (OMZ) present in this region. This natural variability –along with the sparse number of observations available there– partially masks lower frequency fluctuations, including that of anthropogenic origin. In general, the distribution of dissolved oxygen (DO) in the ocean strongly depends on warming because it directly affects oxygen solubility and indirectly by changing ocean circulation, mixing and oxygen respiration (*Schmidtko, et al*., 2017; *Oschlies et al.,* 2018). In the present global warming scenario, both model and observations have shown that ocean DO is decreasing and consequently, expansion and intensification of the OMZs are expected (e.g. *Schmidtko, et al*., 2017; *Lachkar et al*., 2018) with significant impacts on the marine ecosystem and on biogeochemical cycles (e.g. *Breitburg et al*., 2018). Like other regions of the ocean, the OMZ off central Chile is sensitive to the global deoxygenation trend (*Bopp et al*., 2013; *Long et al*., 2016; *Oschiles et al*., 2018), which may contribute to spatially extend and intensify the OMZ in this region. To address this environmental threat much remains yet to be learned about the mechanisms that control natural variability of DO in the southern boundary of the large OMZ of the ESP.

The OMZ of the ESP is closely related to Equatorial Subsurface Water (ESSW), a regional water mass characterized by relatively high salinity, temperature, CO_2 and nutrients, and very low values of DO and pH (*Paulmier et al*., 2008; *Silva et al*., 2009; *Torres et al*., 2011; *Hernandez-Ayon et al*., 2019). This water mass is a key component of the coastal upwelling cell since it is the main source of nutrients to the surface layer. Near the coast of central Chile the ESSW is located just below the waters that form the shallow salinity minimum (*Reid*, 1973; *Wijffels et al*., 2001; *Schneider et al*., 2003; *Karstensen*, 2004), called also Subantarctic Water (SAAW) (e.g. *Silva et al*., 2009), and over the Antarctic Intermediate Water (AAIW). Both, SAAW and AAIW are characterized by low-salinity, relatively low-temperature and high DO, largely contrasting with the ESSW and easily distinguishable in T-S (and T-O) diagrams. The ESSW is transported along the Peruvian and Chilean coasts by the PCUC, which contributes to expand poleward the OMZ (*Paulmier et al*., 2006). This southward flow extends from northern Peru to south-central Chile (*Wooster and Gilmartin*, 1961; *Silva and Neshyba*, 1979; *Pizarro et al*., 2002; *Chaigneau, et al*., 2013) and its northern limb is fed by the South Pacific Tsuchiya jets and to a lesser extent, by the Equatorial Undercurrent (*Montes et al*., 2014). Significant changes in the origin of the source waters that feed the OMZ have been associated to El Niño variability impacting, in turn, the properties of the OMZ off Peru (*Espinoza-Morriberón et al*., 2019), although observations suggest that a significant variance in interannual variance of oxygen content is not linearly related to El Niño there (*Graco et al*., 2017).

Off Peru and Chile the oxycline that denotes the upper limit of the OMZ is quite shallow and abrupt, commonly laying over the 100 m depth (*Paulmier et al*., 2006). Over the continental shelf upwelling-downwelling events and coastally trapped waves modify the depth of this oxycline by transporting oxygen depleted waters to the surface layer (e.g. *Schlosser et al*., 2018; *Pizarro et al*., 2016) or by transporting surface water downward contributing to oxygenate environments that commonly are anoxic (e.g. *Gutierrez et al*., 2008). In contrast, the lower

oxycline is smooth and shows large differences along the coast. It is in particular much deeper (typically > 800 m depth) off Peru than off central Chile (~450 m depth) (e.g. *Silva et al*., 2009; *Fuenzalida et al*., 2009). The offshore extension of the OMZ (demarked here by DO = 45 μM) decreases rapidly southward reaching about 200 km near 30ºS and only ~25 km near 37ºS (*Silva et al*., 2009; *Fuenzalida et al*., 2009; *Pizarro et al*., 2016). Like off Peru (*Gutierrez et al*., 2008; *Espinoza-Morriberón et al*., 2019), the upper oxycline, as well as the thermocline, off Chile experience large interannual variations, mainly related to the ENSO cycles (e.g. *Morales et al*., 1999; *Pizarro and Montecinos*, 2004) but not only, in particular during periods when the ENSO amplitude is reduced (Graco et al., 2017). Off central Chile seasonal and interannual variation of coastal upwelling also modulate the upper oxycline (e.g. *Paulmier et al*., 2006; *Sobarzo et al., 2007*; *Schneider et al*., 2017; *Pizarro-Koch et al*., 2019). In addition, mesoscale eddies play also an important role in the surface and subsurface variability of this region at different time-scales (*Chaigneau and Pizarro*, 2005; *Chaigneau et al*., 2011). Particularly, a specific type of mesoscale eddy, named subsurface or intrathermocline eddies, transports offshore low-oxygen waters and plays an important role in the OMZ dynamics (*Hormazabal et al*., 2013, *Combes et al*., 2015; *Cornejo et al*., 2016; *Frenger et al*., 2018). These subsurface eddies have been associated to instabilities of the Peru-Chile Undercurrent (PCUC) (*Contreras et al*., 2019), and their dynamics are similar to the Cuddies observed in the California Current System (e.g. *Molemaker et al*., 2015). Changes in both the PCUC and mesoscale eddy field contribute to modulate the vertical and offshore extension of the OMZ at seasonal and intraseasonal time scales off central Chile (e.g. *Vergara et al*., 2016; *Frenger et al*., 2018; *Pizarro-Koch et al*., 2019).

Here, we analyze the interannual variability of the extra-tropical OMZ off central Chile (30ºS-38ºS**),** a region that is sensitive to the deoxygenation trend (*Keeling et al*., 2010; *Bopp et al*., 2013; *Oschlies et al*., 2018), but also with large interannual and decadal variability (e.g. *Montecinos et al*., 2003). We take advantage of the recent progresses in coupled physical-biogeochemical modeling for OMZ studies (e.g. *Montes et al*., 2014; *Vergara et al*., 2016; *Mogollon and Calil*, 2017; *Pizarro-Koch et al*., 2019) to investigate the relative role of the meridional –related to the PCUC– and zonal transports of DO over the interannual variability of the OMZ volume.

The main focus of this work is aimed at explaining the contrast between the volume of the OMZ observed in the model between years 2001 and 2007. In those years this volume showed large differences in the study region, despite the fact that during the whole study period the ENSO variability in both the model and observations was relatively weak. Note that during this period a warm (2002-2006) and cold (2000-2001) phase were reported. The last one was related to the end of the strong La Niña (1998-2001) event. The choice of this period is also motivated by the fact that realistic observed atmospheric momentum fluxes are available (i.e. QuikSCAT satellite data) for simulating Eastern Boundary Upwelling System dynamics (EBUS) (c.f *Aguirre et al*., 2012; *Astudillo et al*., 2017) and it corresponds to the period analyzed by *Pizarro-Koch et al*. (2019) for investigating the seasonal cycle of the OMZ, providing benchmark material for the interpretation of the results.

The rest of the paper is organized as follows: the coupled model setup and validation is presented in section 2, in section 3 we describe the interannual changes observed in the extra-tropical OMZ (subsection 3.1) and the associated changes in the integrated DO budget (subsection 3.2). Changes in the PCUC and in the cross-shore DO fluxes are addressed in subsections 3.3 and 3.4, respectively. Finally, in section 4 we present a summary of the main findings and the conclusions.

2 Methods

2.1 Coupled Physical-Biogeochemical Model

In this paper, the model used is the Regional Ocean Model System (ROMS), AGRIF version, coupled to the biogeochemical model named BioEBUS. ROMS is a split-explicit (i.e. the barotropic and baroclinic momentum equations are resolved separately using different time steps), free surface oceanic model that solves the rotating primitive equations, based on the Boussinesq approximation and hydrostatic vertical momentum balance (*Shchepetkin and McWilliams*, 2003, 2005, 2009; *Penven et al.,* 2006). ROMS is discretized using curvilinear coordinate in the horizontal and terrain-following (or sigma) coordinate transformation in the vertical. BioEBUS is a nitrogen-based biogeochemical model specially developed for EBUS (*Gutknecht et al.,* 2013a) following similar methodology than that described by *Montes et al.* (2014), *Vergara et al.* (2016) and *Pizarro-Koch et al.* (2019). BioEBUS model was derived from the nitrogen based $N_2P_2Z_2D_2$ model of *Koné et al.,* (2005) and, in addition to DO, mainly consist of 10 nitrogen state variables, specially adapted to coastal versus off-shore system such as EBUS (*Gutknecht et al.,* 2013a). Those state variables correspond to 6 compartments, having two classes of size for phytoplankton (small-flagellate PS, large-diatoms PL), zooplankton (small-ciliates ZS, large-copepods ZL) and detritus (D; small DS, large DL). Furthermore, 4 other compartment include Dissolved Organic Nitrogen (DON) and three Dissolved Inorganic Nitrogen (DIN) compartments represented by nitrate, nitrite and ammonium. In addition to nitrification, BioEBUS takes into account specific microbial OMZ processes interacting within the DIN pool such as denitrification and anammox. For biogeochemistry, initial and boundary conditions for nitrate and oxygen concentrations are provided by CARS-2006 climatology. For the other biogeochemical tracers (NO_2^-, NH_4^+ and DON) initial and lateral boundary conditions are established using a constant (in time) profiles similar to those described by *Koné et al.,* (2005). The parameters used in the biogeochemical model were the same than those used by *Montes et al.* (2014) and *Vergara et al.* (2016) for the ESP-OMZ off Peru. For a detailed description of the parameters used in this study, please see appendix A in *Montes et al.* (2014). Hereinafter this coupled physical-biogeochemical model will referred as ROMS/BioEBUS.

The evolution of any biological tracer concentration is determined by the advective-diffusive equation. For DO, this equation takes the following form:

$$\frac{\partial DO}{\partial t} = -\nabla \cdot (\mathbf{u} DO) + K_h \nabla^2 DO + \frac{\partial}{\partial z}\left(K_z \partial \frac{DO}{\partial z}\right) + SMS(DO) \quad (1)$$

On the right-hand side (r.h.s), the first three terms represent DO advection (with **u** the velocity vector), K_h and K_z are the horizontal and vertical eddy diffusion, respectively (K_h is equal to 100 m^2s^{-1} in our model and K_z is calculated based on the K-profile parameterization mixing scheme; *Large et al*., (1994)). Note that the model also has numerical diffusion associated with inherent spurious diapycnal mixing of the numerical scheme, so that K_h is empirically adjusted. The *SMS* (sources minus sinks) term includes all biogeochemical processes considered by the model that act as sources and sinks, in this case, for DO. The total physical term (named *PHYS* below) is the summed-up of the advective term ($ADV = \nabla \cdot (\mathbf{u}DO)$) and the horizontal ($K_h \nabla_h^2 DO$) and vertical ($\frac{\partial}{\partial z}\left(K_z \frac{\partial DO}{\partial z}\right)$) mixing, hereafter called *Hmix* and *Vmix,* respectively. Note that *ADV* contains also diffusion (through numerical diffusion) and non-linear advection that can be interpreted as mixing, so that *Hmix* is not the "full" mixing that is taking place in the model (cf. *Vergara et al.,* 2017). The *ADV* can also be represented separately through its contributions related to the different components as: the zonal ($Xadv = u\partial(DO)/\partial x$), meridional ($Yadv = v\partial(DO/\partial y$) and vertical ($Zadv = w\partial(DO)/\partial z$) advection, where *u, v* and *w* are the zonal, meridional and vertical velocity components, respectively. The reader is referred to *Gutknecht et al*. (2013a) for more detailed information about the BioEBUS model.

2.2 Model Setup

We used a similar interannual ROMS (1958-2008) configuration to that used by *Dewitte et al.,* (2012). The model was run for 50 years, however, here we use only the last nine years (2000-2008) for the ROMS/BioEBUS coupled simulation. The horizontal resolution was 1/12º and the domain extends from the North Equatorial Pacific (12°N) to eastern South Pacific (40ºS), and from the South American coast to 95ºW. The vertical resolution was determined by the total depth distributed in 37 vertical levels using the sigma transformation. In this study we focus on the region off central Chile (from 30°S to 38°S, Figure 1a), but a larger domain was necessary in order to correctly grasp the connection with the equatorial variability through coastal-trapped waves, extra-tropical Rossby waves and the PCUC variability (*Pizarro et al*., 2001, 2002; *Ramos et al*., 2008, *Ilig et al*., 2018). The lateral open boundary conditions (temperature, salinity and horizontal velocity) were obtained from SODA 1.4.2 reanalysis (*Smith et al.,* 1992). The SODA 1.4.2 horizontal resolution is 0.25º (latitude) x 0.4º (longitude) and with 40 vertical levels with 10 m spacing near the surface. The atmospheric forcing consists in a statistical downscaling product from NCEP-NCAR (2.5º x 2.5º) data that provides wind stress and wind speed, this method refines the NCEP-NCAR resolution to 0.5º x 0.5 and correct for the biases of the NCEP reanalyses near the Peru-Chile coast. The statistical downscaling model used by *Goubanova et al.* (2011) is constructed from QuikSCAT data (please see *Goubanova et al.,* 2011 for more details). Atmospheric fluxes were derived from the bulk formula using COADS 1º x 1º monthly climatology (*da Silva et al.,* 1994), air temperature, relative humidity and long- and short-wave radiation are also from COADS. The atmospheric forcing is almost equivalent to the original QuikSCAT data over the period 2000-2008, which also motivated us to focus on this period to analyze interannual variability.

2.3 Model Assessment

The hydrodynamics has been formerly validated from satellite and in situ observation focused on mean state and interannual variability by *Dewitte et a*l. (2012) and *Vergara et al*. (2016, 2017). These authors endorse that the model is skillful in simulating the mean SST field (See Fig 1a, c in *Vergara et al*. (2016) and Fig. 3 in *Dewitte et al*. (2012)) as well as other main aspects of the mean circulation (e.g., Peru-Chile Undercurrent and EKE; see Fig. 3 in *Dewitte et al*. (2012)). The SST bias was around (1ºC), the model being colder with respect to observations and EKE with a comparable pattern than altimetry, although with a larger amplitude (see Fig. 1e, f in *Vergara et al*. (2016)).

The biogeochemical variables from the coupled ROMS/BioEBUS model have been validated and used for other studies related to OMZ off Peru and Chile (*Montes et al.,* 2014; *Vergara et al.,* 2016; *Pizarro-Koch et al.* 2019). *Montes et al.* (2014) provide a statistical assessment of the annual mean model skill through Taylor's diagrams. The pattern correlations of physical and biogeochemical fields were larger than 0.85, as well as low standard deviations (i.e. in the order of the observed values) and the centered RMS differences are relatively small (<0.5 of the field's variance). After, *Vergara et al.* (2016) consistently with *Montes et al.* (2014) found that the coupled simulation is skillful in simulating the mean characteristics of OMZ off the Peruvian coast (see Figs 2 and 3 in *Vergara et al.* (2016)). The thickness and OMZ core distribution were realistic and in good agreement with previous studies (see Fig. 2 in *Vergara et al.* (2016)). Furthermore, the simulation is consistent in reproducing the oxygen-consuming processes, as supported by the apparent oxygen utilization (AOU). However, the volume of suboxic water is underestimated by 6 %, which is comparable to the differences obtained by *Montes et al.* (2014). Near the coast and south of ~20ºS the model shows an overestimation of DO. A validation focused in the OMZ off central Chile was recently presented by *Pizarro-Koch et al.,* (2019). They showed that the model has a fair skill in simulating the main features of the region, including upwelling seasonal cycle, vertical structure OMZ, seasonal anomalies of coastal DO, hydrographic patterns (T, S, DO, NO_3^-), and velocity data over the continental slope at the core of the PCUC (for more details please see appendix in *Pizarro-Koch et al*., 2019).

2.4 Interannual time-series and ENSO indices

Model variables were originally stored every 5-days and to obtain interannual time series of the different original and derived –like OMZ_{VOL} and zonal eddy fluxes (see below section 2.5)– variables, we calculate monthly averages based on the 5-days time series. Time series of interannual anomalies were obtained by removing the mean, the linear trend and the seasonal cycle. Then, these monthly times series were low-pass filtered using a moving-average filter of 7 months. We contrast the interannual variability –related to ENSO– during the study period (2000-2008) with other decades. To do this we use the multivariate ENSO index (MEI), the Southern Oscillation Index and the El Niño 3.4 index (data obtained from https://www.esrl.noaa.gov/psd/enso/). The ENSO variability showed a minimum during the 2000-2008 period, when compared with different decades between 1980's and the 2010's.

294 Nevertheless, lower variability was observed in SOI and El Niño 3.4 indices during the 1960's.
295 Thus, the study period can be considered as one of relatively weak ENSO variability.

296

297 2.5 Estimation of advective and diffusive transports

298

299 Advective and eddy fluxes of DO were estimated following the methodology used by *Pizarro-*
300 *Koch et al*. (2019) and *Vergara et al*. (2016). Known such as the Reynolds decomposition and
301 this write as follows:
302

303 $$\emptyset(x,t) = \widetilde{\emptyset}(x,t) + \emptyset'(x,t), \quad (2)$$

304

305 where $\emptyset$ represents DO or any velocity component, $\widetilde{\emptyset}$ is the 3-month running mean and $\emptyset'$ is the
306 deviations from $\widetilde{\emptyset}$. The $\emptyset'$ component accounts for fluctuations having a typical time scale
307 lasting from weeks to a few months so that eddy variability refers here mostly to the mesoscale
308 turbulence. In this work we mainly pay attention to the zonal fluxes –which are approximately
309 offshore in the study region. The zonal mesoscale eddy fluxes of DO were calculated as the
310 covariance between the zonal velocity fluctuations (*u'*) and *DO*' using 3-month periods, i.e. ZEF
311 = $\langle u'DO' \rangle_{3\text{-m}}$, where "$\langle\rangle_{3\text{-m}}$" stands for a 3-month moving average. Meanwhile, the zonal
312 advective flux was estimated as the product of the zonal velocity ($\tilde{u}$) and $\widetilde{DO}$, i.e. ZAF = $\tilde{u}\widetilde{DO}$.
313 Both ZAF and ZEF are originally 5-day time series and can have seasonal and lower frequency
314 variability. Then, to estimate the interannual time series of these fluxes we calculate monthly
315 averages and remove the seasonal cycle to have monthly anomalies time series. Finally these
316 monthly anomalies were low-pass filtered as above.

317

318 **3 Results**

319 3.1 Variability of the extra-tropical OMZ

320 The interannual variability of the OMZ was analyzed using mainly 2 metrics: The OMZ volume
321 (hereafter OMZ_{VOL}) defined as the region where DO ≤ 45 μM between 30°S and 38°S, and the
322 mean DO inside this volume (hereafter OMZ_{DO}). We select the limit of 45 μM (~1 mL L^{-1})
323 because this characterizes hypoxic waters (e.g. *Naqvi et al.,* 2010) impacting most of th
324 ecosystems far from the anoxic center of the ESP OMZ off Peru. The mean value of the OMZ_{VOL}
325 was ~4.5x10^4 km^3, with a thickness and offshore extension that, in average, decrease southward
326 (Figure 1). The core of the OMZ in this region was located over the continental slope centered at
327 ~300 m depth (see contour of DO = 20 μM in Figure 1b), while OMZ_{DO} averaged for the whole
328 period 2000-2008 was 32 μM.

329

330 The OMZ_{VOL} time series showed relatively large interannual variability during the study period
331 (Table 1 and Figure 1c), with maximum and minimum during 2001 and 2007, respectively.
332 Despite the fact that interannual changes related to the ENSO cycles –in both the model and
333 ENSO indices based on observations– were relatively weak during 2000-2008, interannual

changes in the OMZ_{VOL} were quite significant. They were even larger than those associated with the typical seasonal variability (Figure 3a, Table 1). In particular the variation of the OMZ_{VOL} is 3 times larger than the variance of that of the seasonal cyle. The OMZ_{DO} time series also showed large interannual variability, but it was only slightly correlated with the OMZ_{VOL} (Figure 1c; r = −0.62 at 3−month lag, which is significant at 95% confidence level). The OMZ_{VOL} reached a maximum in 2001, which represents an increase of about 38% of the mean value. Other two relative maxima (periods with positive anomalies) were observed in 2006 and 2008, but they were relatively small (less than 5% of the mean value). In fact, the OMZ_{VOL} showed predominantly negative anomalies during 2003-2008 with a minimum during 2007. To visualize the contrast between the years with maximum (2001) and minimum (2007), OMZ_{VOL}, alongshore sections of DO (including the first 80 km from the coast) and the water mass composition of OMZ is depicted in Figure 2. The total OMZ volume for these years is shown in Figures 3b and 3c. Table 1 summarizes the basic statistic for OMZ_{VOL} and OMZ_{DO} time series. Positive anomalies of OMZ_{DO} were observed during 2003 and 2007 with maximum over 2.5 μM (Figure 1c), whereas negative anomalies were observed during 2000, early 2005 and 2008. Note that the largest positive anomaly of OMZ_{DO} −observed during 2007− coincides with a minimum in OMZ_{VOL} (Figure 3c). In contrast, the minimum OMZ_{VOL} observed in 2004 takes place during a period of rapid reduction of OMZ_{DO}, showing that both metrics (OMZ_{VOL} and OMZ_{DO}) are not obviously related. During 2007, the ESSW reduced its proportion inside the OMZ significantly, decreasing rapidly its contribution south of 34°S, while AAIW and SAAW increased (Figure 2e). In contrast, during 2001 water proportion changed only slightly compared to their mean value.

3.2 Interannual DO Budget

To analyze the drivers of DO inside the OMZ off Central Chile we use the advection-diffusion equation (1). Here we follow a similar methodology as *Pizarro-Koch et al*. (2019), who analyzed the seasonal variability in the same region. Table 2 shows the average values of the period and the interannual RMS values for the different terms that make up this equation. The different terms were averaged inside the mean volume conforming the OMZ (i.e. the fixed volume with dissolved oxygen that in average is lower than 45 μM, as shown in Figure 1b). For comparison, the RMS of the seasonal cycle of these terms and their averages for 2001 and 2007 years are also shown. A slight negative trend ($\partial DO/\partial t \sim -0.4$ μM year^{-1} for the period 2000−2008) is present, which may be related to low-frequency variability, e.g. decadal changes (this trend is not analyzed here). The dominant terms in the r.h.s. of (1) are the 3 advective ones (i.e. *Xadv*, *Yadv* and *Zadv*) and the *SMS*. While meridional (*Yadv*) and vertical (*Zadv*) advections contribute in average to ventilate the OMZ, the zonal advection (*Xadv*) contributes to its deoxygenation. The sum of the 3 advective terms is positive and equal to 1.78×10^{-6} μM s^{-1}, which is about the same magnitude as SMS (-1.45×10^{-6} μM s^{-1}). Thus, in average, the physical terms contribute to ventilate the OMZ, while SMS (representing main biogeochemical processes) contribute to reduce DO, particularly oxic decomposition and nitrification dominate the SMS term.

Interannual anomalies of the different terms involved in the balance (1), averaged in the OMZ volume, are shown in Figure 4. The anomalies of the 3 advective terms are of the same order of magnitude (Figure 4b), while the terms involving small-scale (subgrid) mixing are much smaller

(Figure 4c). Thus, interannual anomalies of *PHYS*, which represent all the physical terms in (1), are largely dominated by the advection terms. Note that *PHYS* (dashed red line in Figure 4b) is well correlated with the tendency term (red line in Figure 4a, r=0.7), and that the horizontal advection terms, *Xadv* and *Yadv*, are inversely correlated (blue and magenta lines in Figure 4b, r=-0.9). The SMS averaged in the volume showed anomalies about one order of magnitude smaller than *PHYS*, with a main minimum in 2007 and a secondary minimum in 2001, when OMZ_{VOL} was minimum and maximum, respectively. During 2001, *PHYS* anomalies were slightly positive, while in 2007 they were slightly negative. In both cases the previous year (i.e. 2000 and 2006, *PHYS* showed positive anomalies. The different terms involved in the balance when spatially averaged in the whole OMZ volume, do not show large differences between 2001 and 2007, although both years show large differences in OMZ_{VOL}.

3.3 Interannual Variability of the alongshore flow

Since the work of Eustace R. Gunther (*Gunther*, 1936), the PCUC has been recognized as the current that transport oxygen depleted ESSW poleward along the Chilean coasts, extending southward the OMZ (e.g. *Silva and Neshyba*, 1979; *Silva et al*., 2009). Thus, changes in the PCUC may be associated with the variability of the OMZ (e.g. *Homazabal et al*., 2006). Here, we estimated the transport associated with the PCUC (hereafter $PCUC_{TR}$) by spatially averaging the southward flow (only values smaller than -0.02 m s^{-1}) in a coastal band of 100 km width and between 80 and 800 m depth. The DO inside the region encompassed by the PCUC was also estimated and is referred hereafter as $PCUC_{DO}$. Both, $PCUC_{TR}$ and $PCUC_{DO}$ interannual anomalies at different latitudes are shown in Figure 5. These anomalies were filtered using a similar filter as that used for OMZ_{VOL} and OMZ_{DO} interannual anomalies. Figure 5a shows a large weakness of the $PCUC_{TR}$ during 2007, consistent with the minimum OMZ_{VOL} and with an increase of $PCUC_{DO}$. In general, at interannual timescale a weakness of the $PCUC_{TR}$ is associated with an increase of the $PCUC_{DO}$ during the study period (r = -0.6, which is significantly different from zero at the 95% confidence level). Note that the large changes in the PCUC transport between 2004 and 2008 are consistent in the entire region and a small phase difference between the northern and southern regions observed in Figure 5a indicates a southward propagation of the transport. Poleward propagation along the coast has been also observed in coastal sea level and thermocline depth in both hemisphere and it has been associated to long Rossby wave dynamics (*Clarke and Van Gorder*, 1994; *Pizarro et al*., 2001).

The correlation between $PCUC_{TR}$ and OMZ_{VOL} was rather small, the maximum value was r ~ 0.4 at 3-4 month lags (and not significant at 95%). Nevertheless, the magnitude of the correlation between $PCUC_{TR}$ and OMZ_{DO} was larger (both time series showed an inverse correlation of r = -0.75, significant at 95%) indicating that the $PCUC_{TR}$ variability play a more important role over the intensity of the OMZ than over its volume variability. When the OMZ volume is estimated using just waters with DO < 20 μM –which involves a smaller volume restricted to the near-shore region over the slope and outer shelf (see Figure 1)– the correlation between this volume and the interannual variability of the $PCUC_{TR}$ increases somewhat (r=-0.6) and becomes significant at 95%.

The above results support the idea that the interannual variability of the PCUC has a significant influence on the OMZ variability, particularly over the slope where the PCUC and OMZ cores are located. Nevertheless, the interannual variability of the offshore, vertical and southward extension of the OMZ cannot be fully explained by the PCUC variability. Note that, although during 2007 the $PCUC_{TR}$ showed a largest negative anomaly (consistent with negative anomaly of the OMZ_{VOL}), the large positive anomaly of OMZ_{VOL} observed during 2000-2001 (Figure 1c) corresponds to a period of a slight increase of the $PCUC_{TR}$. In the next section we evaluate the impact of the cross-shore current and the associated transport of DO on the OMZ interannual changes.

3.4 Cross-shore transport of DO

Previous studies have shown that both, advective and eddy cross-shore (approximately zonal in our study region) fluxes may play a significant role in the seasonal variability of the OMZ off Peru and Chile (*Bettencourt et al., 2015*; *Vergara et al*., 2016; *Pizarro-Koch et al*., 2019; *Espinoza-Morriberón et al*., 2019). Note that here the term eddy flux is associated with mesoscale eddy flux and not with small scale (sub-grid) eddies, which are parameterized in the model by lateral mixing (*Hmix* in equation 1). We analyzed the cross-shore DO fluxes along a meridional section centered at 74ºW during years 2001 and 2007, i.e. during the years with maximum and minimum OMZ_{VOL}, respectively. Figures 6a and 6b show that ZAF and ZEF during 2001 (i.e. when OMZ_{VOL} is maximum) have similar order of magnitude, but in average the ZEF is larger and shows positive values between 50 and 500 m depth (Figure 6g, dashed red line) ventilating the OMZ. In contrast, the ZAF is negative in the upper ~300 m and slightly negative below that depth (Figure 4g continuous red line). During 2007 (when the OMZ_{VOL} was minimum) the ZEF was slightly larger than from 2001 (note that in 2001 ZEF was ~30% less than the mean value) and similar to the climatological mean (showed by the black dashed line in Figure 6g), but in 2007 the ZAF was also positive in much of the water column, between ~50 and 500 m depth, reinforcing the ventilation of the OMZ. A striking feature observed in the ZAF is the presence of well defined stripes that alternate onshore and offshore ZAF, which may be related to the presence of meridionally alternating zonal jets (cf. *Belmadani et al*., 2017; *Pizarro-Koch et al*., 2019). The location and intensity of these ZAF stripes changed between 2007 and 2001. The large positive advective transport of DO was located around 35.5°S and 37.5°S in 2007 (Figure 6c). This transport contributed to the ventilation of the southern part of the OMZ and to the associated reduction of the OMZ observed this year (Figure 2c and 3c). In average, between 30°S and 38°S and for the complete period, the ZAF was rather small, about an order of magnitude smaller than the averaged ZEF (Figure 6g, black continue and dashed line, respectively), but ZAF showed large spatial variability (Figure 6e, blue line). Over the whole study region, the ZEFs largely contributed to ventilate the OMZ. Nevertheless, during 2001, when the OMZ_{VOL} was maximum, the mean ZEF was reduced (Figure 6g, dashed red line). Changes in the eddy fluxes are consistent with the reduction and increase of the (mesoscale) eddy kinetic energy observed during 2001 and 2007, respectively (not shown).

In summary, during 2007 the PCUC –that transports water with low DO– was weakened and the zonal eastward flow of highly oxygenated water was increased, both contributing to reduce the OMZ_{VOL}. This year, the zonal eddy flux was similar to its climatological value. In contrast, during 2001 the PCUC was rather normal, but the ZEF, which contributes to ventilate the OMZ,

468 was abnormally smaller and the ZAF was slightly negative. The anomalies in these two zonal
469 fluxes seem to be responsible for the rapid reduction of OMZ_{DO} and the increasing OMZ_{VOL}
470 observed during 2001. Thus, an interplay among the transports of the PCUC, the zonal jets and
471 the eddy fluxes (related to mesoscale eddies) controlled main interannual changes of the OMZ
472 volume during the 2000-2008 period of central Chile.
473

474 **4.- Summary and conclusions**

475

476 Our model results indicate that the OMZ off Central Chile (30°S – 38°S) undergoes substantial
477 interannual changes –typically larger than seasonal variability– even during periods with
478 relatively weak ENSO variability, like the 2000-2008 period. The two main metrics used here to
479 represent the OMZ, namely OMZ_{VOL} and OMZ_{DO}, are only moderately correlated at interannual
480 time scales, that is, the lower values of OMZ_{DO} are not necessarily related to larger values of
481 OMZ_{VOL} and vice versa, suggesting a combination of processes controlling DO changes within
482 the OMZ. Therefore, it is expected that the different terms that make up equation (1) –integrated
483 in the whole control volume– only account for a small fraction of the variability observed in
484 OMZ_{VOL} time series. In fact, these terms do not show significant differences between 2001 and
485 2007, despite the contrast that OMZ_{VOL} shows between those years. The physical terms (grouped
486 in *PHYS*) involved in the DO budget, and particularly the advective ones, dominate the
487 interannual variability of DO. Similar results were observed by *Pizarro-Koch et al*. (2019) for
488 the seasonal variability in our study region.
489

490 During 2007 the PCUC transport experienced a large reduction, and consistently, the waters
491 transported southward by this current increased their DO content. This abnormally weak PCUC
492 transport was associated with the reduction of the OMZ_{VOL} observed this same year. On the other
493 hand, the large OMZ_{VOL} observed in the model during 2001 was not directly related to an
494 increase of the PCUC. During this year, the cross-shore advective flow was, in average negative
495 –removing DO from the OMZ– and the eddy flux which permanently contributes to ventilate the
496 OMZ, was abnormally low. Thus, zonal transport of oxygen related to both advection by zonal
497 jets and mesoscale eddy fluxes may significantly contribute, along with the PCUC, to modulate
498 the southward and offshore extension of the OMZ off central Chile. Changes in the poleward
499 transport of PCUC are mainly related to DO changes in the core of the OMZ over the slope. Our
500 study thus illustrates the interplay between environmental forcing (i.e PCUC transport modulated
501 by equatorial variability) and internal dynamics (i.e eddy flows) in modulating the OMZ off
502 Chile. Besides providing guidance for observational studies and the design of field experiments,
503 these results have implications for interpreting global coupled models that generally do not have
504 the proper resolution to account realistically for the mean PCUC structure and the mean eddy
505 flow. In particular, our study suggests that caution is required when interpreting the low-
506 frequency changes in OMZs and its relationship with equatorial forcing in these global models. It
507 also calls for addressing longer timescale of variability (i.e decadal) considering its potencially
508 important role on both the PCUC transport and eddy activity in this region, which is planned for
509 future work.
510
511
512

513 **Acknowledgments**

514

515 MP-K was supported by a Doctoral Scholarship from CONICYT (Ministry of Education, Chile).
516 This study was carried out under FONDECYT projects 1181872 leaded by OP. Support from
517 FONDECYT 1190276 (leaded by BD), FONDECYT 1140845 (leaded by MR), Millennium
518 Institute of Oceanography, Chile (ICM grant IC 120019), COPAS Sur-Austral (CONICYT PIA
519 CCTE AFB170006) and CRN3070-IAI (US national science Foundation; grant GEO-11280040)
520 is also acknowledged. MP-K thanks financial support for internships at LEGOS and IGP from
521 the REDOC.CTA (Red Doctoral en Ciencia, Tecnología y Ambiente, University of Concepción,
522 Chile) and CONICYT, respectively. BD, OP and MR also acknowledge supports from
523 FONDECYT 1171861 (led by K. Goubanova). This work was granted access to the HPC
524 resources of CALMIP supercomputing center at the Toulouse University under the allocations
525 2017-1044 and 2018-1044. ROMS model code is available at http://www.croco-ocean.org. All
526 input data set and configuration of our ROMS/BIOEBUS simulations are described in section 2.2
527 and in the references therein.
528

529

530

531

532 **References**

533

534 Aguirre, C., Pizarro, O., Strub, P. T., Garreaud, R., & Barth, J. (2012). Seasonal dynamics of the
535 near-surface alongshore flow off central Chile. *Journal of Geophysical Research, 117*,
536 C01006. https://doi.org/10.1029/2011JC007379

537 Astudillo, O., Dewitte, B., Mallet, M., Frappart, F., Rutllant, J. A., Ramos, M., et al. (2017).
538 Surface winds offPeru-Chile: Observing closer to the coast from radar altimetry. Remote
539 Sensing ofEnvironment, 191, 179–196. https://doi.org/10.1016/j.rse.2017.01.010

540 Belmadani, A., E. Concha, D. Donoso, A. Chaigneau, F. Colas, N.A. Maximenko, and E. Di
541 Lorenzo (2017), Striations and preferred eddy tracks triggered by topographic steering of
542 the background flow in the eastern South Pacific. *J. Geophys. Res.-Oceans,122*, 2847-
543 2870, https://doi.org/10.1002/2016JC012348

544 Bettencourt, J. H., C. López, E. Hernández-García, I. Montes, J. Sudre, B. Dewitte, A. Paulmier,
545 and Garçon, V (2015), Boundaries of the Peruvian Oxygen Minimum Zone shaped by
546 coherent mesoscale dynamics. *Nat. Geosci., 8*, 937–940. doi:10.1038/ngeo2570

547 Bopp, L., Resplandy, L., Orr, J. C., Doney, S. C., Dunne, J. P., Gehlen, M., Halloran, P., Heinze,
548 C., Ilyina, T., Séférian, R., Tjiputra, J., and Vichi, M (2013). Multiple stressors of ocean
549 ecosystems in the 21st century: projections with CMIP5 models. *Biogeosciences, 10*,
550 6225-6245. https://doi.org/10.5194/bg-10-6225-2013

551 Breitburg, D., Levin, L. A., Oschlies, A., Grégoire, M., Chavez, F. P., Conley, D. J., ... &
552 Jacinto, G. S. (2018). Declining oxygen in the global ocean and coastal waters. *Science,*
553 *359* (6371), eaam 7240. http://dx.doi.org/10.1126/science.aam7240

554 Chaigneau, A., & Pizarro, O. (2005). Eddy characteristics in the eastern South Pacific. *J.*
555 *Geophys. Res. Oceans, 110*(C6). https://doi.org/10.1029/2004JC002815

556 Chaigneau, A., Le Texier, M., Eldin, G., Grados, C., & Pizarro, O. (2011). Vertical structure of
557 mesoscale eddies in the eastern South Pacific Ocean: A composite analysis from
558 altimetry and Argo profiling floats. *J. Geophys. Res. Oceans*, *116*(C11).
559 https://doi.org/10.1029/2011JC007134

560 Chaigneau, A., Dominguez, N., Eldin, G., Vasquez, L., Flores, R., Grados, C., & Echevin, V.
561 (2013). Near-coastal circulation in the Northern Humboldt Current System from
562 shipboard ADCP data *J. Geophys. Res. Oceans*, *118*, 5251–5266. https://doi.org/
563 10.1002/jgrc.20328

564 Clarke, A. J., & Van Gorder, S. (1994). On ENSO coastal currents and sea levels. *Journal of*
565 *Physical Oceanography, 24*(3), 661-680.

566 Combes, V., S. Hormazábal, and E. Di Lorenzo (2015), Interannual variability of the subsurface
567 eddy field in the Southeast Pacific, *J. Geophys. Res. Oceans*, *120*, 4907–4924,
568 doi:10.1002/ 2014JC010265.

569 Contreras, M., Pizarro, O., Dewitte, B., Sepulveda, H. H., & Renault, L. (2019). Subsurface
570 mesoscale eddy generation in the ocean off central Chile. *J. Geophys. Res. Oceans*,
571 *124*(8), 5700-5722. https://doi.org/10.1029/2018JC014723

572 Cornejo D'Ottone, M., Bravo, L., Ramos, M., Pizarro, O., Karstensen, J., Gallegos, M., ... &
573 Karp-Boss, L. (2016). Biogeochemical characteristics of a long-lived anticyclonic eddy
574 in the eastern South Pacific Ocean. *Biogeosciences*, *13*(10), 2971-2979. DOI:
575 10.5194/bg-13-2971-2016

576 da Silva, A. M., Young, C. C., & Levitus, S. (1994). *Atlas ofSurface Marine Data 1994, vol. 1,*
577 *Algorithms and Procedures, NOAA Atlas NESDIS* (Vol. 6, p. 83). NOAA, Silver, Spring,
578 Md.

579 Dewitte, B., Vazquez-Cuervo, J., Goubanova, K., Illig, S., Takahashi, K., Cambon, G., et al.
580 (2012). Change in El Niño flavours over 1958– 2008: Implications for the long-term
581 trend of the upwelling off Peru. *Deep Sea Research Part II: Topical Studies in*
582 *Oceanography, 77-80*, 143–156. https://doi.org/10.1016/j.dsr2.2012.04.011

583 Espinoza-Morriberón, D., Echevin, V., Colas, F., Tam, J., Gutierrez, D., Graco, M., Ledesma, J.,
584 & Quispe-Ccalluari, C. (2019). Oxygen Variability During ENSO in the Tropical South
585 Eastern Pacific. *Frontiers in Marine Science*, *5*, 526.
586 https://doi.org/10.3389/fmars.2018.00526

587 Frenger, I., D. Bianchi, C. Sührenberg, A. Oschlies, J. Dunne, C. Deutsch, et al. (2018),
588 Biogeochemical role of subsurface coherent eddies in the ocean: Tracer cannonballs,
589 hypoxic storms, and microbial stewpots?. *Global Biogeochemical Cycles*, *32*, 226–249.
590 https://doi.org/10.1002/2017GB005743

591 Fuenzalida, R., Schneider, W., Garces, J., Bravo, L., & Lange, C. (2009). Vertical and horizontal
592 extension of the oxygen minimum zone in the eastern South Pacific Ocean. *Deep Sea*
593 *Research Part II: Topical Studies in Oceanography*, *56*, 992–1003.
594 https://doi.org/10.1016/j. dsr2.2008.11.001

595 Goubanova, K., Echevin, V., Dewitte, B., Codron, F., Takahashi, K., Terray, P., & Vrac, M.
596 (2011). Statistical downscaling of sea-surface wind over the Peru–Chile upwelling
597 region: diagnosing the impact of climate change from the IPSL-CM4 model. *Climate*
598 *Dynamics, 36*(7–8), 1365–1378. https://doi.org/10.1007/s00382-010-0824-0

599 Graco M., S. Purca, B. Dewitte, C. G. Castro, O. Moron, J. Ledesma, G. Flores and D. Gutierrez,
600 2017: The OMZ and nutrients features as a signature of interannual and low frequency
601 variability off the Peruvian upwelling system. *Biogeosciences*, *14*, 4601-4617.

602 Gunther, E. R. (1936), *A report on oceanographic investigations in the Peru Coastal Curren,*
603 *Discovery Rep. 13*, pp. 107-276, Cambridge Univ. Press, Cambridge, U. K.

604 Gutknecht, E., Dadou, I., Le Vu, B., Cambon, G., Sudre, J., Garçon, V., et al. (2013). Coupled
605 physical/biogeochemical modeling including O2-dependent processes in Eastern
606 Boundary Upwelling Systems: Application in the Benguela. *Biogeosciences, 10*(1), 1–22.
607 https://doi. org/10.5194/bg-10-1-2013

608 Gutiérrez, D., Enríquez, E., Purca, S., Quipúzcoa, L., Marquina, R., Flores, G., et al. (2008).
609 Oxygenation episodes on the continental shelf of central Peru: remote forcing and benthic
610 ecosystem response. *Prog. Oceanogr.* 79, 177–189. doi: 10.1016/j.pocean.2008.10.025

611 Hernandez-Ayon, Jose M., et al. "Dynamics of the Carbonate System Across the Peruvian
612 Oxygen Minimum Zone." *Frontiers in Marine Science 6* (2019): 617.
613 https://doi.org/10.3389/fmars.2019.00617

614 Hormazábal, S., Combes, V., Morales, C. E., Correa-Ramírez, M. A., Di Lorenzo, E., & Nuñez,
615 S. (2013). Intrathermocline eddies in the coastal transition zone offcentral Chile (31–
616 41°S). *J. Geophys. Res. Oceans*, 118,1–11. https://doi.org/10.1002/jgrc.20337

617 Hormazábal, S., Shaffer, G., Silva, N., & Navarro, E. (2006). The Perú-Chile undercurrent and
618 the oxygen minimum zone variability off central Chile. Gayana, 70(1), 37–45.

619 Illig, S., Cadier, E., Bachèlery, M.-L., & Kersalé, M. (2018). Subseasonal coastal-trapped wave
620 propagations in the southeastern Pacific and Atlantic Oceans: 1. A new approach to
621 estimate wave amplitude. Journal ofGeophysical Research: Oceans, 123, 3915–3941.
622 https://doi. org/10.1029/2017JC013539

623 Karstensen, J. (2004). Formation of the South Pacific shallow salinity minimum: A Southern
624 Ocean pathway to the tropical Pacific. Journal of physical oceanography, 34(11), 2398-
625 2412.

626 Keeling, R. F., Körtzinger, A. & Gruber, N. (2010). Ocean deoxygenation in a warming world.
627 *Annu. Rev. Mar. Sci. 2*, 199-229.

628 Koné, V., Machu, E., Penven, P., Garçon, V., Freon, P., & Demarcq, H. (2005). Modeling the
629 primary and secondary productions of the southern Benguela upwelling system: A
630 comparative study through two biogeochemical models. *Global Biogeochemical Cycles*,
631 *19*, GB4021. https://doi.org/10.1029/2004GB002427

632 Lachkar, Zouhair & Levy, Marina & Smith, Shafer. (2018). Intensification and deepening of the
633 Arabian Sea oxygen minimum zone in response to increase in Indian monsoon wind
634 intensity. *Biogeosciences*. *15*. 159-186. 10.5194/bg-15-159-2018.

635 Large, W., McWilliams, J. C., & Doney, S. (1994). Oceanic vertical mixing: A review and
636 model with a nonlocal boundary layer parame- terization. *Reviews of Geophysics*, *32*,
637 363–403. https://doi.org/10.1029/94RG01872

638 Long, M. C., Deutsch, C., & Ito, T. (2016). Finding forced trends in oceanic oxygen. *Global*
639 *Biogeochemical Cycles*, 30(2), 381-397.

640 Mogollón, R. & Calil, P. H. R. (2017). On the effects of ENSO on ocean biogeochemistry in the
641 Northern Humboldt Current System (NHCS): A modeling study. *Journal of Marine*
642 *Systems*, *172*, 137– 159. https://doi.org/10.1016/j.jmarsys.2017.03.011

643 Molemaker, M. J., McWilliams, J. C., & Dewar, W. K. (2015). Submesoscale instability and
644 generation of mesoscale anticyclones near a separation of the California Undercurrent.
645 *Journal of Physical Oceanography*, *45*(3), 613– 629.
646 https://doi.org/10.1175/JPO-D-13-0225.1

647 Montecinos, A., Purca, S., & Pizarro, O. (2003). Interannual-to-interdecadal sea surface
648 temperature variability along the western coast of South America. *Geophysical Research*
649 *Letters*, *30*(11). https://doi.org/10.1029/2003GL017345

650 Montes, I., Dewitte, B., Gutknecht, E., Paulmier, A., Dadou, I., Oschlies, A., & Garçon, V.
651 (2014). High-resolution modeling of the Eastern Tropical Pacific oxygen minimum zone:
652 Sensitivity to the tropical oceanic circulation. *J. Geophys. Res. Oceans*, 119, 5515–5532.
653 https://doi.org/10.1002/2014JC009858

654 Morales, C. E., S. Hormazábal, and J. L. Blanco (1999), Interannual variability in the mesoscale
655 distribution of the depth of the upper boundary of the oxygen minimum layer off northern
656 Chile (18–24S): Implications for the pelagic system and biogeochemical cycling. *J. Mar.*
657 *Res*, *57*, 909–932. https://doi.org/10.1357/002224099321514097

658 Naqvi, S. W. A., H. W. Bange, L. Farias, P. M. S. Monteiro, M. I. Scraton, and J. Zhang (2010),
659 Marine hypoxia/anoxia as a source of CH4 and N2O. *Biogeosciences*, *7*, 2159–2190.
660 doi:10.5194/bg-7-2159-2010

661 Oschlies, A., Brandt, P., Stramma, L., & Schmidtko, S. (2018). Drivers and mechanisms of
662 ocean deoxygenation. *Nature Geoscience*, *11*(7), 467-473.
663 https://doi.org/10.1038/s41561-018-0152-2

664 Paulmier, A., Ruiz-Pino, D., Garçon, V., Farias, L. (2006). Maintaining of the East South pacific
665 oxygen minimum zone (OMZ) off Chile. *Geophysical Research Letter*, *33*, L20601.
666 https://doi.org/10.1029/2006GL026801

667 Paulmier, A., Ruiz-Pino, D., Garçon, V. (2008). The oxygen minimum zone (OMZ) off Chile as
668 intense source of CO2 and N2O. *Continental Shelf Research*, *28 (*20), 2746-2756.
669 https://doi.org/10.1016/j.csr.2008.09.012

670 Penven, P., Echevin, V, Pasapera, J, Colas, F and Tam, J. (2005). Average circulation, seasonal
671 cycle, and mesoscale dynamics of the Peru Current System: A modeling approach, *J.*
672 *Geophys. Res., 110*, C10021, doi:10.1029/2005JC002945.

673 Pizarro, O., Clarke, A. J., & Van Gorder, S. (2001). El Niño sea level and currents along the
674 South American coast: Comparison of obser- vations with theory. *Journal of Physical*
675 *Oceanography*, *31*, 1891–1903.
676 https://doi.org/10.1175/1520-0485(2001)031<1891:ENOSLA>2.0. CO;2

677 Pizarro, O., Shaffer, G., Dewitte, B., & Ramos, M. (2002). Dynamics of seasonal and interannual
678 variability ofthe Peru-Chile Undercurrent. *Geophysical Research Letters*, *29*(12), 1581.
679 https://doi.org/10.1029/2002GL014790

680 Pizarro, O. & Montecinos, A. (2004). Interdecadal variability of the thermocline along the west
681 coast of South America. *Geophysical Research Letters*, *31*(20).
682 https://doi.org/10.1029/2004GL020998

683 Pizarro, O., Ramírez, N., Castillo, M. I., Cifuentes, U., Rojas, W., & Pizarro-Koch, M. (2016).
684 Underwater glider observations in the oxygen minimum zone off central Chile. *Bulletin*
685 *of the American Meteorological Society*, *97*(10), 1783-1789.
686 https://doi.org/10.1175/BAMS-D-14-00040.1

687 Pizarro-Koch, M., Pizarro, O., Dewitte, B., Montes, I., Ramos, M., Paulmier, A., & Garcon, V.
688 (2019). Seasonal variability of the southern tip of the oxygen minimum zone in the
689 Eastern South Pacific (30º-38ºS): A Modeling Study. *J. Geophys. Res. Oceans*. 124,
690 8574- 8604. https://doi.org/10.1029/2019JC015201

691 Ramos, M., B. Dewitte, O. Pizarro, and G. Garric (2008), Vertical propagation of extratropical
692 Rossby waves during the 1997–1998 El Nin ˜o off the west coast of South America in a
693 medium-resolution OGCM simulation, *Geophysical Research Letters*, *113*, C08041,
694 doi:10.1029/2007JC004681.

695 Reid, J. L. (1973). The shallow salinity minima of the Pacific Ocean. *In Deep Sea Research and*
696 *Oceanographic Abstracts,* 20, (1), 51-68. https://doi.org/10.1016/0011-7471(73)90042-9

697 Schlosser, C., Streu, P., Frank, M., Lavik, G., Croot, P. L., Dengler, M., & Achterberg, E. P.
698 (2018). H 2 S events in the Peruvian oxygen minimum zone facilitate enhanced dissolved
699 Fe concentrations. *Sci Rep*, *8, 12642*. https://doi.org/10.1038/s41598-018-30580-w

700 Schmidtko, S., Stramma, L. & Visbeck, M. (2017). Decline in global oceanic oxygen content
701 during the past five decades. *Nature* 542, 335-339. https://doi.org/10.1038/nature21399

702 Schneider, W., Fuenzalida, R., Rodríguez-Rubio, E., Garcés-Vargas, J., & Bravo, L. (2003).
703 Characteristics and formation of eastern South Pacific intermediate water. *Geophysical*
704 *Research Letters*, *30*(11). https://doi.org/10.1029/2003GL017086

705 Schneider, W., Donoso, D., Garcés-Vargas, J., & Escribano, R. (2017). Water-column cooling
706 and sea surface salinity increase in the upwelling region off central-south Chile driven by
707 a poleward displacement of the South Pacific High. *Progress in Oceanography*, *151*, 38-
708 48. https://doi.org/10.1016/j.pocean.2016.11.004

709 Shchepetkin, A. F., & McWilliams, J. C. (2003). A method for computing horizontal
710 pressure-gradient force in an oceanic model with a nonaligned vertical coordinate. *J.*
711 *Geophys. Res. Oceans*, 108(C3). https://doi.org/10.1029/2001JC001047

712 Shchepetkin, A., & McWilliams, J. C. (2005). The regional oceanic modeling system (ROMS): a
713 split-explicit, free-surface, topography- following- coordinate oceanic model. Ocean
714 Modelling, 9,347–404. https://doi.org/10.1016/j.ocemod.2004.08.002

715 Shchepetkin, A. F., & McWilliams, J. C. (2009). Correction and commentary for "Ocean
716 forecasting in terrain-following coordinates: Formulation and skill assessment of the
717 regional ocean modeling system" by Haidvogel et al., J. Comp. Phys. 227, pp. 3595–
718 3624. *Journal of Computational Physics*, *228*(24), 8985-9000.
719 https://doi.org/10.1016/j.jcp.2009.09.002

720 Silva, N., & Neshyba, S. (1979). On the southernmost extension of the Peru-Chile Undercurrent.
721 *Deep Sea Research Part I. Oceanographic Research Papers*, *26*, 1387–1393.
722 https://doi.org/10.1016/0198-0149(79)90006-2

723 Silva, N., Rojas, N., & Fedele, A. (2009). Water masses in the Humboldt Current System:
724 properties, distribution, and the nitrate deficit as a chemical water mass tracer for
725 equatorial subsurface water off Chile. *Deep Sea Research Part II: Topical Studies in*
726 *Oceanography*, *56*, 1004–1020. https://doi.org/10.1016/j.dsr2.2008.12.013

727 Smith, R.D., J. K. Dukowicz, R. C. Malone (1992), Parallel ocean general circulation modeling.
728 *Physica D, 60*, 38–61. doi:10.1016/0167-2789(92)90225-C

729 Sobarzo, M., Bravo, L., Donoso, D., Garcés-Vargas, J., & Schneider, W. (2007). Coastal
730 upwelling and seasonal cycles that influence the water column over the continental shelf
731 off central Chile. *Progress in Oceanography*, *75*, 363–382. https://doi.org/10.1016/j.
732 pocean.2007.08.022

733 Torres, R., et al. (2011), Air-sea CO2 fluxes along the coast of Chile: From CO_2 outgassing in
734 central northern upwelling waters to CO2 uptake in southern Patagonian fjords, J.
735 Geophys. Res., 116, C09006, doi:10.1029/2010JC006344.

736 Vergara, O., B. Dewitte, I. Montes, V. Garçon, M. Ramos, A. Paulmier, and O. Pizarro (2016),
737 Seasonal variability of the oxygen minimum zone off Peru in a high-resolution regional
738 coupled model. *Biogeosciences*, *13*, 4389–4410. doi:10.5194/bg-13-4389-2016

739 Vergara, O., B. Dewitte, M. Ramos, and O. Pizarro (2017), Vertical energy flux at ENSO time
740 scales in the subthermocline of the Southeastern Pacific. *J. Geophys. Res. Oceans*, 122.
741 doi:10.1002/2016JC012614

742 Wijffels, S. E., Toole, J. M., & Davis, R. (2001). Revisiting the South Pacific subtropical
743 circulation: A synthesis of World Ocean Circulation Experiment observations along 32 S.
744 *J. Geophys. Res. Oceans*, *106*(C9), 19481-19513.

745 Wooster, W. S., and M. Gilmartin (1961), The Peru–Chile Undercurrent. *J. Mar. Res*., 19, 97–
746 122.
747

748 **Figures Captions**

749

750 **Figure 1**. Climatological mean of the dissolved oxygen (DO) at 300 m depth in the eastern South
751 Pacific Oxygen Minimum Zone (ESP-OMZ) obtained from CARS 2009 climatology (a). The
752 area of study defined here such as the extra-tropical region of ESP-OMZ is located between 30°S
753 - 38°S and 76º W – and the coast (black square). A 3-D annual mean volume of the extra-tropical
754 OMZ modeled defined here as the region with 9-year (2000-2008) mean DO ≤ 45 μM (red
755 isosurface) (b). The shading colour represents the spatial DO distribution modeled at 300m
756 depth. The interannual anomalies of the OMZ volume (red line; OMZ_{VOL}) and the DO within
757 OMZ (black line; OMZ_{DO}) obtained from the model (c).

758

759 **Figure 2**. Annual mean of the DO meridional section during 2001(a) and 2007(b) for the coastal
760 band (region from the coast to 80 km offshore). The vertical mean of the DO sections (c) and the
761 difference between both periods (d). Background color in (μM) and the isopycnals of 1026.2 and
762 1026.8 kgm^{-3} are shown overlaid in white. Water masses percentage estimated between 1026.2
763 and 1026.8 kgm^{-3} isopycnals (e). The water masses are Subantarctic Water, (SAAW; 11.5ºC,
764 33.8), Equatorial Subsurface Water (ESSW; 12.5ºC, 34.9) and Antarctic Intermediate Water
765 (AAIW; 3ºC, 34). The water mass and their thermohaline indices (T, S) indicated above were
766 obtained from *Silva et al.*, 2009 and were used here to compute the water mass proportions.

767

768 **Figure 3**. Seasonal cycles (black square-line) and monthly time series for 2001 (red square-line)
769 and 2007 (blue square-line) of the extratropical OMZ volume between 2000-2008 years (a). The
770 red and blue dashed line represented the annual mean and the standard deviation of the seasonal
771 cycle volume is represented with black error bar. 3-D distribution of the annual mean of the
772 extratropical OMZ volume (red isosurface) for 2001 (b) and 2007 (c) years.

773

774 **Figure 4.** Interannual DO budget within the mean OMZ volume (see Figure 1b). Interannual
775 anomalies of DO and DO rate of change ($\partial DO/\partial T$) (a). The different terms of the right-hand side
776 of Eq. (1) are also shown (b): The physical term (*PHYS* red dashed line) is the summed-up
777 contribution of advection and mixing. The advection term (*ADV*) is composed, in turn, by zonal
778 (*Xadv*, magenta line), meridional (*Yadv*, blue line) and vertical (*Zadv*, cyan line) advections. The
779 mixing terms are the summed-up contribution of the horizontal diffusion (*Hmix*; grey line) and
780 vertical diffusivity (*Vmix*, dark green line) (c). The biogeochemical fluxes (*SMS*, light green line)
781 represent the "source-minus-sink" contribution to the DO rate of change due to biogeochemical
782 processes, among them are: photosynthetic production (dark-green line), oxic decomposition
783 (dark-magenta line), excretion (sky line) and nitrification (yellow line) (d).

784

785 **Figure 5.** Interannual anomalies of the alongshore southward transport associated to the PCUC
786 modeled (in Sv, 1 Sv = 10^6 m^3s^{-1}) (a) and mean DO inside the PCUC (in μM) defined by the
787 isopleth of -0.02 m s^{-1} in the first 150 km from the coast and above 700m depth (c). The root
788 mean square of (RMS) of the interannual variability of $PCUC_{TR}$ and $PCUC_{DO}$ is shown in (b) and
789 (d) respectively. Mean of the interannual anomalies of both $PCUC_{TR}$ and $PCUC_{DO}$ for the whole

790 region (e). The red line represents the PCUC transport, note that a positive value indicates high
791 southward transport. The black line represents the average DO inside the PCUC.

792

793 **Figure 6.** Annual mean of the zonal DO transport along meridional section at 74ºW between 30º
794 and 38ºS during 2001 and 2007 periods represented separately by the sum between the mean
795 zonal advective fluxes ($\langle \widetilde{\boldsymbol{u}}\widetilde{DO} \rangle$, (a) and (c)) and the zonal mesoscale eddy fluxes ($\langle \mathbf{u}'DO' \rangle$, (b)
796 and (d)). The shading color represented eastward (red) and westward (blue) flux (in m s^{-1} μM).
797 The $\langle \widetilde{\boldsymbol{u}}\widetilde{DO} \rangle$ and $\langle \mathbf{u}'DO' \rangle$ integrated between 50-500m depth is shown in (e) and (f) respectively
798 while vertical mean of the section is shown in (g).

799

800 **Table Captions**

801

802 **Table 1.** Root mean square (RMS) and descriptive statistics of the seasonal and interannual
803 variability of the OMZ_{VOL} (in km^3) and OMZ_{DO} (μM s^{-1}).

804

805 **Table 2.** Root mean square (RMS) of the seasonal and interannual variability of the DO
806 concentration and the different terms of the DO budget in a a fixed volume defined as the region
807 with 9-year (2000-2008) mean DO ≤ 45 μM, as shown in Figure 1b. The mean (2000-2008) and
808 annual mean to 2001 and 2007 for DO and each term of the DO budget also is presented. The
809 physical term (*PHYS*) is the summed-up contribution of all advection and mixing terms to the
810 rate of change of DO (∂DO/∂t). The advection terms are the zonal (*Xadv*), meridional (*Yadv*) and
811 vertical (*Zadv*) advections. The subgrid mixing terms are the summed-up contribution of the
812 horizontal diffusion (*Hmix*) and vertical diffusivity (*Vmix*). The biogeochemical fluxes (*SMS*)
813 represents the "source-minus-sink" contribution to the ∂DO/∂t due to biogeochemical processes.
814 The *SMS* term is decomposed in photosynthetic production, oxic decomposition, excretion and
815 nitrification. The DO is in μM and DO budget terms are in μM s^{-1}.
816

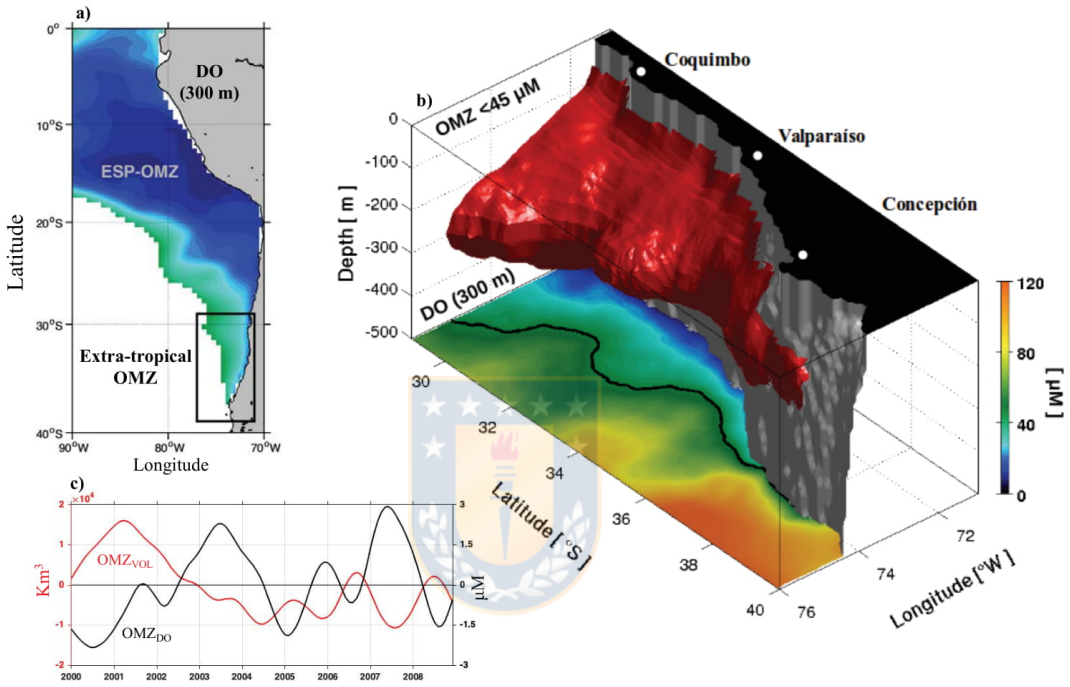

Figure 1. Climatological mean of the dissolved oxygen (DO) at 300 m depth in the eastern South Pacific Oxygen Minimum Zone (ESP-OMZ) obtained from CARS 2009 climatology (a). The area of study defined here such as the extra-tropical region of ESP-OMZ is located between 30°S - 38°S and 76° W – and the coast (black square). A 3-D annual mean volume of the extra-tropical OMZ modeled defined here as the region with 9-year (2000-2008) mean DO ≤ 45 µM (red isosurface) (b). The shading colour represents the spatial DO distribution modeled at 300m depth. The interannual anomalies of the OMZ volume (red line; OMZ_{VOL}) and the DO within OMZ (black line; OMZ_{DO}) obtained from the model (c).

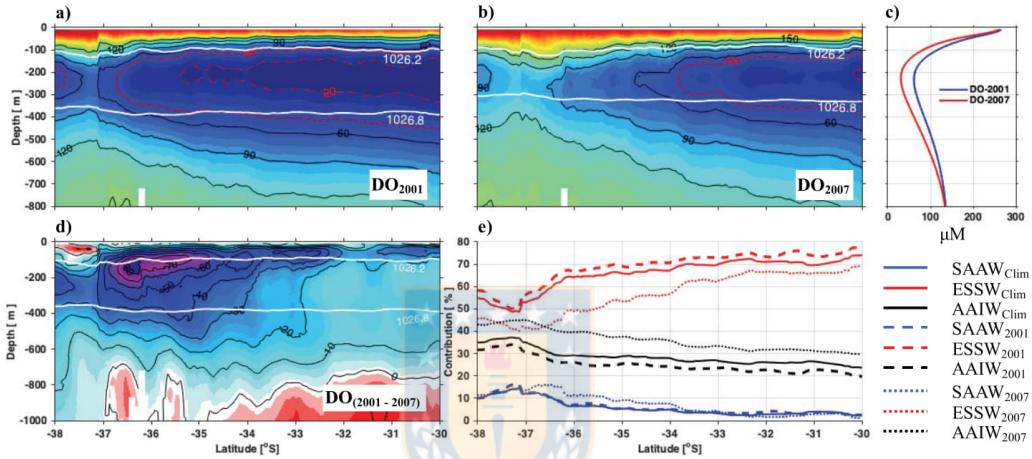

Figure 2. Annual mean of the DO meridional section during 2001(a) and 2007(b) for the coastal band (region from the coast to 80 km offshore). The vertical mean of the DO sections (c) and the difference between both periods (d). Background color in (µM) and the isopycnals of 1026.2 and 1026.8 kgm^{-3} are shown overlaid in white. Water masses percentage estimated between 1026.2 and 1026.8 kgm^{-3} isopycnals (e). The water masses are Subantarctic Water, (SAAW; 11.5ºC, 33.8), Equatorial Subsurface Water (ESSW; 12.5ºC, 34.9) and Antarctic Intermediate Water (AAIW; 3ºC, 34). The water mass and their thermohaline indices (T, S) indicated above were obtained from *Silva et al.*, 2009 and were used here to compute the water mass proportions.

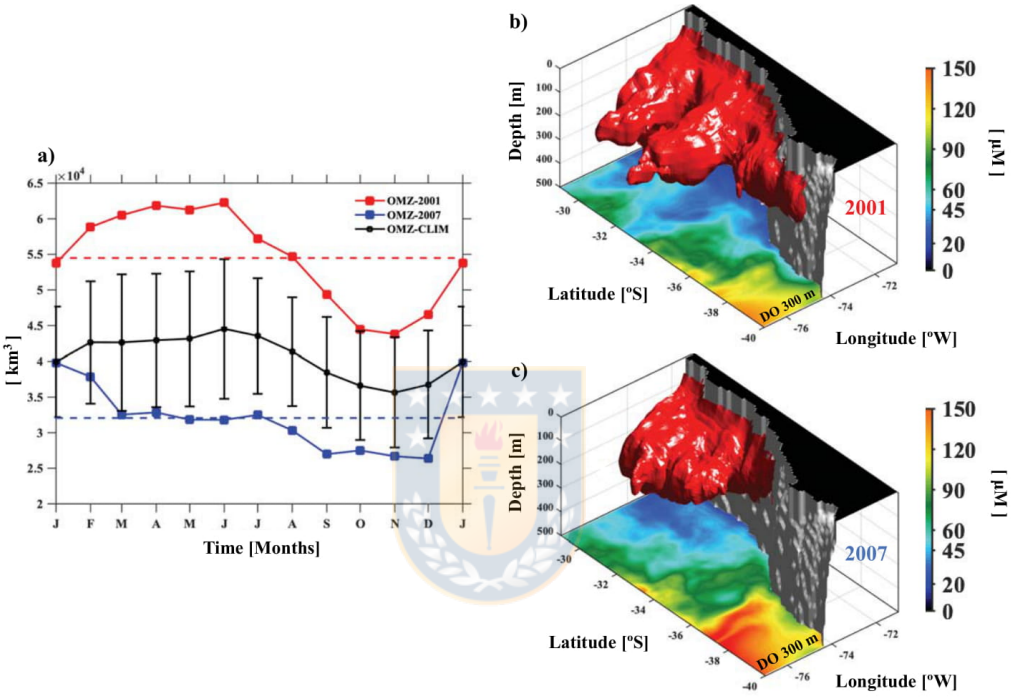

Figure 3. Seasonal cycles (black square-line) and monthly time series for 2001 (red square-line) and 2007 (blue square-line) of the extratropical OMZ volume between 2000-2008 years (a). The red and blue dashed line represent the annual mean and the standard deviation of the seasonal cycle volume is represented with black error bar. 3-D distribution of the annual mean of the extratropical OMZ volume (red isosurface) for 2001 (b) and 2007 (c) years.

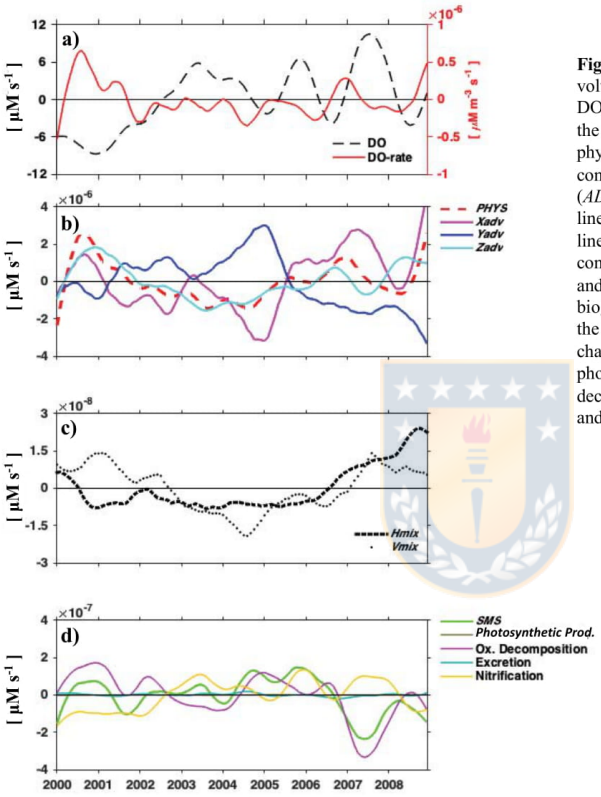

Figure 4. Interannual DO budget within the mean OMZ volume (see Figure 1b). Interannual anomalies of DO and DO rate of change (∂DO/∂T) (a). The different terms of the right-hand side of Eq. (1) are also shown (b): The physical term (*PHYS* red dashed line) is the summed-up contribution of advection and mixing. The advection term (*ADV*) is composed, in turn, by zonal (*Xadv*, magenta line), meridional (*Yadv*, blue line) and vertical (*Zadv*, cyan line) advections. The mixing terms are the summed-up contribution of the horizontal diffusion (*Hmix*; grey line) and vertical diffusivity (*Vmix*, dark green line) (c). The biogeochemical fluxes (*SMS*, light green line) represent the "source-minus-sink" contribution to the DO rate of change due to biogeochemical processes, among them are: photosynthetic production (dark-green line), oxic decomposition (dark-magenta line), excretion (sky line) and nitrification (yellow line) (d).

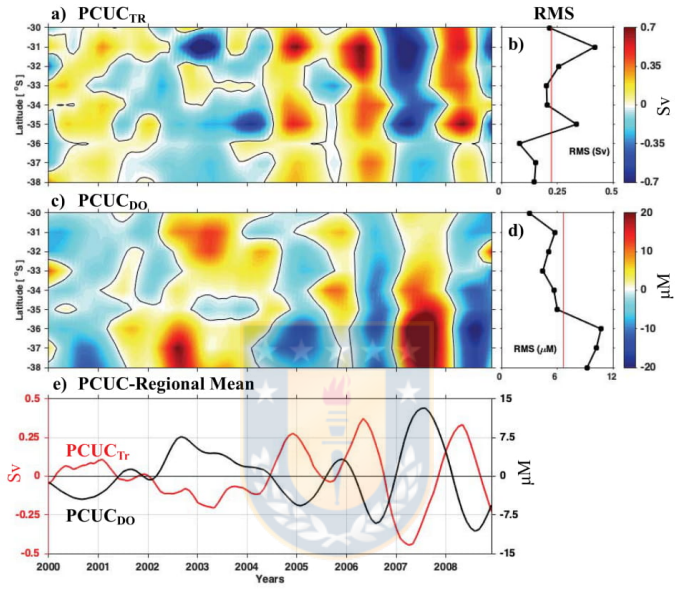

Figure 5. Interannual anomalies of the alongshore southward transport associated to the PCUC modeled (in Sv, 1 Sv = 10^6 m^3s^{-1}) (a) and mean DO inside the PCUC defined by the isopleth of -0.02 m s^{-1} in the first 150 km from the coast and above 700m depth (c). The root mean square of (RMS) of the interannual variability of $PCUC_{TR}$ and $PCUC_{DO}$ is shown in (b) and (d) respectively. Mean of the interannual anomalies of both PCUC transport and its DO inside for the whole region (e). The red line represents the PCUC transport, note that a positive value indicates high southward transport. The black line represents the average DO inside the PCUC.

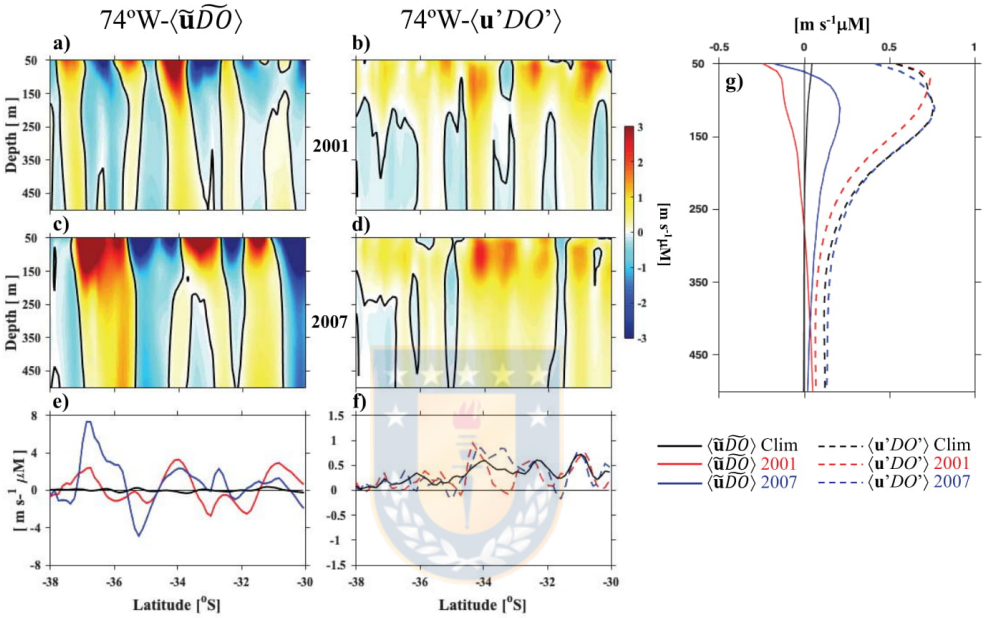

Figure 6. Annual mean of the zonal DO transport along meridional section at 74ºW between 30º and 38ºS during 2001 and 2007 periods represented separately by the sum between the mean zonal advective fluxes (⟨$\tilde{\mathbf{u}}\tilde{DO}$⟩, (a) and (c)) and the zonal mesoscale eddy fluxes (⟨**u**'*DO*'⟩, (b) and (d)). The shading color represented eastward (red) and westward (blue) flux (in m s^{-1} μM). The ⟨$\tilde{\mathbf{u}}\tilde{DO}$⟩ and ⟨**u**'*DO*'⟩ integrated between 50-500m depth is shown in e) and f) respectively while vertical mean of the section is shown in (g).

Table 1. Root mean square (RMS) and descriptive statistics of the seasonal and interannual variability of the OMZ_{VOL} (in km^3) and OMZ_{DO} ($\mu M\ s^{-1}$).

	Seasonal RMS	Interannual RMS	2001 Average	2007 Average	[2000-2008] Average	Max	Min
OMZ_{VOL} ($\leq 45\ \mu M$)[a]	2.3e3	0.75e4	5.5e4	3.2e4	4.0e4	6.3e4	2.6e4
OMZ_{VOL} ($\leq 20\ \mu M$)[b]	1.8e4	0.37e4	1.5e4	4.9e3	1.1e4	2.2e4	1.2e3
OMZ_{DO} [a]	0.7	1.4	28.1	31.0	28.4	33.0	24
OMZ_{DO} [b]	0.6	0.8	12.0	14.0	12.2	17.0	9.0

Table 2. Root mean square (RMS) of the seasonal and interannual variability of the DO concentration and the different terms of the DO budget in a a fixed volume defined as the region with 9-year (2000-2008) mean DO ≤ 45 μM, as shown in Figure 1b. The mean (2000-2008) and annual mean to 2001 and 2007 for DO and each term of the DO budget also is presented. The physical term (*PHYS*) is the summed-up contribution of all advection and mixing terms to the rate of change of DO (∂DO/∂t). The advection terms are the zonal (*Xadv*), meridional (*Yadv*) and vertical (*Zadv*) advections. The subgrid mixing terms are the summed-up contribution of the horizontal diffusion (*Hmix*) and vertical diffusivity (*Vmix*). The biogeochemical fluxes (*SMS*) represent the "source-minus-sink" contribution to the ∂DO/∂t due to biogeochemical processes. The SMS term is decomposed in photosynthetic production, oxic decomposition, excretion and nitrification. The DO is in μM and DO budget terms are in μM s^{-1}.

DO Budget Terms	Seasonal RMS	Interannual RMS	Mean [2000-2008] Average	2001 Average	2007 Average
DO	3.2	5.1	32	26	41
∂DO/∂t	5.40e-7	2.21e-7	-1.31e-8	-1.08e-7	4.50e-8
PHYS	1.02e-6	1.02e-6	1.78e-6	2.12e-6	2.29e-6
Xadv	1.60e-6	1.59e-6	-4.43e-6	-5.41e-6	-1.88e-6
Yadv	0.60e-6	1.40e-6	3.85e-6	4.07e-6	2.27e-6
Zadv	0.48e-6	0.92e-6	2.35e-6	3.43e-6	1.85e-6
Hmix	7.40e-9	8.90e-9	-2.86e-8	-3.36e-8	-1.75e-8
Vmix	1.01e-8	0.89e-8	4.76e-8	5.57e-8	5.46e-8
SMS	2.21e-7	9.53e-8	-1.45e-6	-1.49e-6	-1.65e-6
Photosynthetic production	1.95e-9	0.52e-9	6.86e-9	6.60e-9	7.00e-9
Oxic depcomposition	1.48e-7	1.18e-7	-7.32e-7	-6.86e-7	-1.04e-6
Excretion	2.54e-8	7.73e-9	-1.02e-7	-1.05e-7	1.06e-7
Nitrification	1.00e-7	8.48e-7	-6.60e-9	-7.52e-6	-5.46e-6

5. DISCUSIÓN

En septiembre de 2018, en la ciudad de Kiel, Alemania, se realizó una conferencia sobre el problema de la desoxigenación de los océanos, a partir de la discusión sostenida en esta reunión los participantes dieron a conocer a la comunidad internacional una declaración titulada "*El Océano pierde su aliento*" (*The Ocean is losing its breath;* https://www.ocean-oxygen.org/declaration). Los puntos más importantes de esta declaración indican que las aguas que han agotado su oxígeno en los océanos se han expandido cuatro veces durante los últimos 50 años, llegando incluso a perder hasta el 40% de su OD. Esta pérdida de OD amenaza la vida marina, los ecosistemas del océano, el hábitat y la biodiversidad, especialmente en las comunidades costeras. La declaración argumenta que el calentamiento global de la Tierra afecta la distribución de OD en el océano en dos formas i) disminuyendo su solubilidad (principalmente en las regiones tropicales) y ii) aumentando la estratificación de la columna de agua, disminuyendo la mezcla y la ventilación debido a la circulación oceánica lo que implica una limitación en el intercambio de oxígeno océano-atmósfera, y a su vez el intercambio con el océano profundo. No obstante, esta desoxigenación no sería sólo una consecuencia, sino que además puede ser un factor amplificador del calentamiento global a través de una mayor producción de gases de efecto invernadero que se originan en aguas pobres en OD. La declaración enfatiza la importancia de generar estrategias para mitigar y eventualmente revertir la desoxigenación y sus impactos ecológicos, las cuales deben ser desarrolladas conjuntamente entre los ámbitos científico y social teniendo como base un mayor conocimiento de las ZMOs.

Específicamente en Chile, las aguas que bañan la zona costera desde Arica a Puerto Montt contienen aguas subsuperficiales extraordinariamente pobres en oxígeno, sin embargo, aún es muy poco lo que se conoce acerca de la variabilidad natural de esta ZMO y cómo el calentamiento global está impactando en ella. En este contexto, el presente trabajo de tesis contribuye al conocimiento de esta ZMO, particularmente a los mecanismos que controlan su variabilidad en escalas de tiempo que se extienden de meses a algunos años. Conocer estos mecanismos es fundamental para entender como el océano regional y la ZMO evolucionará durante las próximas décadas.

Las aguas con bajo oxígeno frente a Chile son parte de la gran ZMO del océano Pacífico Suroriental (PSO) que abarca desde el Pacífico ecuatorial hasta la región central de Chile, esta última (30°– 40°S), considerada como la frontera sur de la ZMO del PSO. En efecto, esta frontera presenta una dinámica espacial y temporal diferente a la región ecuatorial y tropical de las costas de Perú y norte de Chile (e.g. *Czeschel et al*., 2011; *Montes at al*., 2010; *Strub et al*., 1998, 2019), siendo particularmente sensible a la extensión (e intensificación) de la ZMO y, en general, al calentamiento global.

En este estudio se utilizó un modelo hidrodinámico tridimensional de resolución 1/12º (ROMS) acoplado a un modelo biogeoquímico (BioEBUS) y se evaluó la variabilidad estacional e interanual en el balance de OD mediante el análisis de las contribuciones de procesos físicos de advección (horizontal y vertical) y mezcla, y de los procesos biogeoquímicos. Los resultados del modelo apoyan la hipótesis de que la variabilidad de la CSPC es un mecanismo relevante sobre la variabilidad de la ZMO como ha sido previamente reportado (e.g. *Gunther*, 1936; *Silva and Neshyba,* 1979, *Huyer et al*., 1991; *Strub et al*., 1998; *Hormazabal*., 2006; *Silva et al*., 2009). La mayor parte de la variabilidad estacional del OD se asocia con cambios en la proporción de la masa de agua AESS (transportada por la CSPC) más que con cambios generados por procesos biogeoquímicos. Este resultado está de acuerdo con la alta correlación entre el OD y la salinidad al interior del volumen de la ZMO a lo largo del año. No obstante, otros procesos físicos como los remolinos de mesoescala y las corrientes zonales también demostraron tener un rol fundamental en la variabilidad espacial y temporal de la ZMO.

Los remolinos de mesoescala (ciclónicos y anticiclónicos) ejercen una influencia importante en el transporte vertical y horizontal de calor, sal, temperatura y otras propiedades físicas, biológicas y químicas en el océano (*McGillicuddy et al*., 2015). Estas estructuras ocupan alrededor del 30% de la superficie del océano y contienen más del 80% de la energía cinética de la circulación oceánica (*Chelton et al*., 2007; *Chaigneau et al*., 2009). En la cuenca del Pacífico Sur Oriental, *Combes et al*. (2015) mediante modelación numérica observaron una asimetría en el número de remolinos superficiales y subsuperficiales. En la superficie dominan levemente los remolinos ciclónicos sobre los anticiclónicos, mientras que en la capa subsuperficial asociada a la ZMO esta relación es inversa, dominando los remolinos

anticiclónicos inducidos por inestabilidades de la CSPC cerca de la costa de Perú y Chile (*Thomsen et al*., 2016; *Contreras et al*., 2019). En los sistemas de surgencia de borde oriental, estos remolinos subsuperficiales representan el ~30-55% de la totalidad de los remolinos anticiclónicos, alcanzando un radio aproximado de 60 km y una extensión vertical de ~500 m (*Pegliasco et al*., 2015; *Barceló-Llull et al*., 2017). En el océano Pacífico, la propagación de estos remolinos hacia el oeste son capaces de transportar las propiedades de las aguas costeras (aguas hipóxicas ricas en nutrientes) hacia el giro subtropical (*Chaigneau et al*., 2009*; Combes et al., 2015; Hormazabal et al*., 2013) impactando en gran medida el volumen de la ZMO, y representando aproximadamente el 10% del transporte de oxígeno y nutrientes en la picnoclina (*Colas et al*., 2012; *Cornejo et al.,* 2016; *Frenger et al*., 2018).

Los mecanismos a través de los cuales los remolinos de mesoescala transportan propiedades horizontalmente (o a lo largo de superficies de igual densidad), se pueden tratar, por una parte, como procesos de difusión turbulenta utilizando las correlaciones entre fluctuaciones para estimar el transporte, por ejemplo ($\langle u'C' \rangle$, $\langle v'C' \rangle$), donde (u,v) son las componentes zonal y meridional de la velocidad y C es la concentración de algún compuesto disuelto, las ()' denotan perturbación respecto de un promedio de tiempo superior a la escala típica de los remolinos de mesoescala (el promedio representado por $\langle\ \rangle$). Esta fue justamente la aproximación utilizada en el presente estudio. Por otro lado, los remolinos pueden jugar también un rol advectivo (*Lee, et al*., 1997; *Zhang et al*., 2014), transportando sustancias disueltas gradiente arriba (es decir desde regiones de menor concentración de C hacia regiones de mayor concentración). En nuestra región de estudio los remolinos se propagan hacia el oeste transportando oxígeno desde regiones cercanas a la costa con bajas concentraciones de OD, hacia regiones oceánicas con aguas que están, comúnmente, mucho mejor ventiladas. Junto con transportar aguas con bajo OD, estos remolinos transportan, nutrientes, microbios y otras substancias que crean ambientes anómalos con características propias de la OMZ, en regiones alejadas de la costa (*Frenger et al*., 2018). El rol que juegan estos remolinos en la expansión de la ZMO frente a Chile y el papel que podrían jugar los eventos de bajo oxígeno en la ecología regional requiere de estudios con un enfoque diferente al abordado aquí.

Adicional a esto, las corrientes zonales de mesoescala o estriaciones también cumplen un rol importante en la variabilidad del borde oceánico de la ZMO. Estas corrientes alternadas hacia el este y el oeste tienen una escala meridional de 300-500 km, extendiéndose zonalmente por miles de kilómetros con una alta coherencia vertical a lo largo de cientos de metros en profundidad. Los estudios que han descrito estas características se han basado en diferentes aproximaciones tales como altimetría satelital (*Maximenko et al*., 2005), boyas Argo (*Cravatte et al*., 2012), datos de cruceros oceanográficos (*Stramma et al*., 2008, 2010; *Brand et al*., 2008, 2012, 2015) y modelos numéricos tanto globales como regionales (*Sinha y Richards*, 1999; *Davis et al*., 2013; *Belmadani et al*., 2017; *Delpech et al*., 2020). Pese a esto, son poco los estudios que han evaluado las implicancias de estas estructuras sobre trazadores biogeoquímicos (*Dietze and Löptien*, 2013; *Duteil et al*., 2014; *Cabré et al*., 2015; *Delpech et al*., 2020). Si bien estas corrientes zonales presentan velocidades débiles, cercanas a ~1cm s^{-1}, se ha descrito que pueden ser capaces de transportar calor (*Buckingham et al.,* 2014), contribuir a la mezcla de trazadores (*Chen y Flierl*, 2015), transportar detritus marinos en la superficie (*Maes et al*., 2016) e incluso modificar los vientos cercanos a la superficie (*Taguchi et al*., 2012).

Por tanto y en base a este contexto, a continuación, se discute en mayor detalle cómo estos mecanismos físicos (variaciones en la CSPC y estructuras de mesoescala) estarían influenciando la variabilidad estacional e interanual del OD y la ZMO frente a la región central de Chile.

5.1 Transporte Meridional de OD: El rol de la Corriente Subsuperficial de Perú-Chile

Dentro de las corrientes que componen el SCH, la CSPC es clave en el transporte meridional subsuperficial de OD (así como de nutrientes y otras propiedades biológicas y físico-químicas) desde la región ecuatorial a la región extratropical, siendo fundamental en los cambios de volumen e intensidad de la ZMO. Note que la CSPC transporta OD en una dirección contraria al gradiente predominante, por lo que se representa mejor diciendo que transporta aguas con bajo OD. Los resultados del primer capítulo evidencian una buena relación entre la variabilidad semianual de la CSPC y la extensión zonal, volumen, profundidad media y términos advectivos dominantes en el presupuesto de OD al interior de la ZMO. Específicamente, el volumen de la

ZMO presentó dos valores mínimos y máximos a lo largo del año, alcanzando el volumen mínimo absoluto (y máxima concentración de OD) aproximadamente uno a dos meses después de que la CSPC mostrara su valor mínimo de transporte hacia el sur.

La componente semianual del ciclo estacional de la CSPC es principalmente de origen ecuatorial, mientras que los armónicos anuales son el resultado de una combinación del forzamiento de viento ecuatorial y local (*Pizarro et al*., 2002; *Shaffer et al*., 1997, 1999). A lo largo de la costa oeste de Sudamérica, el cambio estacional de los vientos varía en amplitud y fase –frente a Perú los máximos vientos favorables a la surgencia ocurren en invierno, mientras que en la costa centro-sur de Chile (~35°S - 40°S) estos tienen lugar en verano– lo que también podría introducir una variabilidad semianual en la CSPC. *Vergara et al*. (2016c) mediante modelación numérica demostraron que la disminución del rotor del viento (anomalías ciclónicas del rotor) impacta la intensidad del transporte de la CSPC hacia el sur. Pese a esto, el efecto del viento sobre la ZMO no fue abordado directamente en este estudio, dado que el objetivo principal fue evaluar los impactos de la variabilidad del transporte de la CSPC y de las estructuras de mesoescala a nivel subsuperficial sobre la ZMO. Sin embargo, futuros trabajos deberían ser orientados a la evaluación del efecto del viento (esfuerzo y rotor) sobre la ZMO, dada la proyección de aumento en la magnitud de los vientos para la región (*Garreaud y Falvey*, 2009; *Oerder et al*., 2018), y su potencial influencia sobre la circulación, surgencia costera y los procesos biogeoquímicos locales (ej. productividad biológica, flujos de carbono y nitrógeno, acidificación del agua, entre otros).

En contraste con la variabilidad semianual observada en las diferentes métricas del volumen de la ZMO, el ciclo estacional de la oxiclina y la disponibilidad de OD en la columna de agua sobre la plataforma continental frente a Concepción (~36.5º S) están asociados a un único armónico anual. En esta latitud, la profundidad mínima de la oxiclina coincide con los vientos favorables a la surgencia costera, similar a lo reportado en otras zonas del norte de Chile (20°S y 24°S; *Reyes et al*., 2007, Figura 158). En este sentido, los cambios estacionales de OD sobre la plataforma continental estarían más asociados con la surgencia anual que con los factores (*e.g*. la CSPC) que controlan su concentración en el núcleo de la ZMO sobre el talud continental. Otros antecedentes también muestran una variabilidad intraestacional e interanual

de la oxiclina asociada con procesos ecuatoriales remotos como las ondas atrapadas a la costa forzadas por ondas ecuatoriales de Kelvin. Estas ondas además de perturbar la picnoclina y la oxiclina, impactan la CSPC y la advección a lo largo de la costa (*Shaffer et al.,* 1997, *Morales et al.,* 1999; *Ulloa et al.,* 2001; *Illig et al.,* 2018a, b). Sin embargo, la variabilidad del OD sobre la plataforma continental y su relación con la surgencia costera no fue analizada en este estudio debido a que se requiere i) una simulación con mejor resolución espacial para representar correctamente la plataforma continental y los procesos físicos que podrían ser relevantes tales como la formación de frentes y remolinos de sub-mesoescala (*Thomsen et al*., 2016), y ii) un modelo que permita representar los procesos biogeoquímicos en los sedimentos y su interacción con los procesos que tienen lugar en la plataforma, tales como la acumulación de materia orgánica, biopertubación, nitrificación y desnitrificación, entre otros (*Gutknecht et al*., 2013a, b).

A escala interanual, la amplitud de las anomalías de los procesos biogeoquímicos (principalmente respiración oxigénica y nitrificación) fue significativamente menor respecto de los procesos físicos (principalmente advección) que suceden al interior del volumen de la ZMO. Los resultados indicaron que la amplitud de la variabilidad interanual de la ZMO es ~30% mayor que la variabilidad estacional, incluso durante periodos con eventos ENOS débiles, como lo fue el periodo analizado 2000-2008. Debido a esto, los resultados obtenidos podrían interpretarse como un análisis de la variabilidad natural del sistema, es decir, el modo de variabilidad interna del océano levemente influenciado por forzamientos externos.

En el segundo capítulo se abordó la influencia que la CSPC ejerce sobre la variabilidad interanual de la ZMO frente a la región central de Chile. Para este propósito, las anomalías interanuales del volumen de la ZMO fueron contrastadas con el transporte hacia el sur de la CSPC. Los resultados mostraron que la CSPC tiene un rol clave en la modulación del contenido de OD en el núcleo de la ZMO sobre el talud continental. Asimismo, se observó una disminución del ~30% en el volumen de la ZMO durante el año 2007 en conjunto con un debilitamiento del transporte de la CSCP, aumentando de manera constante el contenido de OD en las aguas transportadas hacia el sur. En contraste, un aumento en el volumen de la ZMO fue observado durante el año 2001 junto con una leve anomalía positiva del transporte de la CSPC, indicando

que este mecanismo por sí solo no explica en su totalidad el incremento del volumen, y que, por tanto, otros procesos físicos estarían co-modulando la variabilidad de la ZMO, tales como los remolinos de mesoescala. En este sentido y en base a los estudios recientes que han demostrado que la CSPC es relevante para la generación y formación de los remolinos de mesoescala subsuperficiales (*Thomsen et al*., 2016; *Frenger et al*., 2018; *Contreras et al*., 2019), se pudo establecer que i) la CSPC como mecanismo físico influye directamente sobre la intensidad de la ZMO mediante el transporte meridional hacia el sur de la AESS, y ii) la CSPC influye indirectamente sobre el volumen de la ZMO debido a un transporte zonal hacia aguas oceánicas producto de la generación de remolinos de mesoescala subsuperficiales.

5.2 Transporte Zonal de OD: El rol de las Corrientes Zonales y los Flujos Turbulentos de Mesoescala

Conforme a la dominancia de los procesos físicos sobre los procesos biogeoquímicos en el balance de OD al interior de la ZMO a escalas estacional e interanual, la componente zonal (este-oeste) de la advección fue el término físico más relevante en el balance de OD en la región de estudio. En consecuencia, la advección zonal (asociada al flujo medio) y los flujos turbulentos de OD, asociados a la actividad de mesoescala, fueron evaluados con mayor detalle a escala estacional e interanual. En términos de la advección zonal de OD, la región oceánica estuvo marcada por la presencia de bandas zonales intercaladas (positivas y negativas), siendo las bandas positivas (hacia el este) las asociadas con flujos de OD hacia la costa (ventilando la ZMO), mientras que, las bandas negativas (hacia el oeste) estuvieron asociadas con la expansión de la ZMO costa afuera. Este tipo de estructuras zonales han sido previamente reportadas como mecanismo de ventilación de las ZMOs principalmente en la región ecuatorial (*Tsuchiya et al*., 1992; *Schott et al*., 1995, 1998, *Brandt et al*., 2008, 2010, 2012), sin embargo, se conoce muy poco acerca del impacto sobre la ZMO de estos flujos zonales en regiones extratropicales.

Estas estructuras zonales también conocidas como estriaciones se han observado en diferentes regiones del océano (ej. *Maximenko et al*., 2005; *Brand et al*., 2010; *Cravatte et al*., 2012; *Belmadani et al*., 2017; *Xia et al*., 2020). Frente a Chile central, las inestabilidades de la CSPC provocadas por la fricción topográfica inducen una vorticidad relativa capaz de

desencadenar la formación de estriaciones espacialmente coherentes con las rutas de los remolinos de mesoescala (*Davis et al*., 2014; *Belmadani et al*., 2017). Horizontalmente pueden alcanzar cientos de km y presentar una estructura vertical coherente en profundidad. Aunque su velocidad promedio es pequeña (~1 cm s^{-1}), tienen la capacidad de transportar masa y calor (*Buckingham et al*., 2014), así como también contribuir de manera significativa a la mezcla de trazadores biogeoquímicos (*Chen and Flierl*, 2015).

A pesar de la compleja estructura zonal del transporte de OD, el ciclo anual promedio de las corrientes zonales en la región de estudio presentó una marcada variabilidad semianual, transportando aguas con bajo oxígeno costa afuera, extendiendo el volumen de la ZMO hacia la región oceánica. Este transporte fue mínimo durante la transición de invierno-primavera asociado a un debilitamiento de la CSPC, lo que en conjunto produjo una reducción en el volumen total de la ZMO y un aumento en la concentración de OD al interior del mismo. A escala interanual, la posición e intensidad de estas corrientes zonales fueron determinantes en la variabilidad de la ZMO, tal como se evidenció durante el año 2007, en donde el flujo neto de OD positivo (hacia el este) estuvo asociado con una notable disminución en el volumen de la ZMO en ~30% con respecto al volumen climatológico para todo el periodo considerado (2000-2008). Si bien el término advectivo medio representó aproximadamente el 80% del total del transporte zonal de OD, el restante ~20% estuvo asociado a flujos turbulentos de mesoescala.

El ciclo anual de los flujos turbulentos presentó una alta variabilidad intraestacional con una dirección promedio preferente hacia la costa, contribuyendo al transporte de OD hacia la ZMO durante todo el año, es decir, éste sería un mecanismo físico clave en la ventilación de la ZMO. Un ejemplo de esto se observó durante el año 2001 cuando los flujos turbulentos disminuyeron ~30% y el volumen de la ZMO se incrementó en un ~38%, resaltando el rol que cumplen los flujos turbulentos sobre la variabilidad espacial y temporal de la ZMO. Estos resultados son consistentes con otros estudios previamente realizados en la ZMO frente a Perú y Chile. *Vergara et al*. (2016a) indicaron que el ciclo anual de la ZMO frente a Chile es modulado en gran medida por los flujos turbulentos de OD con un impacto altamente heterogéneo tanto en los bordes como en la estructura vertical de la ZMO. Mientras que, *Bettencourt et al*. (2015) utilizando modelación numérica con enfoque langrangiano y un

análisis de exponentes de Lyapunov demostraron que a profundidades medias (entre 380-600 m) las estructuras de mesoescala cumplen dos funciones relevantes en los bordes de la ZMO: En primer lugar, la trayectoria y la posición media de los flujos turbulentos delimitan y mantienen los bordes de la ZMO y, en segundo lugar, la variabilidad de alta frecuencia de estos flujos inyecta OD hacia la ZMO, siendo mayores que el flujo advectivo medio.

En resumen, tanto el ciclo anual como la variabilidad interanual del transporte zonal de OD, están relacionados con la advección de los chorros zonales (bandas intercaladas), los flujos turbulentos asociados a los remolinos de mesoescala y el transporte hacia el sur de la CSPC, modulando la extensión oceánica y meridional hacia el sur de la ZMO. Cabe notar que el transporte zonal de OD es indirectamente controlado por inestabilidades de la CSPC en la banda costera (~100 km) debido a la formación de los remolinos anticiclónicos subsuperficiales incidiendo también en la localización de los jets zonales. De este modo, la CSPC y su variabilidad ejercerían un control clave sobre la ZMO. Por otra parte, nuestros resultados mostraron que la variabilidad de la ZMO es directamente influenciada por la intensidad de los chorros zonales y la ventilación asociada a los flujos turbulentos de remolinos sobre la frontera oceánica de la ZMO, impactando de esta forma la distribución lateral de OD. En este sentido, los resultados sugieren que este tipo de jets o chorros zonales en conjunto con los flujos turbulentos contribuyen de igual manera que la CSPC al transporte de OD desde y hacia la ZMO, sin embargo, la influencia zonal principalmente modula la forma y extensión del límite oceánico de la ZMO. Futuros estudios deben enmarcarse en este aspecto, incluyendo experimentos de sensibilidad en los modelos numéricos, considerando que la representación de la actividad de mesoescala depende críticamente de una serie de parámetros que incluyen la resolución horizontal, y la interacción océano-atmósfera debido a la actividad de mesoescala. Una parametrización debe dar cuenta, además, del transporte advectivo asociado a los remolinos de mesoescala, particularmente aquellos que presentan un núcleo cercano al núcleo de la ZMO.

5.3 Evaluación y perspectivas de la Modelación Biogeoquímica

El modelo acoplado (ROMS-BioEBUS) usado en este estudio, al igual que la mayoría de las investigaciones basadas en herramientas de modelación y/o simulación numérica tienen

un error asociado a la exactitud con la que los modelos logran representar los procesos oceanográficos que ocurren en el océano. Debido a esto, la evaluación de los modelos es un paso importante en todo trabajo de investigación basado en este tipo de herramientas. Esta evaluación consiste en la comparación estadística entre las variables oceanográficas modeladas y observaciones directas, con el propósito de determinar la capacidad del modelo de reproducir los valores promedios y la variabilidad espacial y temporal de las variables analizadas (Espinoza-*Morriberon et al*., 2016; *Lettmann et al*., 2020). En este estudio, la simulación fue evaluada en términos de la temperatura superficial del mar (TSM), la salinidad, la clorofila-a (Clo-a), el ciclo anual y la variabilidad interanual del OD, y de la CSPC. Para esto, la TSM y Clo-a extraídas del modelo fueron comparadas con los datos satelitales obtenidos del sensor AQUA-MODIS, el OD y la salinidad fueron contrastados con los datos de la climatología CARS y la serie de tiempo de una estación costera perteneciente a la Universidad de Concepción (conocida como Estación 18; e.g. *Farías et al*., 2018), en tanto que, la CSPC fue comparada con mediciones directas de corrientes realizada en un anclaje ubicado en el talud continental cerca de los 30ºS (*Pizarro et al*., 2001).

Los resultados de estos análisis mostraron que el modelo sobreestima (subestima) la concentración de OD (la profundidad de la oxiclina) al interior de la ZMO muy cerca de la costa, sobre la plataforma continental (La estación 18 se ubica a menos de 100 m de profundidad, en la parte interior de la plataforma) y subestima el transporte meridional de la CSPC en un 30-40% en 30°S. Por otra parte, el RMSE de la TSM y la Clo-a modelada fue de 0.7ºC y 0.4 mg C d^{-1} respectivamente, mientras que la energía cinética de remolinos fue sobreestimada. Adicional a esto, el modelo biogeoquímico BioEBUS demostró ser altamente sensible a la velocidad de descomposición de la materia orgánica y su distribución vertical, así como también a la velocidad de hundimiento del material particulado (*Gutknecht et al*., 2013a, b). Estos sesgos podrían afectar las conclusiones obtenidas sobre el rol de la CSPC en la variabilidad de la ZMO, debido a que la concentración de OD es sensible a la cantidad de oxígeno advectado hacia el sur por la CSPC.

Para evaluar la influencia que podrían tener estos sesgos sobre los resultados obtenidos es necesario realizar experimentos de sensibilidad para la región, lo cual no fue incluido en el

presente trabajo. Sin embargo, a continuación, se presentan algunas estrategias para disminuir el error asociado y mejorar el estado medio en futuras simulaciones físico-biogeoquímicas para la región. En primer lugar, incluir un forzamiento atmosférico que represente de mejor forma la interacción océano-atmosfera sobre la actividad de mesoescala (Oerder *et al*., 2018) y el decaimiento del viento (drop-off) cerca de la costa, dado que la mayoría de los productos atmosféricos utilizados como forzantes sobreestiman la intensidad del viento en esta región (*Astudillo et al*., 2017, 2019), implicando una sobreestimación en la intensidad de la surgencia costera, un mayor enfriamiento de la TSM y pérdida de OD en la columna de agua debido a una alta tasa de producción/exportación de materia orgánica. En segundo lugar, se deben ajustar los parámetros biogeoquímicos para la región específica de estudio, tales como la tasa máxima de crecimiento del fitoplancton, la nitrificación y los procesos anamox, entre otros, dado que los parámetros utilizados en este modelo fueron originalmente adecuados para simular la ZMO frente a Perú (Montes *et al*., 2014). Esto requiere de un trabajo exhaustivo de recopilación de información oceanográfica regional y, para algunos casos, de complementar la información actualmente existente con nuevas observaciones. Por último, es importante, especialmente en la región centro sur, incorporar la descarga de los ríos, además de incluir un compartimiento asociado a la dinámica biogeoquímica del sedimento, el cual podrían actuar como sumidero importante de OD cerca de la costa (*Bianucci et al*., 2012; *Adams et al*., 2013; *Siedlecki et al*., 2015).

A pesar de las limitaciones del modelo utilizado en este trabajo, la simulación reproduce adecuadamente la dinámica fundamental del Sistema de Borde Oriental frente a la costa central de Chile, caracterizado por una surgencia activa (pasiva) durante primavera/verano (otoño/invierno) con un alta (baja) productividad biológica en las capas superficiales del océano. Representa además el transporte hacia el sur de aguas con bajo contenido de OD por la CSPC, permitiendo abordar las preguntas planteadas sobre la interacción de los procesos físicos y biogeoquímicos tanto de la CSPC como de la ZMO. Finalmente, el uso de estas herramientas de modelación permite analizar una amplia cantidad e interacción de procesos físicos-biogeoquímicos a distintas escalas espacio-temporales de variabilidad, proporcionando además una guía para futuros experimentos de campo de estudios basados en observaciones.

6. CONCLUSIONES

Este trabajo de tesis doctoral es una contribución al conocimiento y entendimiento de la dinámica estacional e interanual de la ZMO en la región central de Chile. El objetivo principal del presente estudio fue analizar las contribuciones relativas de algunos procesos físicos, como la advección y la mezcla turbulenta, y algunos procesos biogeoquímicos que se asumieron relevantes para la variabilidad estacional e interanual del oxígeno disuelto en la columna de agua, frente a la costa central de Chile (30ºS-38ºS). Para cumplir este objetivo, se utilizó un modelo acoplado físico-biogeoquímico para evaluar la variabilidad de la ZMO-PSO entre los 30°S y 38°S, región que corresponde a la frontera sur de esta ZMO.

De acuerdo a los análisis de validación, el modelo demostró capturar adecuadamente la estructura media de la variabilidad espacial y temporal de la ZMO, aunque el OD fue sobreestimado cerca de la zona costera y en el extremo sur del dominio. Respecto del análisis del presupuesto estacional e interanual de OD al interior del volumen de la ZMO (definida como el volumen de agua con OD < 45 μM) se pudo concluir que los flujos de OD asociados a la actividad biológica son un orden de magnitud menores que los flujos de OD relacionados con procesos físicos. En este sentido, los procesos biogeoquímicos contribuyeron solamente un ~10-20% en el presupuesto estacional e interanual de oxígeno, indicando que el balance de OD en la región de estudio está controlado por los procesos físicos, principalmente por la advección y mezcla. Los términos advectivos fueron relevantes tanto a escala estacional como interanual, y dentro de estos, las componentes zonal y meridional de la advección de OD fueron dominantes por sobre la advección vertical. En relación a los términos asociados a la mezcla (horizontal y vertical), estos fueron menores en comparación con los términos advectivos, no obstante, fueron del mismo orden de magnitud que los observados por los procesos biogeoquímicos, y podrían tener un mayor protagonismo en el presupuesto del OD en otras escalas de variabilidad temporal. Asimismo, los resultados obtenidos sugieren que la variabilidad estacional e interannual del volumen de la ZMO está altamente relacionada con las aguas subsuperficiales con altos valores de salinidad (>34.5) y la CSPC, lo que concuerda con estudios previos que han reportado la relación existente entre la ZMO y la masa de agua AESS caracterizada además por un alto contenido de nutrientes y CO_2.

En este sentido, los resultados evidenciaron una estrecha relación entre la variabilidad estacional del transporte de la CSPC y la ZMO, observando que el ciclo anual del transporte hacia el sur por parte de la CSPC se relaciona con un mayor volumen de agua con bajo contenido de OD frente a Chile central. A escala interanual, la CSPC impactó principalmente la intensidad de la ZMO y secundariamente su volumen, aunque esta modulación no fue homogénea a lo largo de la costa debido a la ocurrencia de otros procesos físicos simultáneos capaces de perturbar el transporte meridional de la CSPC y de contribuir directamente a la ventilación y extensión hacia el oeste de la ZMO. Por una parte, la intensidad y variabilidad espacial de las corrientes zonales (jets) asociadas al flujo medio mostraron ser un mecanismo importante en la conformación de las características promedio y las anomalías de la ZMO. Estos jets zonales intercalados (positivos y negativos) se observan mayormente en la región oceánica, siendo los jets positivos (hacia el este) los asociados con flujos de OD hacia la costa quienes ventilan la ZMO, mientras que, los jets negativos (hacia el oeste) estuvieron asociados principalmente con la expansión de la ZMO costa afuera. Por otra parte, otro mecanismo clave en la ventilación del la ZMO son los flujos turbulentos de OD asociados a la actividad de mesoescala. En general, estos flujos turbulentos presentan una alta variabilidad intraestacional y su dirección es positiva (hacia el este) permanente e impacta directamente las tasas de ventilación estacional e interanual de la ZMO.

Finalmente concluimos que el transporte meridional de OD por la CSPC regula aproximadamente el 60% los cambios estacionales e interanuales del OD, impactando fuertemente el talud continental asociado al núcleo de la ZMO. A esto se suma el rol que cumplen los jets zonales y flujos turbulentos mayormente sobre la variabilidad espacial y temporal del borde oceánico de la ZMO frente a la zona central de Chile.

7. REFERENCIAS

- Adams, K.A., Barth, J.A. and Chan, F., 2013. Temporal variability of near-bottom dissolved oxygen during upwelling off central Oregon. *Journal of Geophysical Research: Oceans*, *118*(10), pp.4839-4854.

- Aguirre, C., O. Pizarro, P. T. Strub, R. Garreaud, J. Barth (2012), Seasonal dynamics of the near-surface alongshore flow off central Chile. J. Geophys. Res. 117, C01006. http://dx.doi.org/10.1029/2011JC007379

- Aguirre, C., R. Garreaud, J. Rutllant (2014), Surface ocean response to synoptic-scale variability in wind stress and heat fluxes off south-central Chile. Dyn. Atmos. Ocean. 65, 64-85. http://dx.doi.org/10.1016/j.dynatmoce.2013.11.001

- Anderson, J. J., A. Okubo, A. Robbins, and A. Richards (1982), A model for nitrite and nitrate distributions in oceanic oxygen minimum zones, Deep Sea Res. ,29, 1113–1140.

- Arevalo-Martínez, D.L., Kock, A., Löscher, C.R., Schmitz, R.A. and Bange, H.W., 2015. Massive nitrous oxide emissions from the tropical South Pacific Ocean. *Nature Geoscience*, *8*(7), pp.530-533.

- Astudillo, O., et al. (2017), Surface winds off Peru-Chile: Observing closer to the coast from radar altimetry. Remote Sensing of Environment. Vol. (191), Pages 179-196. https://doi.org/10.1016/j.rse.2017.01.010

- Astudillo, O., Dewitte, B., Mallet, M., Rutllant, J. A., Goubanova, K., Frappart, F., et al. (2019). Sensitivity of the near-shore oceanic cir- culation off Central Chile to coastal wind profiles characteristics. Journal ofGeophysical Research: Oceans, 124, 4644–4676. https://doi. org/10.1029/2018JC014051

- Barceló-Llull, B., Sangrà, P., Pallàs-Sanz, E., Barton, E.D., Estrada-Allis, S.N., Martínez-Marrero, A., Aguiar-González, B., Grisolía, D., Gordo, C., Rodríguez-Santana, Á. and Marrero-Díaz, Á., 2017. Anatomy of a subtropical intrathermocline eddy. Deep Sea Research Part I: Oceanographic Research Papers, 124, pp.126-139.

- Bakun, A. C.S. Nelson (1991), The seasonal cycle of wind-stress curl in subtropical eastern boundary current regions. Journal of Physical Oceanography 21: 1815-1834. https://doi.org/10.1175/1520-0485(1991)021<1815:TSCOWS>2.0.CO;2

- Blanco, J. L., A. C. Thomas, M. E. Carr & P. T. Strub. (2001). Seasonal climatology of hidrographic conditions in the upwelling region off northern Chile. J. Geophys. Res., 106, 11.451-11.467.

- Belmadani, A., E. Concha, D. Donoso, A. Chaigneau, F. Colas, N.A. Maximenko, and E. Di Lorenzo (2017), Striations and preferred eddy tracks triggered by topographic steering of the background flow in the eastern South Pacific. J. Geophys. Res.-Oceans,122 (4), 2847-2870, doi:10.1002/2016JC012348.

- Bertagnolli, A.D. and Stewart, F.J., 2018. Microbial niches in marine oxygen minimum zones. *Nature Reviews Microbiology*, *16*(12), pp.723-729.

- Bettencourt, J. H., López, C., Hernández-García, E., Montes, I., Sudre, J., Dewitte, B., et al. (2015). Boundaries of the Peruvian Oxygen Minimum Zone shaped by coherent mesoscale dynamics. Nature Geoscience, 8, 937–940. https://doi.org/10.1038/ngeo2570

- Bianucci, L., K. Fennel and K. L. Denman (2012), Role of sediment denitrification in water column oxygen dynamics: comparison of the North American East andWest Coasts, Biogeosciences, 9, 2673– 2682, doi:10.5194/bg-9-2673-2012, 2012.

- Bopp, L., Le Quéré, C., Heimann, M., Manning, A.C. and Monfray, P., 2002. Climate-induced oceanic oxygen fluxes: Implications for the contemporary carbon budget. Global Biogeochemical Cycles, 16(2), pp.6-1.

- Brandt, P., Hormann, V., Bourles, B., Fischer, J., Schott, F.A., Stramma, L. and Dengler, M., 2008. Oxygen tongues and zonal currents in the equatorial Atlantic. *Journal of Geophysical Research: Oceans*, *113*(C4).

- Brandt, P., Greatbatch, R. J., Claus, M., Didwischus, S. H., Hormann, V., Funk, A., Hahn, J., Krahmann, G., Fischer, J., and Körtzinger, A.: Ventilation of the equatorial Atlantic by the equatorial deep jets, J. Geophys. Res.-Oceans, 117, C12015, 2012

- Brandt, P., Bange, H.W., Banyte, D., Dengler, M., Didwischus, S.H., Fischer, T., Greatbatch, R.J., Hahn, J., Kanzow, T., Karstensen, J. and Körtzinger, A., 2015. On the role of circulation and mixing in the ventilation of oxygen minimum zones with a focus on the eastern tropical North Atlantic. *Biogeosciences (BG)*, *12*, pp.489-512.

- Breitburg, D., Levin, L.A., Oschlies, A., Grégoire, M., Chavez, F.P., Conley, D.J., Garçon, V., Gilbert, D., Gutiérrez, D., Isensee, K. and Jacinto, G.S., 2018. Declining oxygen in the global ocean and coastal waters. *Science*, *359*(6371).

- Buckingham, C. E. & Cornillon, P. C. The contribution of eddies to striations in absolute dynamic topography. J. Geophys. Res. Ocean. 118, 448–461 (2013).

- Cabré, A., Marinov, I., Bernardello, R. and Bianchi, D., 2015. Oxygen minimum zones in the tropical Pacific across CMIP5 models: mean state differences and climate change trends. *Biogeosciences*, *12*(18), pp.5429-5454.

- Cantarero, S.I., Henríquez-Castillo, C., Dildar, N., Vargas, C.A., Von Dassow, P., Cornejo-D'Ottone, M. and Sepúlveda, J., 2020. Size-fractionated contribution of microbial biomass to suspended organic matter in the Eastern Tropical South Pacific oxygen minimum zone. *Frontiers in Marine Science*, *7*, p.745.

- Czeschel, R., Stramma, L., Schwarzkopf, F.U., Giese, B.S., Funk, A. and Karstensen, J., 2011. Middepth circulation of the eastern tropical South Pacific and its link to the oxygen minimum zone. *Journal of Geophysical Research: Oceans*, *116*(C1).

- Chaigneau, A., Eldin, G. and Dewitte, B., 2009. Eddy activity in the four major upwelling systems from satellite altimetry (1992–2007). *Progress in Oceanography*, *83*(1-4), pp.117-123.

- Chaigneau, A., N. Dominguez, G. Eldin, L. Vasquez, R. Flores, C. Grados, and V. Echevin (2013), Near-coastal circulation in the Northern Humboldt Current System from shipboard ADCP data. J. Geophys. Res. Oceans, 118. doi:10.1002/jgrc.20328

- Chelton, D.B., Schlax, M.G., Samelson, R.M. and de Szoeke, R.A., 2007. Global observations of large oceanic eddies. *Geophysical Research Letters*, *34*(15).

- Chen, R., and G. R. Flierl (2015), The contribution of striations to the eddy energy budget and mixing: Diagnostic frameworks and results in a quasigeostrophic barotropic system with mean flow, J. Phys. Oceanogr., 45, 2095–2113, doi:10.1175/JPO-D-14-0199.1.

- Callbeck, C.M., Lavik, G., Stramma, L., Kuypers, M.M. and Bristow, L.A., 2017. Enhanced nitrogen loss by eddy-induced vertical transport in the offshore Peruvian oxygen minimum zone. *PLoS One*, *12*(1), p.e0170059.

- Chan, F., Barth, J.A., Kroeker, K.J., Lubchenco, J. and Menge, B.A., 2019. The dynamics and impact of ocean acidification and hypoxia. *Oceanography*, *32*(3), pp.62-71.

- Chavez, F.P. and Messié, M., 2009. A comparison of eastern boundary upwelling ecosystems. *Progress in Oceanography*, *83*(1-4), pp.80-96.

- Cline, J.D. and Richards, F.A., 1972. OXYGEN DEFICIENT CONDITIONS AND NITRATE REDUCTION IN THE EASTERN TROPICAL NORTH PACIFIC OCEAN 1. *Limnology and Oceanography*, *17*(6), pp.885-900.

- Codispoti, L. A., Brandes, J. A., Christensen, J. P., Devol, A. H., Naqvi, S. W. A., Paerl, H. W., and Yoshinari, T. (2001). The oceanic fixed nitrogen and nitrous oxide budgets: Moving targets as we enter the anthropocene?, Sci. Mar., 65(S2), 85–105, doi:10.3989/scimar.2001.65s285.

- Colas, F., J. C. McWilliams, X. Capet, J. Kurian (2012), Heat balance and eddies in the Peru-Chile current system. Clim. Dyn. 39 (1–2), 509–529.

- Combes, V., S. Hormazábal, and E. Di Lorenzo (2015), Interannual variability of the subsurface eddy field in the Southeast Pacific, J. Geophys. Res. Oceans, 120, 4907–4924, doi:10.1002/ 2014JC010265.

- Contreras, M., Pizarro, O., Dewitte, B., Sepulveda, H.H. and Renault, L., 2019. Subsurface mesoscale eddy generation in the ocean off central Chile. *Journal of Geophysical Research: Oceans*, *124*(8), pp.5700-5722.

- Cornejo, M., Farías, L. (2012). Meridional variability of the vertical structure and air-sea fluxes of N2O off central Chile (30-40°S). Progress in Oceanography 92(1), 33-42. doi: 10.1016/j.pocean.2011.07.016

- Cornejo D'Ottone, M., Bravo, L., Ramos, M., Pizarro, O., Karstensen, J., Gallegos, M., Correa-Ramirez, M., Silva, N., Farias, L. and Karp-Boss, L., 2016. Biogeochemical characteristics of a long-lived anticyclonic eddy in the eastern South Pacific Ocean. *Biogeosciences (BG)*, *13*(10), pp.2971-2979.

- Cravatte, S., W.S Kessler & F. Marin (2012), Intermediate zonal jets in the tropical Pacific Ocean observed by Argo floats. Journal of Physical Oceanography, 42(9), 1475-1485. https://doi.org/10.1175/JPO-D-11-0206.1

- da Silva, A. M., C. C. Young, and S. Levitus (Eds.) (1994), Atlas of Surface Marine Data 1994, vol. 1, Algorithms and Procedures, NOAA Atlas NESDIS, vol. 6, 83 pp., NOAA, Silver, Spring, Md.

- Davis, A., Di Lorenzo, E., Luo, H., Belmadani, A., Maximenko, N., Melnichenko, O., & Schneider, N. (2014). Mechanisms for the emer- gence of ocean striations in the North Pacific. Geophysical Research Letters, 41, 948–953. https://doi.org/10.1002/2013GL057956

- Dadou, I., Lamy, F., Rabouille, C., Ruiz-Pino, D., Andersen, V., Bianchi, M., and Garc¸on, V.: An integrated biological pump model from the euphotic zone to the sediment: a 1-D applica- tion in the Northeast tropical Atlantic, Deep Sea Res. Pt II, 48, 2345–2381, 2001.

- Dadou, I., Evans, G., and Garc¸on, V.: Using JGOFS in situ and ocean color data to compare biogeochemical models and esti- mate their parameters in the subtropical North Atlantic Ocean, J. Mar. Res., 62, 565–594, 2004.

- Daneri, G., Dellarossa, V., Quiñones, R., Jacob, B., Montero, P. and Ulloa, O., 2000. Primary production and community respiration in the Humboldt Current System off Chile and associated oceanic areas. *Marine Ecology Progress Series*, *197*, pp.41-49.

- Debreu, L., Marchesiello, P., Penven, P. and Cambon, G., 2012. Two-way nesting in split-explicit ocean models: Algorithms, implementation and validation. Ocean Modelling, 49, pp.1-21.

- Delpech, A., Cravatte, S., Marin, F., Ménesguen, C. and Morel, Y., 2020. Deep Eddy Kinetic Energy in the Tropical Pacific from Lagrangian Floats. *Journal of Geophysical Research: Oceans*, *125*(8), p.e2020JC016313.

- Dewitte, B., et al. (2012), Change in El Niño flavours over 1958–2008: Implications for the long-term trend of the upwelling off Peru. Deep-Sea Res. Part. II, 77–80, 143–156. doi:10.1016/j.dsr2.2012.04.011

- Dietze, H. and Löptien, U., 2013. Revisiting “nutrient trapping” in global coupled biogeochemical ocean circulation models. *Global Biogeochemical Cycles*, *27*(2), pp.265-284.

- Duteil, O., Schwarzkopf, F.U., Böning, C.W. and Oschlies, A., 2014. Major role of the equatorial current system in setting oxygen levels in the eastern tropical Atlantic Ocean: A high-resolution model study. *Geophysical Research Letters*, *41*(6), pp.2033-2040.

- Escribano, R., Hidalgo, P. and Krautz, C., 2009. Zooplankton associated with the oxygen minimum zone system in the northern upwelling region of Chile during March 2000. *Deep Sea Research Part II: Topical Studies in Oceanography*, *56*(16), pp.1083-1094.

- Espinoza-Morriberón, D., Echevin, V., Colas, F., Tam, J., Gutierrez, D., Graco, M., Ledesma, J. and Quispe-Ccalluari, C., 2019. Oxygen Variability During ENSO in the Tropical South Eastern Pacific. *Frontiers in Marine Science*, *5*, p.526.

- Farías, L., Faúndez, J., & Sanhueza-Guevara, S. (2018). Temporal dynamics of dissolved inorganic nitrogen (DIN) in the aphotic layer of a coastal upwelling system with variable dissolved oxygen. Journal of Marine Systems, 103087.

- Fennel, K. and Testa, J.M., 2019. Biogeochemical controls on coastal hypoxia. *Annual Review of Marine Science*, *11*, pp.105-130.

- Frenger, I., Bianchi, D., Stührenberg, C., Oschlies, A., Dunne, J., Deutsch, C., Galbraith, E. and Schütte, F., 2018. Biogeochemical role of subsurface coherent eddies in the ocean: Tracer cannonballs, hypoxic storms, and microbial stewpots. *Global Biogeochemical Cycles*, *32*(2), pp.226-249.

- Fuenzalida, R., W. Schneider, J. Garces, L. Bravo, and C. Lange (2009), Vertical and horizontal extension of the oxygen minimum zone in the eastern South Pacific Ocean. Deep Sea Res., Part II, 56, 992–1003. doi:10.1016/j.dsr2.2008.11.001

- Garreaud, R.D. and Falvey, M., 2009. The coastal winds off western subtropical South America in future climate scenarios. International Journal of Climatology: A Journal of the Royal Meteorological Society, 29(4), pp.543-554.

- Galán, A., Molina, V., Thamdrup, B., Woebken, D., Lavik, G., Kuypers, M.M. and Ulloa, O., 2009. Anammox bacteria and the anaerobic oxidation of ammonium in the oxygen minimum zone off northern Chile. Deep sea research part II: topical studies in oceanography, 56(16), pp.1021-1031.

- Gobler, C.J. and Baumann, H., 2016. Hypoxia and acidification in ocean ecosystems: coupled dynamics and effects on marine life. *Biology letters*, *12*(5), p.20150976.

- Gray, J.S., Wu, R.S., Or, Y.Y., (2002). Effect of hypoxia and organic enrichment on the coastal marine environment. Marine Ecology Progress Series 238, 249–279.

- Griffies, S.M., Böning, C., Bryan, F.O., Chassignet, E.P., Gerdes, R., Hasumi, H., Hirst, A., Treguier, A.M. and Webb, D., 2000. Developments in ocean climate modelling. *Ocean Modelling*, *2*(3-4), pp.123-192.

- Gewin,. V. (2010). Dead in the Water. NATURE New Feature, vol 466, 12 August.

- Goubanova, K., V. Echevin, B. Dewitte, F. Codron, K. Takahashi, P. Terray, and M. Vrac (2011), Statistical downscaling of sea-surface wind over the Peru–Chile upwelling region: diagnosing the impact of climate change from the IPSL-CM4 model. Clim. Dyn., 36 (7–8), 1365–1378. doi:10.1007/s00382-010-0824-0

- Gregg, W. W., & Rousseaux, C. S. (2019). Global ocean primary production trends in the modern ocean color satellite record (1998–2015). *Environmental Research Letters*, **14**(12), 1998–2015. https://doi.org/10.1088/1748-9326/ab4667

- Gruber, N. and Sarmiento, J.L., 1997. Global patterns of marine nitrogen fixation and denitrification. *Global Biogeochemical Cycles*, *11*(2), pp.235-266.

- Gruber, N. and Galloway, J.N., 2008. An Earth-system perspective of the global nitrogen cycle. *Nature*, *451*(7176), pp.293-296.

- Gunther, E. R. (1936), A report on oceanographic investigations in the Peru Coastal Curren, Discovery Rep. 13, pp. 107-276, Cambridge Univ. Press, Cambridge, U. K.

- Gutknecht, E., et al. (2013a), Coupled physical/biogeochemical modeling including O_2-dependent processes in Eastern Boundary Upwelling Systems: Application in the Benguela. Biogeosciences, 10, 3559–3591. doi:10.5194/bg-10-1-2013

- Gutknecht, E., Dadou, I., Marchesiello, P., Cambon, G., Le Vu, B., Sudre, J., et al. (2013b). Nitrogen transfers off Walvis Bay: A 3-D coupled physical/biogeochemical modeling approach in the Namibian Upwelling System. Biogeosciences, 10, 4117–4135.

- Hameau, A., Frölicher, T., Mignot, J. and Joos, F., 2020. Is deoxygenation detectable before warming in the thermocline. *Biogeosciences*, *17*(7), pp.1877-1895.

- Helly, J.J., L. A. Levin (2004), Global distribution of naturally occurring marine hypoxia on continental margins. Deep-Sea Research I 51, 1159–1168. https://doi.org/10.1016/j.dsr.2004.03.009

- Hidalgo, P., Escribano, R., Fuentes, M., Jorquera, E. and Vergara, O., 2012. How coastal upwelling influences spatial patterns of size-structured diversity of copepods off central-southern Chile (summer 2009). *Progress in Oceanography*, *92*, pp.134-145.

- Holland, H.D. 2006. The oxygenation of the atmosphere and oceans. Philosophical Transactions of The Royal Society 361: 903-915

- Hormazábal, S., G. Shaffer, N. silva, and E. Navarro (2006), The Perú-Chile undercurrent and the oxygen minimum zone variability off central Chile, Gayana 70 (1), 37-45.

- Hormazábal, S., V. Combes, C.E. Morales, M.A. Correa-Ramírez, E. Di Lorenzo, S. Nuñez (2013), Intrathermocline eddies in the coastal transition zone off central Chile (31–41°S). J. Geophys. Res. Oceans 118, 1–11, doi:10.1002/jgrc.20337.

- Huyer, A., M. Knoll, T. Paluszkiewicz, and R. L. Smith (1991), The Peru Undercurrent: A study in variability. Deep-Sea Res., 38 (Suppl. 1), 247–279. https://doi.org/10.1016/S0198-0149(12)80012-4

- Ito, T., & Follows, M. J. (2013). Air-sea disequilibrium of carbon dioxide enhances the biological carbon sequestration in the Southern Ocean. *Global Biogeochemical Cycles*, **27**, 1129– 1138. https://doi.org/10.1002/2013GB004682

- Illig, S., Bachèlery, M.-L., & Cadier, E. (2018). Subseasonal coastal-trapped wave propagations in the southeastern Pacific and Atlantic Oceans: 2. Wave characteristics and connection with the equatorial variability. Journal ofGeophysical Research: Oceans, 123, 3942–3961. https://doi.org/10.1029/2017JC013540

- Illig, S., Cadier, E., Bachèlery, M.-L., & Kersalé, M. (2018). Subseasonal coastal-trapped wave propagations in the southeastern Pacific and Atlantic Oceans: 1. A new approach to estimate wave amplitude. Journal ofGeophysical Research: Oceans, 123, 3915–3941. https://doi. org/10.1029/2017JC013539

- José, Y.S., Stramma, L., Schmidtko, S. and Oschlies, A., 2019. ENSO-driven fluctuations in oxygen supply and vertical extent of oxygen-poor waters in the oxygen minimum zone of the Eastern Tropical South Pacific. *Biogeosciences Discussions*, pp.1-20.

- Kämpf J., Chapman P. (2016) The Peruvian-Chilean Coastal Upwelling System. In: Upwelling Systems of the World. Springer, Cham. https://doi.org/10.1007/978-3-319-42524-5_5

- Kamykowski, D. and Zentara, S.J., 1990. Hypoxia in the world ocean as recorded in the historical data set. Deep-Sea Research, 37(12), pp.1861-1874.

- Karstensen, J., L. Stramma, and M. Visbeck (2008), Oxygen minimum zones in the eastern tropical Atlantic and Pacific oceans. Prog. Oceanogr., 77, 331–350. https://doi.org/10.1016/j.pocean.2007.05.009

- Keeling, R.F., Körtzinger, A. and Gruber, N., 2010. Ocean deoxygenation in a warming world. *Annual review of marine science*, *2*, pp.199-229.

- Kessler, W.S., 2006. The circulation of the eastern tropical Pacific: A review. *Progress in Oceanography*, *69*(2-4), pp.181-217.

- Koné, V., E. Machu, P. Penven, V. Garçon, P. Freon, and H. Demarcq (2005), Modeling the primary and secondary productions of the southern Benguela upwelling system: A comparative study through two biogeochemical models. Global Biogeochem. Cycles, 19, GB4021. doi: 10.1029/2004GB002427

- Large, W., J. C. McWilliams, and S. Doney (1994), Oceanic vertical mixing: A review and model with a nonlocal boundary layer parameterization. Rev. Geophys., 32, 363–403. doi:10.1029/94RG01872

- Levin, L.A., A. E. Rathburn, A.E. Gutierrez, P. Munoz, A. Shankle (2002), Benthic processes on the Peru margin: a transect across the oxygen minimum zone during the 1997–1998 El Niño. Prog. Oceanogr 53, 1-27. https://doi.org/10.1016/S0079-6611(02)00022-8

- Lettmann, K.A., Hahner, F., Schakau, V., Wüllner, T. and Kohlmeier, C., 2020. A modelling study of hydrodynamical and biogeochemical processes within the California Upwelling System. arXiv preprint arXiv:2008.12749.

- Levin, L.A., 2018. Manifestation, drivers, and emergence of open ocean deoxygenation. *Annual review of marine science*, *10*, pp.229-260.

- Leth, O. and Shaffer, G., 2001. A numerical study of the seasonal variability in the circulation off central Chile. *Journal of Geophysical Research: Oceans*, *106*(C10), pp.22229-22248.

- Llanillo, P. J., J. L. Pelegrí, C. M. Duarte, M. Emelianov, M. Gasser, J. Gourrion, and A. Rodrıguez-Santana (2012), Meridional and zonal changes in water properties along the continental slope off central and northern Chile, Cienc. Mar., 38, 307–332, doi:10.7773/cm.v38i1B.1814.

- Luyten, J.R., Pedlosky, J. and Stommel, H., 1983. The ventilated thermocline. *Journal of Physical Oceanography*, *13*(2), pp.292-309.

- Maes, C., B. Blanke, and E. Martinez (2016), Origin and fate of surface drift in the oceanic convergence zones of the eastern Pacific, Geophys. Res. Lett., 43, 3398–3405, doi:10.1002/2016GL068217.

- Marchesiello, P., McWilliams, J.C. and Shchepetkin, A., 2001. Open boundary conditions for long-term integration of regional oceanic models. *Ocean modelling*, *3*(1-2), pp.1-20.

- McGillicuddy Jr, D.J., 2015. Formation of intrathermocline lenses by eddy–wind interaction. *Journal of Physical Oceanography*, *45*(2), pp.606-612.

- Maßmig, M., Lüdke, J., Krahmann, G., and Engel, A.: Bacterial degradation activity in the eastern tropical South Pacific oxygen minimum zone, Biogeosciences, 17, 215–230, https://doi.org/10.5194/bg-17-215-2020, 2020.

- Maximenko, N. A., Bang, B., & Sasaki, H. (2005). Observational evidence of alternating zonal jets in the world ocean. Geophysical Research Letters, 32, L12607. https://doi.org/10.1029/2005GL022728

- McCreary, J. P. (1981). A linear stratified ocean model of the coastal undercurrent, Phil. Trans. R. Soc. London, Ser. A, 302, 385– 413.

- McCreary, J.P., P.K. Kundu, and S.Y. Chao. (1987). On the dynamics of the California Current System, J. Mar. Res., 45 (1), 1–32

- Melzner, F., Mark, F.C., Seibel, B.A. and Tomanek, L., 2020. Ocean acidification and coastal marine invertebrates: tracking CO2 effects from seawater to the cell. *Annual Review of Marine Science*, *12*, pp.499-523.

- Melzner, F., Thomsen, J., Koeve, W., Oschlies, A., Gutowska, M.A., Bange, H.W., Hansen, H.P. and Körtzinger, A., 2013. Future ocean acidification will be amplified by hypoxia in coastal habitats. *Marine Biology*, *160*(8), pp.1875-1888.

- Mogollón, R. and Calil, P.H., 2017. On the effects of ENSO on ocean biogeochemistry in the Northern Humboldt Current System (NHCS): A modeling study. *Journal of Marine Systems*, *172*, pp.137-159.

- Montes, I., F. Colas, X. Capet, and W. Schneider (2010), On the pathways of the equatorial subsurface currents in the Eastern Equatorial Pacific and their contributions to the Peru-Chile Undercurrent. J. Geophys. Res., 115, C09003. doi:10.1029/2009JC005710

- Montes, I., W. Schneider, F. Colas, B. Blanke, and V. Echevin (2011), Subsurface connections in the eastern tropical Pacific during La Nina 1999–2001 and El Ni~no 2002–2003, J. Geophys. Res., 116, C12022, doi:10.1029/2011JC007624.

- Montes, I., B. Dewitte, E. Gutknecht, A. Paulmier, I. Dadou, A. Oschlies, and V. Garçon (2014), High-resolution modeling of the Eastern Tropical Pacific oxygen minimum zone: Sensitivity to the tropical oceanic circulation. J. Geophys. Res.-Oceans, 119, 5515–5532. doi:10.1002/2014JC009858

- Morales, C. E., S. Hormazábal, and J. L. Blanco (1999), Interannual variability in the mesoscale distribution of the depth of the upper boundary of the oxygen minimum layer off northern Chile (18–24S): Implications for the pelagic system and biogeochemical cycling. J. Mar. Res., 57, 909–932. https://doi.org/10.1357/002224099321514097

- Morel, A., and J. F. Berthon (1989), Surface pigments, algal biomass profiles, and potential production of euphotic layer: Relationship reinvestigated in view of remote-sensing applications. Limnol. Oceanogr., 34, 1545–1562. doi: 10.4319/lo.1989.34.8.1545

- Muñoz, R., and R. Garreaud (2005), Dynamics of the low level jet off the west coast of subtropical South America. Mon. Weather Rev. 133, 3661–3677. https://doi.org/10.1175/MWR3074.1

- Naqvi, S. W. A., H. W. Bange, L. Farias, P. M. S. Monteiro, M. I. Scraton, and J. Zhang (2010), Marine hypoxia/anoxia as a source of CH4 and N2O. Biogeosciences, 7, 2159–2190. doi:10.5194/bg-7-2159-2010

- Oerder, V., Colas, F., Echevin, V., Masson, S. and Lemarié, F., 2018. Impacts of the mesoscale ocean-atmosphere coupling on the Peru-Chile ocean dynamics: The current-induced wind stress modulation. *Journal of Geophysical Research: Oceans*, *123*(2), pp.812-833.

- Oschlies, A., Koeve, W., Landolfi, A. and Kähler, P., 2019. Loss of fixed nitrogen causes net oxygen gain in a warmer future ocean. *Nature communications*, *10*(1), pp.1-7.

- Oschlies, A., Brandt, P., Stramma, L. and Schmidtko, S., 2018. Drivers and mechanisms of ocean deoxygenation. *Nature Geoscience*, *11*(7), pp.467-473.

- Paulmier, A., Ruiz-Pino, D. and Garçon, V., 2011. CO_2 maximum in the oxygen minimum zone (OMZ).

- Paulmier, A., and D. Ruiz-Pino (2009), Oxygen minimum zones (OMZs) in the modern ocean. Prog. Oceanogr., 80 (3–4), 113–128. doi: 10.1029/j.pocean.2008.08.001

- Paulmier, A., D. Ruiz-Pino, V. Garçon, and L. Farias (2006), Maintaining of the East South Pacific Oxygen Minimum Zone (OMZ) off Chile. Geophys. Res. Lett., 33, L20601, doi:10.1029/2006GL026801

- Penven, P., Echevin V, Pasapera J, Colas F, Tam J. (2005). Average circulation, seasonal cycle, and mesoscale dynamics of the Peru Current System: A modeling approach. J. Geophys. Res. 110: C10021, doi: 10.1029/2005JC002945.

- Pegliasco, C., Chaigneau, A., Morrow, R. and Dumas, F., 2020. Detection and tracking of mesoscale eddies in the Mediterranean Sea: A comparison between the Sea Level Anomaly and the Absolute Dynamic Topography fields. *Advances in Space Research*.

- Pizarro, O., A. J. Clarke, and S. Van Gorder (2001), El Niño sea level and currents along the South American coast: Comparison of observations with theory. J. Phys. Oceanogr., 31, 1891–1903. https://doi.org/10.1175/1520-0485(2001)031<1891:ENOSLA>2.0.CO;2

- Pizarro, O., G. Shaffer, B. Dewitte, and M. Ramos (2002), Dynamics of seasonal and interannual variability of the Peru-Chile Undercurrent. Geophys. Res. Lett., 29, 1581. doi:10.1029/2002GL014790

- Pedlosky, J., Pratt, L.J., Spall, M.A. and Helfrich, K.R., 1998. Circulation around islands and ridges. Oceanographic Literature Review, 6(45), pp.897-898.

- Portela, E., Kolodziejczyk, N., Vic, C. and Thierry, V., 2020. Physical mechanisms driving oxygen subduction in the global ocean. *Geophysical Research Letters*, *47*(17), p.e2020GL089040.

- Renault, L., B. Dewitte, M. Falvey, R. Garreaud, V. Echevin, F. Bonjean (2009), Impact of the atmospheric coastal jet off central Chile on sea surface temperature from satellite observations (2000–2007). J. Geophys. Res. 114, C08006. doi:10.1029/2008JC005083

- Reyes et al. (2007), Monitoreo de las condiciones bio-oceanográficas entre la I y IV regiones, año 2006. IFOP Proyecto FIP 2006-01. Octubre 2007.

- Rich, J.J., Arevalo, P., Chang, B.X., Devol, A.H. and Ward, B.B., 2020. Anaerobic ammonium oxidation (anammox) and denitrification in Peru margin sediments. *Journal of Marine Systems*, *207*, p.103122.

- Ruiz-Fernández, P., Ramírez-Flandes, S., Rodríguez-León, E. and Ulloa, O., 2020. Autotrophic carbon fixation pathways along the redox gradient in oxygen-depleted oceanic waters. *Environmental Microbiology Reports*, *12*(3), pp.334-341.

- Rutllant, J.O.S.É. and Montecino, V.I.V.I.A.N., 2002. Multiscale upwelling forcing cycles and biological response off north-central Chile. Revista Chilena de Historia Natural, 75(217), p.e231.

- Sánchez-Velasco, L., Godínez, V.M., Ruvalcaba-Aroche, E.D., Márquez-Artavia, A., Beier, E., Barton, E.D. and Jiménez-Rosenberg, S.P.A., 2019. Larval Fish Habitats and Deoxygenation in the Northern Limit of the Oxygen Minimum Zone off Mexico. *Journal of Geophysical Research: Oceans*, *124*(12), pp.9690-9705.

- Shepherd, J.G., Brewer, P.G., Oschlies, A. and Watson, A.J., 2017. Ocean ventilation and deoxygenation in a warming world: introduction and overview.

- Schmidtko, S., Stramma, L., & Visbeck, M. (2017). Decline in global oceanic oxygen content during the past five decades. *Nature*, **542**(7641), 335– 339. https://doi.org/10.1038/nature21399

- Schneider, W., Donoso, D., Garcés-Vargas, J. and Escribano, R., 2017. Water-column cooling and sea surface salinity increase in the upwelling region off central-south Chile driven by a poleward displacement of the South Pacific High. Progress in Oceanography, 151, pp.38-48.

- Schneider, W., R. Fuenzalida, E. Rodríguez-Rubio, J. Garcés-Vargas and L. Bravo. (2003). Characteristics and formation of Eastern South Pacific Intermediate Water. Geophysical Research Letters, 30 (11): 1581.

- Schunck, H., et al. (2013), Giant Hydrogen Sulfide Plume in the Oxygen Minimum Zone off Peru Supports Chemolithoautotrophy. PLoS ONE 8(8): e68661. doi:10.1371/journal.pone.0068661.

- Schott, F. A., Stramma, L., and Fischer, J.: The warm water inflow into the western tropical Atlantic boundary regime, spring 1994, J. Geophys. Res.-Oceans, 100, 24745–24760, 1995.

- Schott, F. A., Fischer, J., and Stramma, L.: Transports and pathways of the upper-layer circulation in the western tropical Atlantic, J. Phys. Oceanogr., 28, 1904–1928, 1998

- Shaffer, G., O. Pizarro, L. Djurfeldt, S. Salinas, and J. Ruttlant (1997), Circulation and low-frequency variability near the Chilean coast: Remotely forced fluctuations during the 1991–1992 El Niño. J. Phys. Oceanogr., 27, 217–235. https://doi.org/10.1175/1520-0485(1997)027<0217:CALFVN>2.0.CO;2

- Shaffer, G., S. Hormazábal, O. Pizarro, and S. Salinas (1999), Seasonal and interannual variability of currents and temperature off central Chile. J. Geophys. Res., 104, 29,951–29,961. doi: 10.1029/1999JC900253

- Shchepetkin, A., J.C. McWilliams (2005), The regional oceanic modeling system (ROMS): a split-explicit, free-surface, topography-following- coordinate oceanic model. Ocean Model. 9, 347–404. https://doi.org/10.1016/j.ocemod.2004.08.002

- Siedlecki, S. A., N. S. Banas, K. A. Davis, S. Giddings, B. M. Hickey, P. MacCready, T. Connolly and S. Geier, S (2015), Seasonal and interannual oxygen variability on the Washington and Oregon continental shelves, J. Geophys. Res.-Oceans, 120, 608–633, doi:10.1002/2014JC010254.

- Silva, N., and S. Neshyba (1979), On the southernmost extension of the Peru-Chile Undercurrent, Deep Sea Res., Part A, 26, 1387–1393. doi:10.1016/0198-0149(79)90006-2

- Silva, N., N. Rojas, A. Fedele (2009), Water masses in the Humboldt Current System: properties, distribution, and the nitrate deficit as a chemical water mass tracer for equatorial subsurface water off Chile. Deep-Sea Res. II 56, 1004–1020. https://doi.org/10.1016/j.dsr2.2008.12.013

- Sinha, B & Richards, K (1999), Jet structure and scaling in Southern Ocean models. J. Phys.Oceanogr. 29, 1143–1155.

- Smith, R.D., J. K. Dukowicz, R. C. Malone (1992), Parallel ocean general circulation modeling. Physica D 60, 38–61. doi:10.1016/0167-2789(92)90225-C

- Stewart, F.J. Ulloa, O. DeLong, E. (2012). Microbial metatranscriptomics in a permanent marine oxygen minimun zone. Environmental Microbiology.14(1), 23-40

- Stramma, L., Johnson, G.C., Sprintall, J. and Mohrholz, V., 2008. Expanding oxygen-minimum zones in the tropical oceans. *science*, *320*(5876), pp.655-658.

- Stramma, L., Johnson, G.C., Firing, E. and Schmidtko, S., 2010. Eastern Pacific oxygen minimum zones: Supply paths and multidecadal changes. *Journal of Geophysical Research: Oceans*, *115*(C9).

- Stramma, L., Prince, E.D., Schmidtko, S., Luo, J., Hoolihan, J.P., Visbeck, M., Wallace, D.W., Brandt, P. and Körtzinger, A., 2012. Expansion of oxygen minimum zones may reduce available habitat for tropical pelagic fishes. *Nature Climate Change*, *2*(1), pp.33-37.

- Stramma, L., Oschlies, A. and Schmidtko, S., 2012. Mismatch between observed and modeled trends in dissolved upper-ocean oxygen over the last 50 yr. *Biogeosciences (BG)*, *9*(10), pp.4045-4057.

- Stramma, L., S. Schmidtko, LA, Levin, GC. Johnson (2010), Ocean oxygen minima expansions and their biological impacts. Deep-Sea Res. I 57:587–95. https://doi.org/10.1016/j.dsr.2010.01.005

- Strub, P. T., V. Montecino, J. Ruttlant, and S. Salinas (1998), Coastal ocean circulation off western South America, in the sea, vol. 11, The Global Coastal Ocean: Regional Studies and Syntheses, edited by A.R. Robinson and K. H. Brink, pp. 273-314, John Wiley, Hoboken, N. J

- Strub, P.T., Combes, V., Shillington, F.A. and Pizarro, O., 2013. Currents and processes along the eastern boundaries. In *International Geophysics* (Vol. 103, pp. 339-384). Academic Press.

- Strub, P.T., James, C., Montecino, V., Rutllant, J.A. and Blanco, J.L., 2019. Ocean circulation along the southern Chile transition region (38°–46° S): Mean, seasonal and interannual variability, with a focus on 2014–2016. *Progress in Oceanography*, *172*, pp.159-198.

- Suntharalingam, P., Sarmiento, J. L., & Toggweiler, J. R. (2000), Globalsignificance of nitrous-oxide production and transport from oceanic low-oxygenzones: A modeling study. Global Biogeochemical Cycles, 14, 1353–1370. https://doi.org/10.1029/1999GB900100

- Suntharalingam, P., Buitenhuis, E., Le Quere, C., Dentener, F., Nevison, C., & Butler, J. (2012). Quantifying the Impact of Anthro-pogenic Nitrogen Depositionon Oceanic Nitrous Oxide. Geophysical Research Letters, 39, L07605. https://doi.org/10.1029/2011GL050778

- Vergara, O., B. Dewitte, I. Montes, V. Garçon, M. Ramos, A. Paulmier, and O. Pizarro (2016a), Seasonal variability of the oxygen minimum zone off Peru in a high-resolution regional coupled model. Biogeosciences, 13, 4389–4410. doi:10.5194/bg-13-4389-2016

- Vergara, O., Echevin, V., Sepulveda, H. H., Colas, F., & Quiñones, R. (2016c). Modeling the seasonal dynamics of the Peru-Chile under- current of Central Chile (30-40°S). Continental ShelfResearch, 123,61–79. https://doi.org/10.1016/j.csr.2016.04.001

- Taguchi, B., R. Furue, N. Komori, A. Kuwano-Yoshida, M. Nonaka, H. Sasaki, and W. Ohfuchi (2012), Deep oceanic zonal jets constrained by fine-scale wind stress curls in the South Pacific Ocean: A high-resolution coupled GCM study, Geophys. Res. Lett., 39, L08602, doi: 10.1029/2012GL051248.

- Thomsen, S., T. Kanzow, G. Krahmann, R. J. Greatbatch, M. Dengler and G. Lavik (2016), The formation of a subsurface anticy-clonic eddy in the Peru-Chile Undercurrent and its impact on the near-coastal salinity, oxygen, and nutrients distributions, J. Geo- phys. Res.-Oceans, 121, 476–501, doi:10.1002/2015JC010878.

- Tyrrell, T. (1999). The relative influences of nitrogen and phosphorus on oceanic primary production. Nature 400, 525–531

- Thamdrup, B., Dalsgaard, T., Jensen, M.M., Ulloa, O., Farías, L. and Escribano, R., 2006. Anaerobic ammonium oxidation in the oxygen-deficient waters off northern Chile. Limnology and Oceanography, 51(5), pp.2145-2156.

- Toggweiler, J. R., K. Dixon, and W. S. Broecker. (1991). The Peru upwelling and the ventilation of the South Pacific thermocline. J. Geophys. Res., 96(C11): 20,467-20,497.

- Torres, R., Pantoja, S., Harada, N., González, H.E., Daneri, G., Frangopulos, M., Rutllant, J.A., Duarte, C.M., Rúiz-Halpern, S., Mayol, E. and Fukasawa, M., 2011. Air-sea CO_2 fluxes along the coast of Chile: From CO2 outgassing in central northern upwelling waters to CO2 uptake in southern Patagonian fjords. *Journal of Geophysical Research: Oceans*, *116*(C9).

- Tsuchiya, M., 1975. Subsurface countercurrents in the eastern equatorial Pacific Ocean.

- Tsuchiya, M., Talley, L. D., and Mccartney, M. S.: An eastern Atlantic section from Iceland southward across the equator, Deep- Sea Res. Pt. A, 39, 1885–1917, 1992.

- Tutasi, P. and Escribano, R., 2020. Zooplankton diel vertical migration and downward C flux into the oxygen minimum zone in the highly productive upwelling region off northern Chile. *Biogeosciences*, *17*(2), pp.455-473.

- Ulloa O., R. Escribano, S. Hormazábal, R. Quiñones, R. González and M. Ramos (2001), Evolution and biological effects of the 1997-98 El Niño in the upwelling ecosystem off northern Chile. *Geophys Res Lett*., 28:1591–1594. https://doi.org/10.1029/2000GL011548

- Ulloa, O., D. E. Canfield, E. F. DeLong, R. M. Letelier, F. J. Stewart (2012), Microbial oceanography of anoxic oxygen minimum zones. Proc. Natl. Acad. Sci. U.S.A. 109,15996-16003. doi:10.1073/pnas.1205009109

- Yakusev, E.V., Neretin, L.N., 1997. One-dimensional modelling of nitrogen and sulphur cycles of the aphotic zone of the Black and Arabian Seas. Global Biogeochemical Cycles 11, 401–414.

- Warren, B.A., 1981. The shallow oxygen minimum of the South Indian Ocean. Deep Sea Research Part A. Oceanographic Research Papers, 28(8), pp.859-864.

- Wishner, K.F., Seibel, B. and Outram, D., 2020. Ocean deoxygenation and copepods: coping with oxygen minimum zone variability.

- Wyrtki, K. (1962), The oxygen minima in relation to ocean circulation. Deep Sea Res. Oceanogr. Abstr., 9, 11–23. https://doi.org/10.1016/0011-7471(62)90243-7.

- Xia, Y., Du, Y., Qiu, B., Cheng, X., Wang, T. and Xie, Q., 2020. The characteristics of the mid-depth striations in the North Indian Ocean. *Deep Sea Research Part I: Oceanographic Research Papers*, p.103307.